JOURNAL OF PHYSICS OF THE EARTH

Volume IX June 1961 Number 1

CONTENTS

PUBLISHED JOINTLY BY

THE SEISMOLOGICAL SOCIETY OF JAPAN
THE GEODETIC SOCIETY OF JAPAN
THE VOLCANOLOGICAL SOCIETY OF JAPAN

JOURNAL OF PHYSICS OF THE EARTH

The object of the publication of JOURNAL OF PHYSICS OF THE EARTH is to provide an international medium for the publication of original contributions in the field of geophysical science, more particularly concerning with physical properties and conditions of and phenomena occurring in the solid part of the earth.

The JOURNAL is open to any one who wishes to contribute his (or her) article. But the authors are, in principle, requested to pay page charges necessary for publishing their respective articles. The authors receive 100 copies of reprints free of charge.

In order to serve the purposes for which this JOURNAL is published, all contributions should be written in widely understandable languages, such as English, French and German, etc. Contributions should be sent to the Editor or to one of the Associate Editors.

For the time being, this JOURNAL will be issued at variable prices and at irregular intervals. The price of this issue is 200 yen inside Japan and $1.00 for foreign countries, the latter including postage.

Subscriptions may be made through Charles E. Tuttle Co., Booksellers and publishers; Rutland, Vermont, U.S.A. or 15, Edogawa-cho, Bunkyo-ku, Tokyo, Japan.

JOURNAL OF PHYSICS OF THE EARTH, VOL. 9, No. 1, 1961

Vibration of an Elastic Globe with a Homogeneous Mantle over a Homogeneous Core. Vibrations of the First Class

By

Yasuo SATÔ and Tosimatu MATUMOTO,

Earthquake Research Institute.

(Read at the E.R.I. March 28, 1961.—Received March 31, 1961.)

1. Introduction

Several years ago the same authors (MATUMOTO and SATÔ: 1954) theoretically studied the torsional oscillation period of the earth having a homogeneous mantle and core. Because of the assumption adopted that the core was a perfectly liquid or rigid body, it was presumed that the condition at the boundary surface was either free from stress or vanishing displacement. On the other hand, however, we have reports that the core is neither perfect liquid nor rigid (JEFFREYS: 1959; PRESS: 1956; SCHLANGER: 1959), and it is desirable to know the effect of finite rigidity on the period and mode of vibration, so that we may examine the possibility of detecting the core rigidity by means of the free oscillation period. The assumption of a homogeneous mantle and core is not a satisfactory one in view of our present knowledge of the earth's structure, but a simplified assumption will make the general nature clear and give us a clue for further study.

2. Characteristic equation

The displacement and stress components for the torsional vibration were given before. (Subscript o refers to the mantle and i the core.)

$$u_0 = 0$$

$$v_0 = \frac{-im}{n(n+1)} \cdot \frac{1}{\sqrt{r}} \begin{pmatrix} B\, J_{n+1/2}(k_0 r) \\ B' Y_{n+1/2}(k_0 r) \end{pmatrix} \cdot \frac{1}{\sin\theta} P_n^m(\cos\theta) \cdot \exp(im\varphi) \cdot \exp(ipt)$$

$$w_0 = \frac{1}{n(n+1)} \cdot \frac{1}{\sqrt{r}} \begin{pmatrix} B\, J_{n+1/2}(k_0 r) \\ B' Y_{n+1/2}(k_0 r) \end{pmatrix} \cdot \frac{d}{d\theta} P_n^m(\cos\theta) \cdot \exp(im\varphi) \cdot \exp(ipt)$$

for the mantle

$$b \leq r \leq a \tag{2.1}$$

a and b being the outer and inner radius of the mantle respectively, and

$$u_i = 0$$

$$v_i = \frac{-im}{n(n+1)} \cdot \frac{1}{\sqrt{r}} E J_{n+1/2}(k_i r) \cdot \frac{1}{\sin\theta} P_n^m(\cos\theta) \cdot \exp(im\varphi) \cdot \exp(ipt)$$

$$w_i = \frac{1}{n(n+1)} \cdot \frac{1}{\sqrt{r}} E J_{n+1/2}(k_i r) \cdot \frac{d}{d\theta} P_n^m(\cos\theta) \cdot \exp(im\varphi) \cdot \exp(ipt)$$

for the core

$$0 \leq r \leq b \tag{2.2}$$

u, v and w are the displacement components for the radial, colatitudinal and azimuthal directions, and

$$k_0^2 = p^2\rho_0/\mu_0 = (p/V_{s0})^2 \quad \text{and} \quad k_i^2 = p^2\rho_i/\mu_i = (p/V_{si})^2 \tag{2.3}$$

where ρ, μ and V_s are the density, rigidity and S wave velocity respectively.

The characteristic equation is given by the continuity of the displacement and stress at the boundary surface as follows

$$D_n = \begin{vmatrix} \xi^3 \frac{\partial}{\partial\xi}(J_{n+1/2}(\xi)\cdot\xi^{-3/2}) & \xi^3 \frac{\partial}{\partial\xi}(Y_{n+1/2}(\xi)\cdot\xi^{-3/2}) & 0 \\ \eta^3 \frac{\partial}{\partial\eta}(J_{n+1/2}(\eta)\cdot\eta^{-3/2}) & \eta^3 \frac{\partial}{\partial\eta}(Y_{n+1/2}(\eta)\cdot\eta^{-3/2}) & \frac{\mu_i}{\mu_0}\zeta^3 \frac{\partial}{\partial\zeta}(J_{n+1/2}(\zeta)\cdot\zeta^{-3/2}) \\ \eta^{1/2} J_{n+1/2}(\eta) & \eta^{1/2} Y_{n+1/2}(\eta) & \zeta^{1/2} J_{n+1/2}(\zeta) \end{vmatrix}$$

$$= \zeta^{1/2} J_{n+1/2}(\zeta) \cdot L_n(\xi, \eta) - \frac{\mu_i}{\mu_0}\zeta^3 \frac{\partial}{\partial\zeta}(J_{n+1/2}(\zeta)\cdot\zeta^{-3/2}) \cdot R_n(\xi, \eta) = 0$$

where

$$\xi = k_0 a, \quad \eta = k_0 b \quad \text{and} \quad \zeta = k_i b = (V_{s0}/V_{si})\eta \tag{2.4}.$$

3. Solution of the equation

The above equation gives a relation between ξ, b/a, k_i/k_0 and μ_i/μ_0. For finding the effect of a thin crust over a homogeneous mantle we

are to assume b/a nearly equal to 1, while for the oscillation of the whole earth having a mantle and core we assume this value $b/a=0.5447$ $(=3470/6370)$. Then the ratio of the rigidity μ_i/μ_0 and that of the density ρ_i/ρ_0 are given as a function of ξ $(\equiv k_0 a=2\pi a/(V_{s0}T)$, $T=$oscillation period) and k_i/k_0 $(=V_{s0}/V_{si})$.

Fig. 1 is the result of numerical computation for μ_i/μ_0 as a function ξ $(=k_0 a)$ and V_{s0}/V_{si}, n being assumed to be 1 and 2, both axes are written in logarithmic scale. There are domains filled by numerals, which indicate the existence of solutions. On the other hand there is no solution for any combination of $k_0 a$ and V_{s0}/V_{si} corresponding to the blank area, because the ratio μ_i/μ_0 (and also ρ_i/ρ_0) turns out to be negative in this area.

Horizontal lines in the figures give solutions either for a liquid or rigid core. $L_n(\xi, \eta)=0$ gives the former, while $R_n(\xi, \eta)=0$ the latter. These equations do not contain any physical quantity connected with the core, therefore the solution has nothing to do with the physical nature of it. A part of the result was given in the previous paper.

Using Figs. 1a, 1b and two other similar figures we can draw the lines of constant (μ_i/μ_0) and those of constant (ρ_i/ρ_0). They are given in the Figs. 2a–2d in linear scale. (A few numerical errors were found in the previous paper, which are corrected here.)

4. Discussion

Since we can easily get the solution to the two extremity cases, namely the perfectly liquid and rigid cores, we are apt to think that the period of oscillation for finite rigidity lies between these two values. But the result of computation turns out not to be so. As the figures in the previous section show, if we keep (ρ_i/ρ_0) finite

$$\text{(Oscillation period)}\to\infty, \quad \text{as} \quad \mu_i\to 0\,.$$
$$\text{(Oscillation period)}=\text{finite}, \quad \text{when} \quad \mu_i=0\,.$$

If there is no core substance at all or the core rigidity is a perfect zero, the energy is not transmitted from the mantle into the core and the simple theory in the previous paper holds. However, if there is an interaction between them, the core has two effects to the oscillation ; namely it gives a restitutive force and also it acts as an inertia. The former shortens the period, while the latter elongates it. If the density ρ_i remains constant and the rigidity μ_i tends to zero, the effect

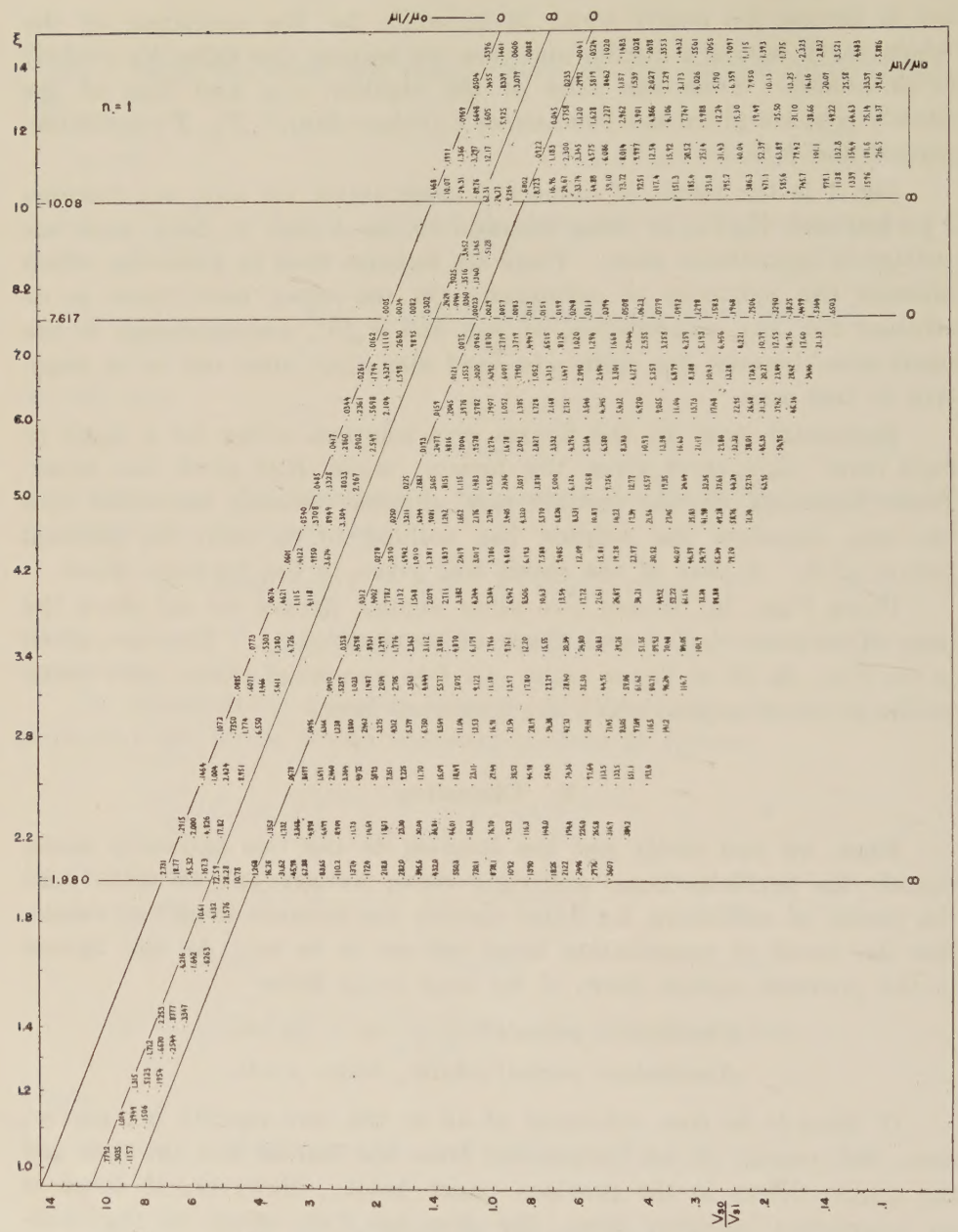

Fig. 1a. μ_1/μ_0 as a function of ξ and (V_{80}/V_{81}).

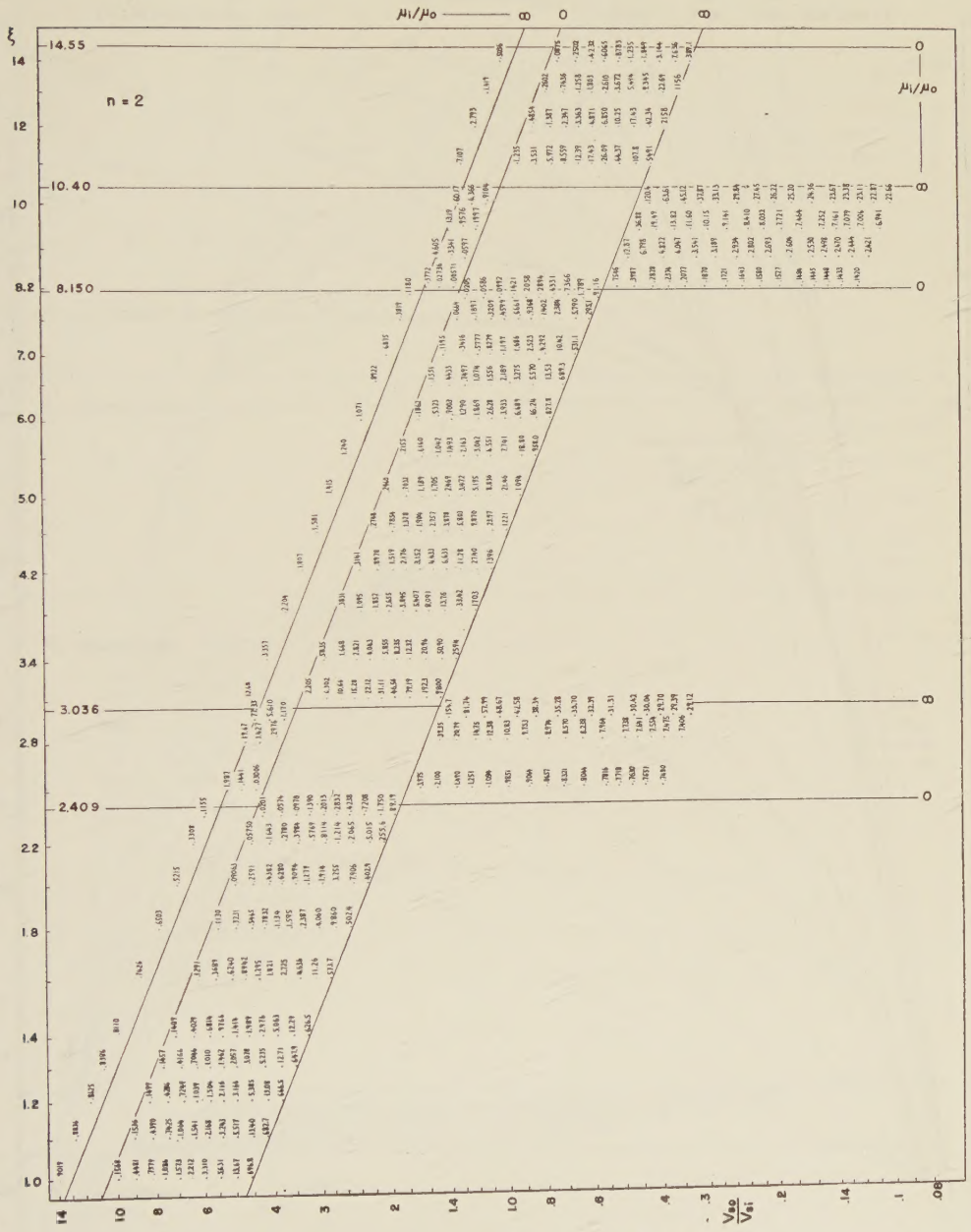

Fig. 1b. μ_1/μ_0 as a function of ξ and (V_{s0}/V_{s1}).

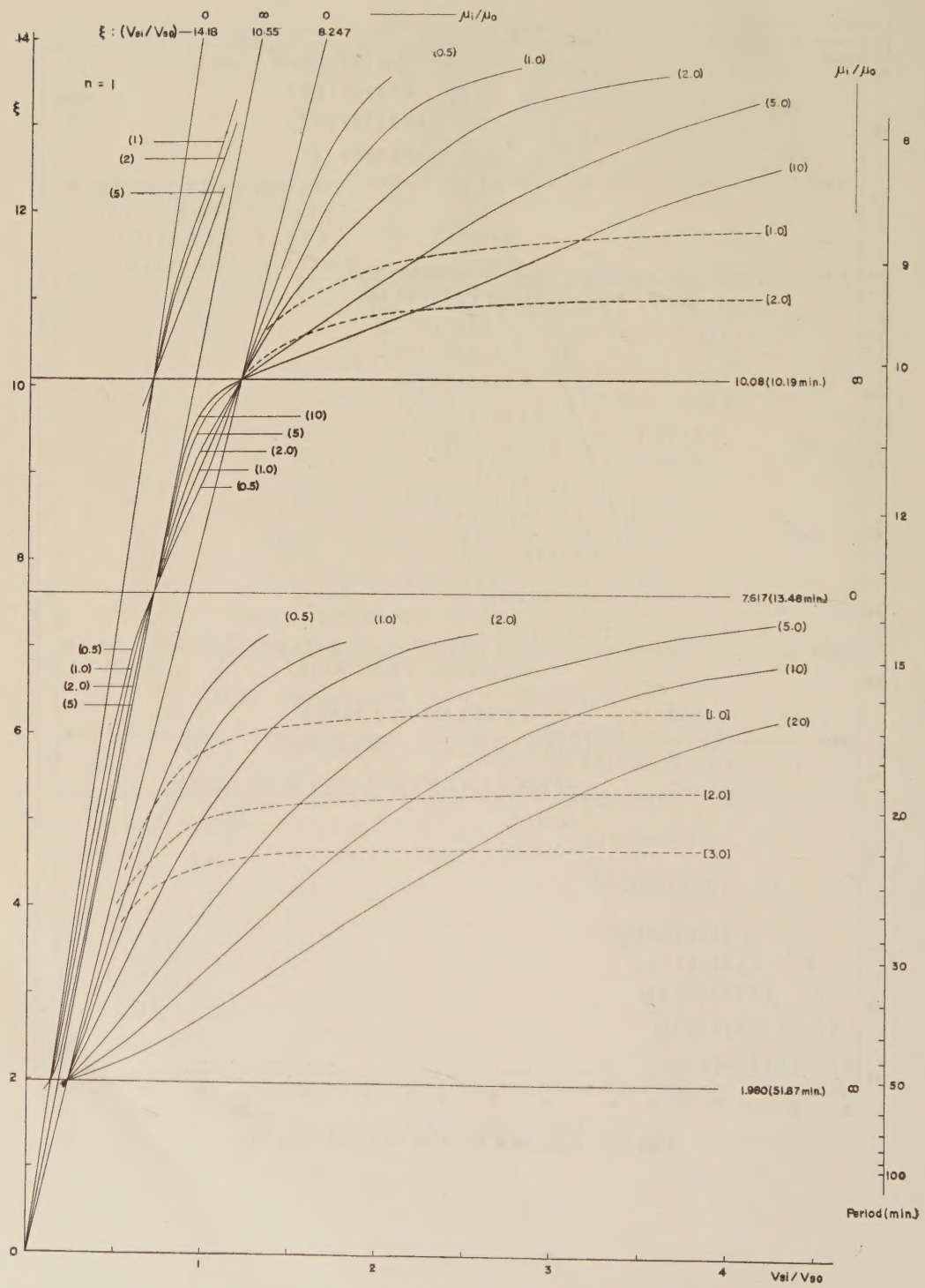

Fig. 2a. Curves of constant μ_i/μ_0 and ρ_i/ρ_0. ( ) gives μ_i/μ_0. [ ] gives ρ_i/ρ_0. V_{s0} is assumed to be 6.5 km/sec.

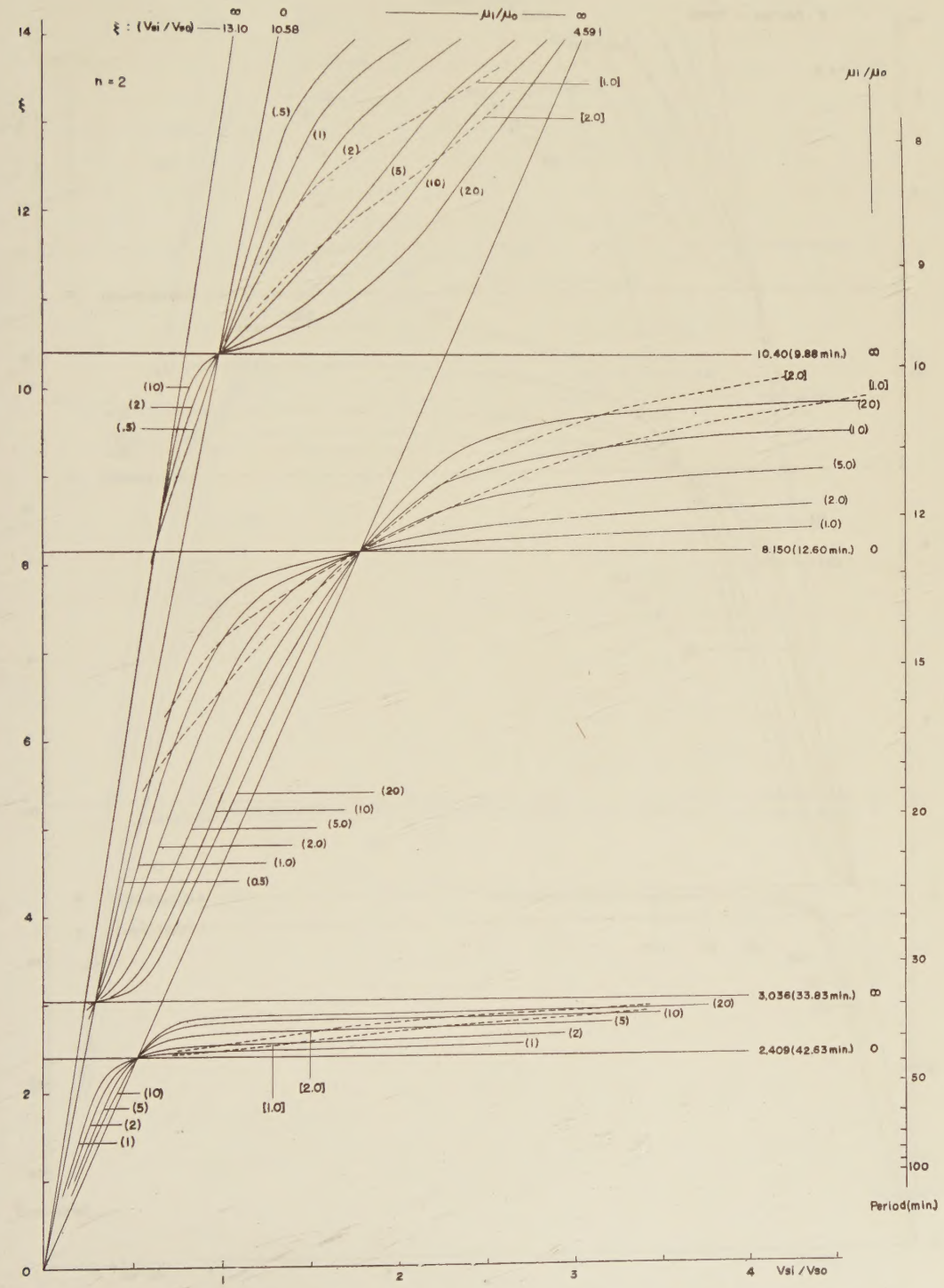

Fig. 2b. Curves of constant μ_i/μ_0 and ρ_i/ρ_0. ( ) gives μ_i/μ_0. [ ] gives ρ_i/ρ_0. V_{s0} is assumed to be 6.5$\frac{1}{4}$km/sec.

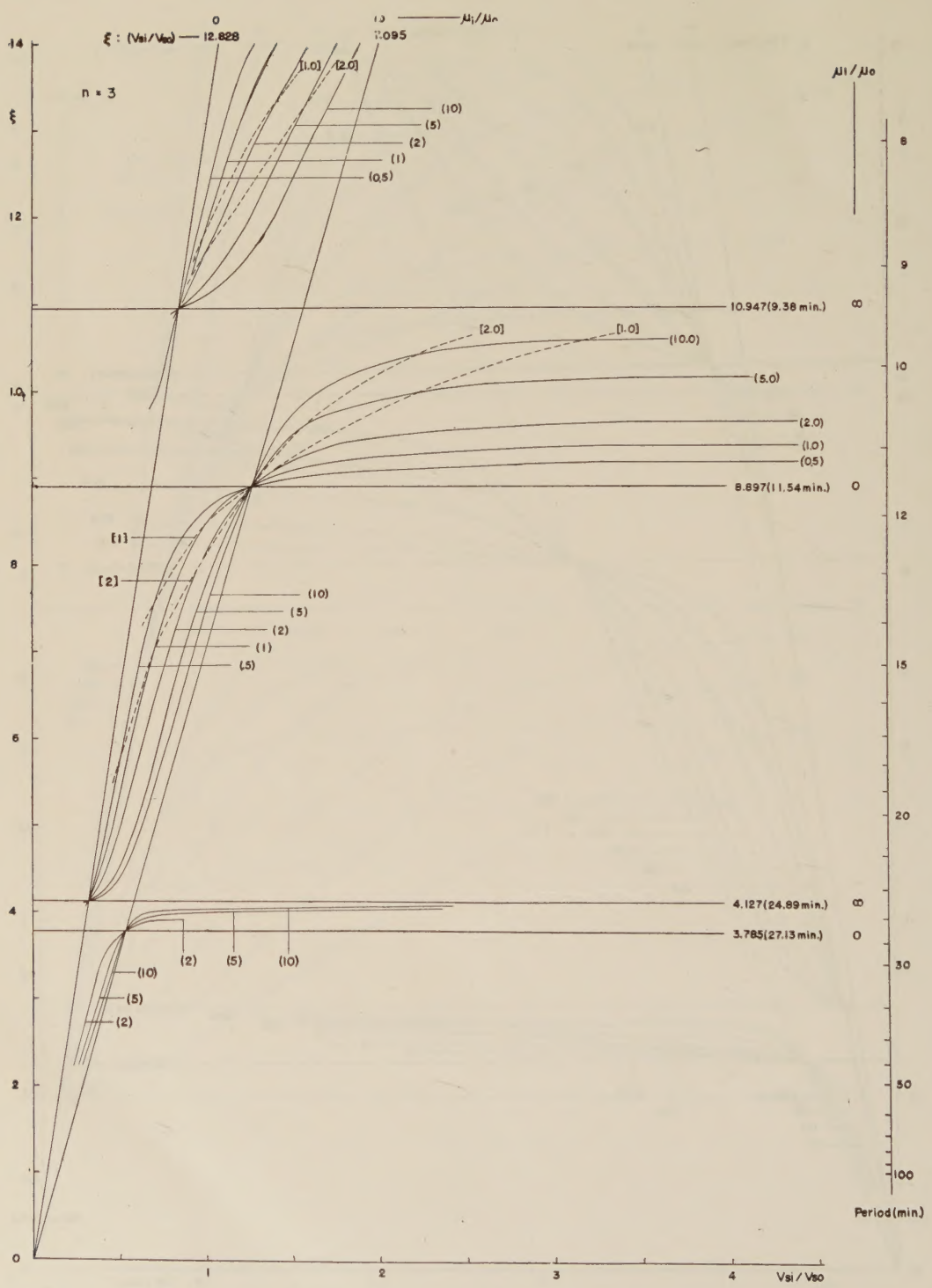

Fig. 2c. Curves of constant μ_i/μ_0 and ρ_i/ρ_0. ( ) gives μ_i/μ_0. [ ] gives ρ_i/ρ_0. V_{s0} is assumed to be 6.5 km/sec.

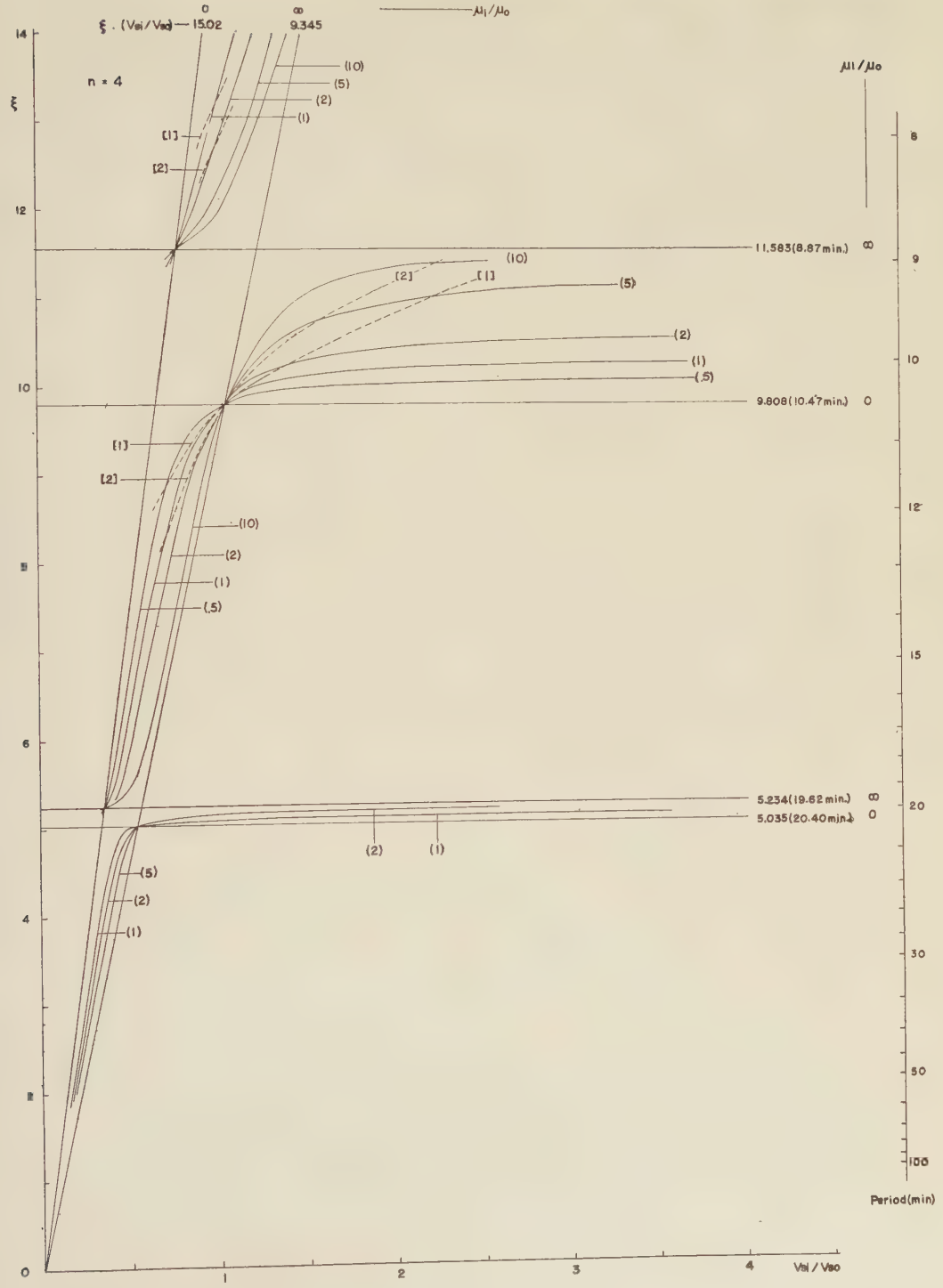

Fig. 2d. Curves of constant μ_i/μ_0 and ρ_i/ρ_0. ( ) gives μ_i/μ_0. [ ] gives ρ_i/ρ_0. V_{s0} is assumed to be 6.5 km/sec.

of the core as an inertia term remains unchanged while the restitutive force becomes weak, and as a result the period becomes extremely long.

This can be interpreted in another way. If we look at the curves

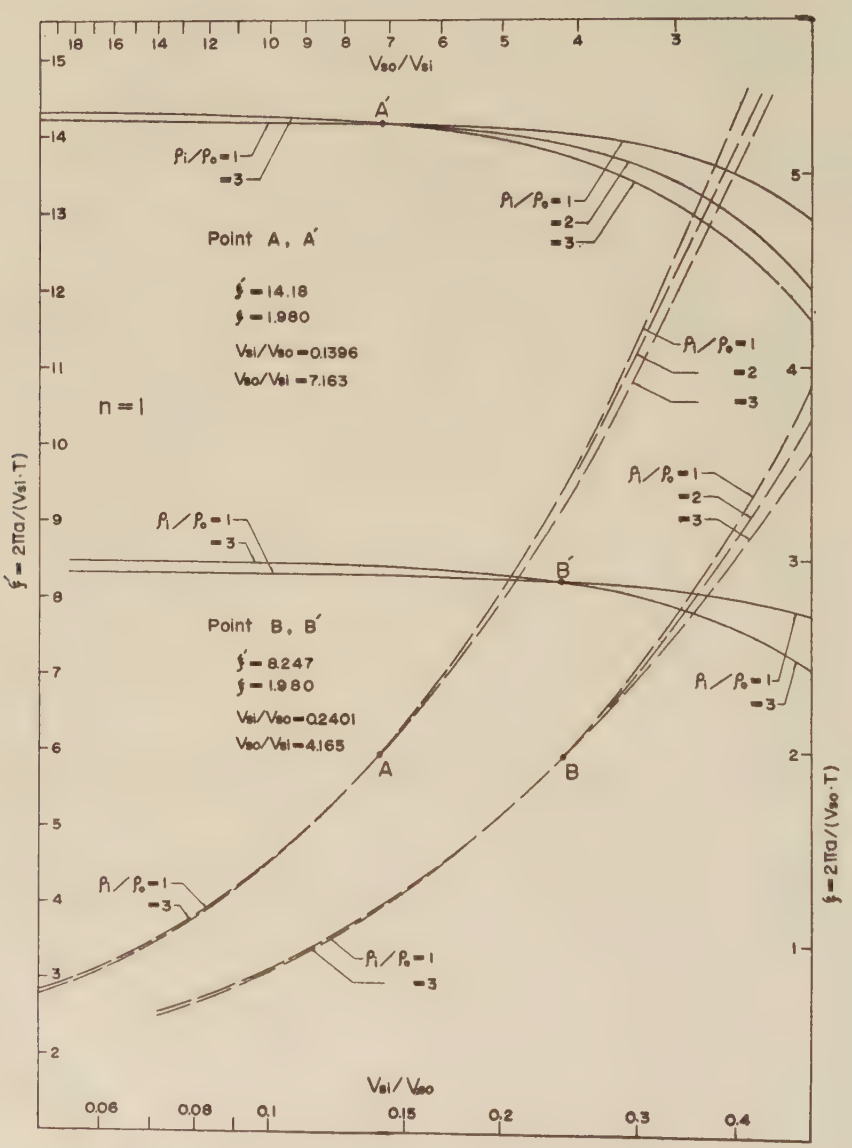

Fig. 3a. Curves of constant ρ_i/ρ_0. Bold lines refer to ξ'-axis. Broken lines refer to ξ-axis.

in Figs. 2a–2d belonging to the fundamental mode, we find (being better in figures of larger n) that they are divided into two parts; one part is nearly horizontal and is independent of V_{si}/V_{s0}, which fact shows that the frequency is approximately determined by the property of the mantle only. While in the other part, ξ is almost proportional to V_{si}/V_{s0}, implying that the outer part of the earth has little effect on the oscillation. Figs. 3a and 3b, which are both written using the ordinate $\xi'=2\pi a/(V_{si}T)$ ($\xi=2\pi a/(V_{s0}T)$ is also given for reference), will make clear the above circumstance. Whatever value μ_i may take, the ratio of the

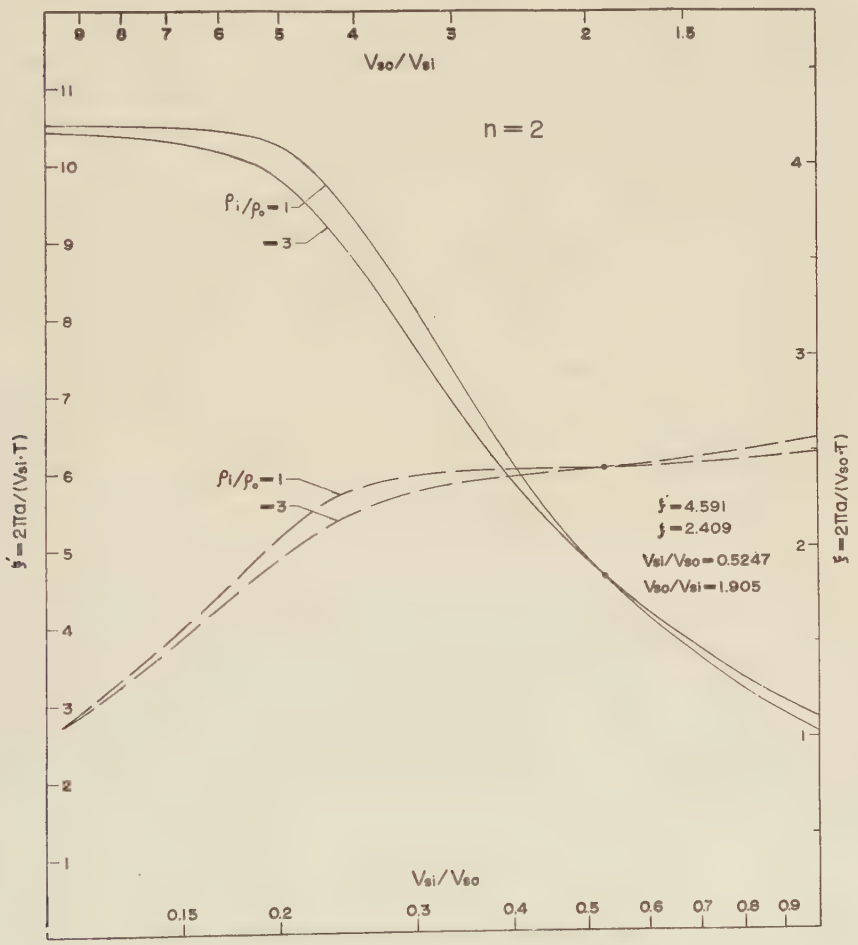

Fig. 3b. Curves of constant ρ_i/ρ_0. Bold lines refer to ξ'-axis. Broken lines refer to ξ-axis.

densities does not change widely, so the curves of constant (ρ_i/ρ_0) are given in these figures. When the shear velocity of the core is low curves are flat, implying the effect of the mantle being small. In this case the displacement in the mantle is, as is seen in the figures of the next section, very small, therefore the oscillation of this kind seems hard to be excited by a source in the upper part of the mantle. Then what will be the significance of the period theoretically obtained ignoring the rigidity of the core? The observed period of free oscillation of the earth agrees with this simple theory (BENIOFF, PRESS and SMITH: 1961; NESS, HARRISON and SLICHTER: 1961; ALSOP, SUTTON and EWING: 1961).

A similar problem was discussed by K. TAZIME (TAZIME: 1959) in his study on the propagation of surface waves in a medium having a very low velocity layer. According to what he suggests the solution which is obtained neglecting the existence of low velocity medium corresponds to the higher mode oscillation with such low velocity medium. When the core rigidity is small, higher mode has generally very large amplitude in the part of core and it seems that a source of disturbance near the surface is not a favorable condition for exciting such a mode. However, when the impedance contrast of two media is large the rate of energy transmission across the boundary is small. Besides the restitutive force at this surface is also small when the core is much less rigid than the mantle. Under such a condition the existence of the core will scarcely affect the oscillation period. Thus a mode of oscillation will exist, which is a higher mode if fully developed, but, in the part of the mantle, has at first a similar feature to the case of perfect liquid core.

In Fig. 4 the left figure represents the fundamental mode where there is a perfect liquid core, while the right figure gives an example of one of the higher modes when the core has small rigidity. ρ_i/ρ_0 and μ_i/μ_0 will not be very far from those of the real earth. A value of period $(=1/\xi)$ is adopted which is nearly equal to the case of perfect liquid. The distribution of displacement in the mantle thus obtained does not differ appreciably, although the feature in the core is completely different.

5. Conclusion

The above discussion leads us to the conclusion that

1) Existence of the core with large rigidity makes the frequency of torsional oscillation higher.

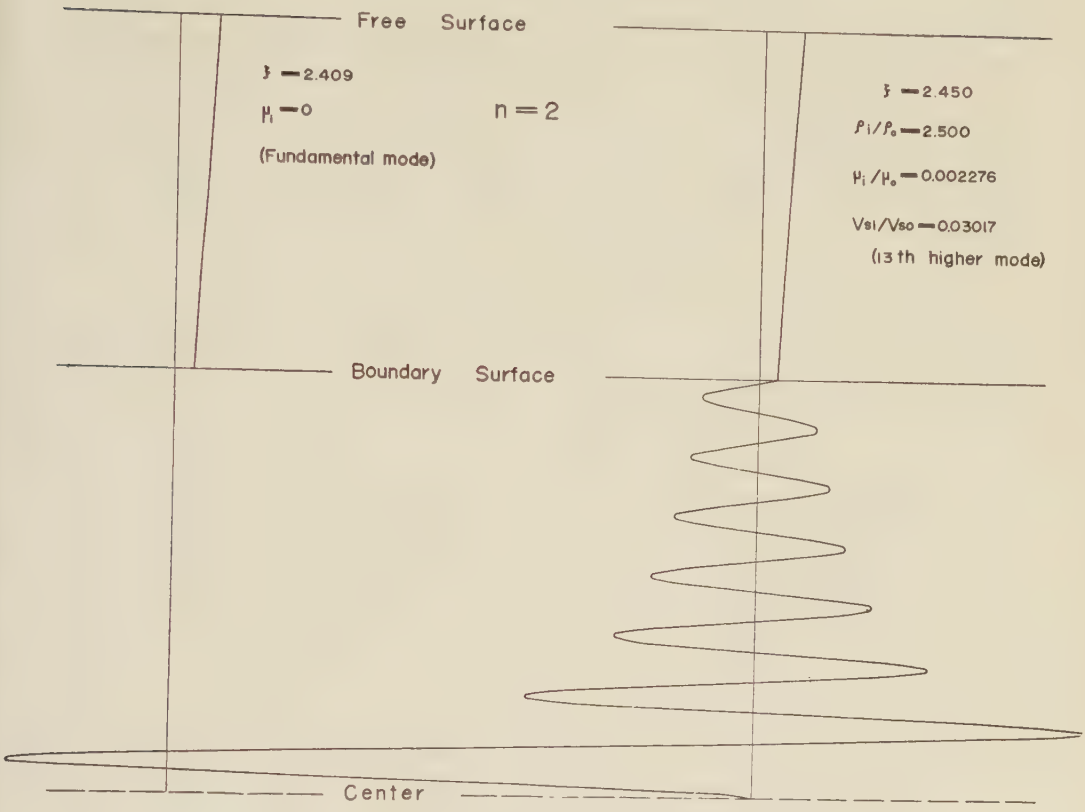

Fig. 4. Amplitude distribution
Left: Core of liquid
Right: Core of small rigidity

2) Existence of the core with small rigidity decreases the frequency of fundamental mode and the period becomes very long.

3) However, when the core rigidity is small, there are higher modes whose periods are nearly equal to those in the case of the perfect liquid core, and the feature of motion in the mantle is also similar.

4) Although the displacement in the core is very large and is completly different from that in the case of perfect liquid, the observed period will be the one for these modes with undeveloped displacement distribution in the core.

6. Distribution of amplitude

To make the feature of oscillation clearer, the distribution of am-

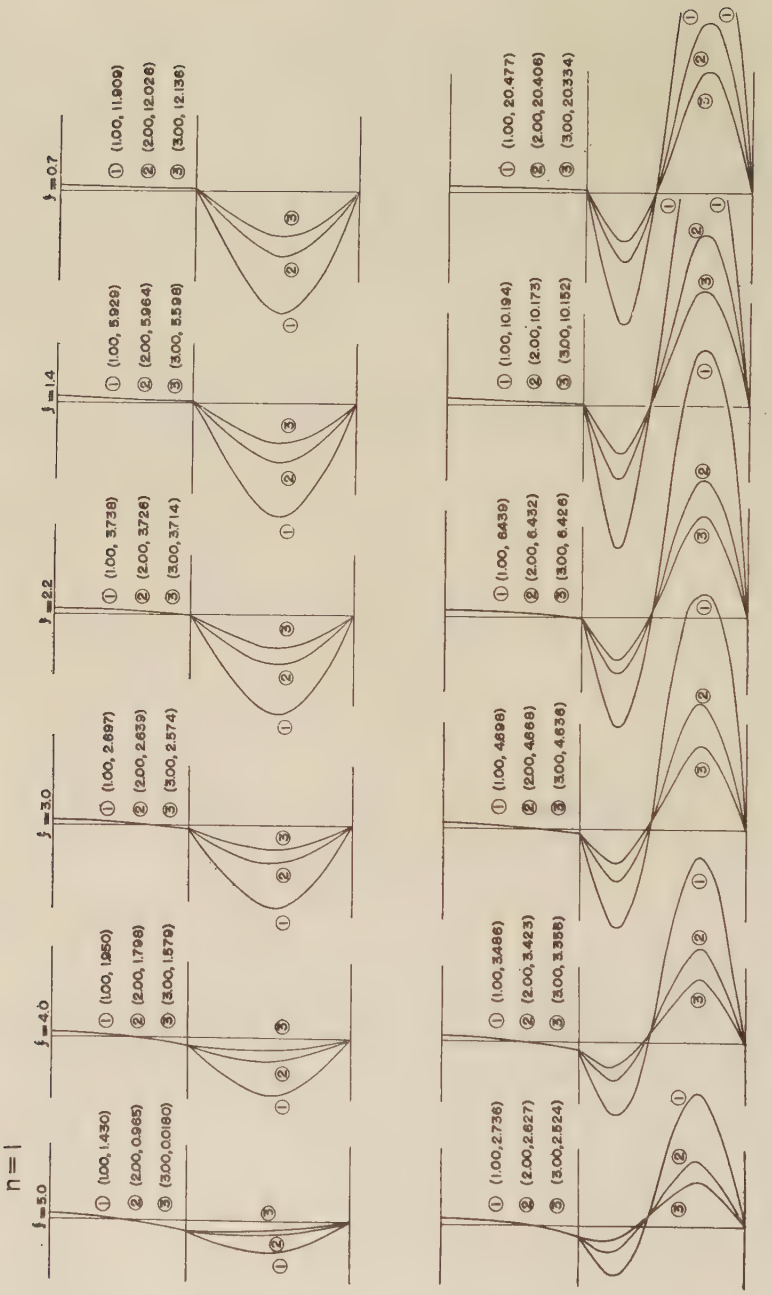

Fig. 5a. Amplitude distribution in the mantle and the core for $n=1$.
Above: 1st higher mode Below: 2nd higher mode
First and second numbers in the parentheses; ρ_i/ρ_0 and V_{s0}/V_{si}.

plitude within the earth was computed for the case $n=1$ and 2 adding to the one given before. Since the density ratio does not vary widely, computation was carried out along the curves of $\rho_i/\rho_0=$const.

As can be expected from Figs. 3a and 3b, corresponding to large values of V_{si}/V_{s0} the energy concentration in the mantle is revealed, while small V_{si}/V_{s0} gives a mode of oscillation which has large displacement in the core.

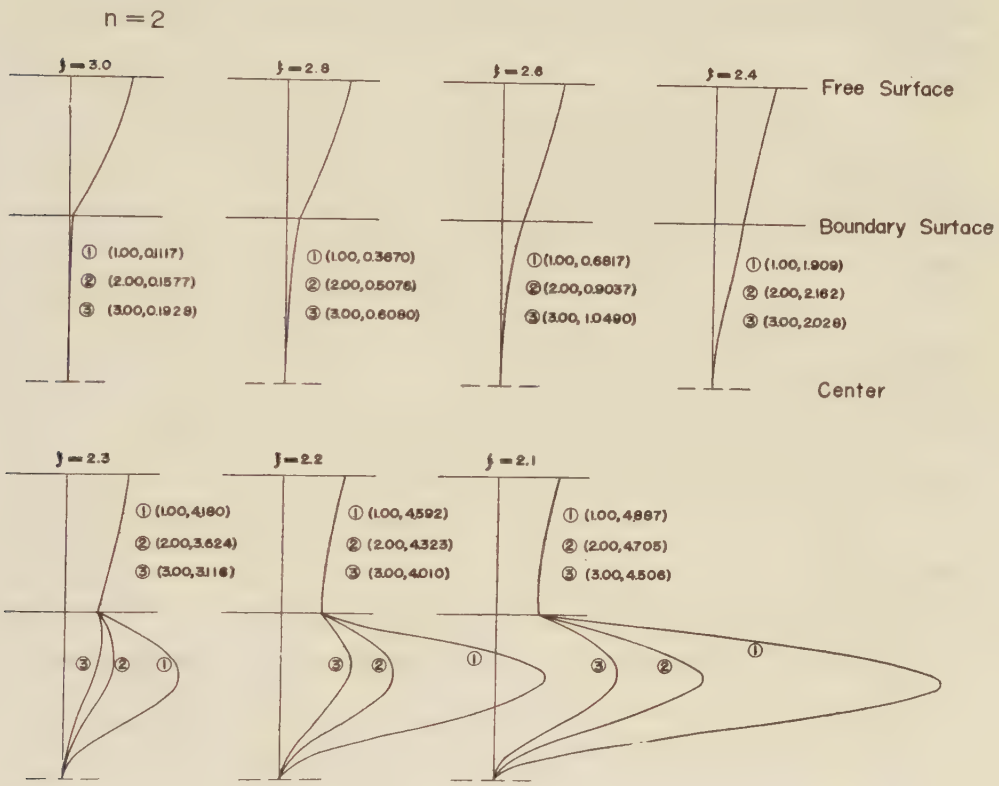

Fig. 5b. Amplitude distribution in the mantle and the core for $n=2$ fundamental mode. First and second numbers in the parentheses; ρ_i/ρ_0 and V_{s0}/V_{si}.

Acknowledgment

This work was started by the authors at the Earthquake Research Institute, Tokyo University, and finished in the U.S.A., while they were working at Watson Research Laboratory and Lamont Geological Observatory. Authors' thanks are due to Dr. W. ECKERT of Watson Research

Laboratory and Dr. M. EWING of Lamont Geological Observatory. They are also indebted to Dr. R. TAKAHASI of Earthquake Research Institute for giving them the chance of making research at the above-mentioned institutions.

It will also be mentioned here that Yasuo SATÔ has been given leave of absence from the University of Tokyo to study at Watson Research Laboratory, New York, and Tosimatu MATUMOTO, too, to study at Lamont Geological Observatory as the Columbia University's Exchange Visitor.

References

ALSOP, L., SUTTON, G. H. and EWING, M.:
1961 "Free Oscillations of the Earth Observed on Strain and Pendulum Seismographs." Journ. Geophys. Res., **66**, 631-641.

BENIOFF, H., PRESS, F. and SMITH, S.:
1961 "Excitation of the Free Oscillations of the Earth by Earthquakes." Journ. Geophys. Res. **66** 605-619.

JEFFREYS, H.:
1959 "The Earth" (Cambridge), § 7.051.

MATUMOTO, T. and SATÔ, Y.:
1954 "On the Vibration of an Elastic Globe with One Layer. The Vibration of the First Class." Bull. Earthq. Res. Inst., **32**, 247-258.

NESS, N. F., HARRISON, J. C. and SLICHTER, L. B.:
1961 "Observations of the Free Oscillations of the Earth." Journ. Geophys. Res. **66**, 621-629.

PRESS, F.:
1956 "Rigidity of the Earth Core." Science, **124**, 1204.

SCHLANGER, A. (Ben-Menahem):
1959 "Free Non-Rigid Vibration of the Earth." Geofisica Pura e Applicata, **43**, 23-35.

TAZIME, K.:
1959 "An Application of the Ray Theory to Stratified Layers (**10**)." Zisin (Journ. Seis. Soc. Japan), **12**, 25-26.

(Contribution no. 497, Lamont Geological Observatory, Columbia University, Palisades, New York)

DISASTER PREVENTION RESEARCH INSTITUTE
KYOTO UNIVERSITY
BULLETINS

Bulletin No. 36 August, 1960

On the Flow and Fracture of Igneous Rocks

By

Shogo MATSUSHIMA

Geophysical Institute, Faculty of Science, Kyoto University, Kyoto

On the Flow and Fracture of Igneous Rocks

By

Shogo MATSUSHIMA

Geophysical Institute, Faculty of Science, Kyoto University, Kyoto
(Communicated by Prof. K. Sassa)

ABSTRACT

1. The stress-strain relations of some igneous rocks for longitudinal and lateral direction were observed. The curves of the longitudinal strain versus stress were approximately linear up to the moment of rupture, but the strain in the lateral direction showed the abrupt increase in the fracture range.

2. It was found that such abrupt increase of the lateral strain was closely related with the flow. The longitudinal creep during the moderate period was almost recovered by the removal of the load, but in the lateral direction, large amount of residual strain was observed after the removal of the load.

3. The empirical formulae of creep for granite were given as follows,

$$S=A_0+A_1e^{-\alpha_1 t}+A_2e^{-\alpha_2 t}+A_3e^{-\alpha_3 t}+B\log t+Ct,$$

for the longitudinal direction, and

$$S=A+B\log t+Ct,$$

for the lateral direction, respectively. In the former equation, the reciprocals of α_1, α_2 and α_3 denote the retardation times. The later equation concurs with the formula given by Griggs and others.

1. If we consider the problems of the occurrence of the earthquake, it seems to be very important to study the rupture mechanism of rocks constituting the earth's crust in the deep place. However, the rocks which exist in the deeper part of the crust must be different from the ones found at the surface of the earth. Moreover, they are under high pressure and high temperature.

In spite of the above circumstances, it may give us some clue of the interpretation of the rupture phenomena in the crust to study the mechanism of fracture of rocks in ordinary states. The experiments reported here

were carried out under an atmospheric pressure and room temperature. In these experiments the simple compressional force was applied to the specimens.

The strain was measured by the strain gauge of the electric resistance type. The strain gauge of this type has high sensitivity and considerable accuracy. Besides, it has a very convenient characteristics such as the any desired strain component can be measured easily. The difficulties caused by the unstability of the indication, which we always encounter in the treatment of the electric instruments during the long period observation, were avoided sufficiently by the use of the unbonded type of strain gauge.

2. It has been reported in many papers that the stress-strain relations in the loading direction for silicate rocks were approximately linear up to the moment of rupture. It may be said that the rocks are the quite elastic and brittle material. It is well known, however, that the rocks are the very porous material, and because of its porous structure, they have the considerably lower value of Poisson's ratio at the incipience of loading than that of the other materials[1]. Then, it may be expected at the rupture stage, that the porous structure will considerably affect to the rupture mechanism for the rocks.

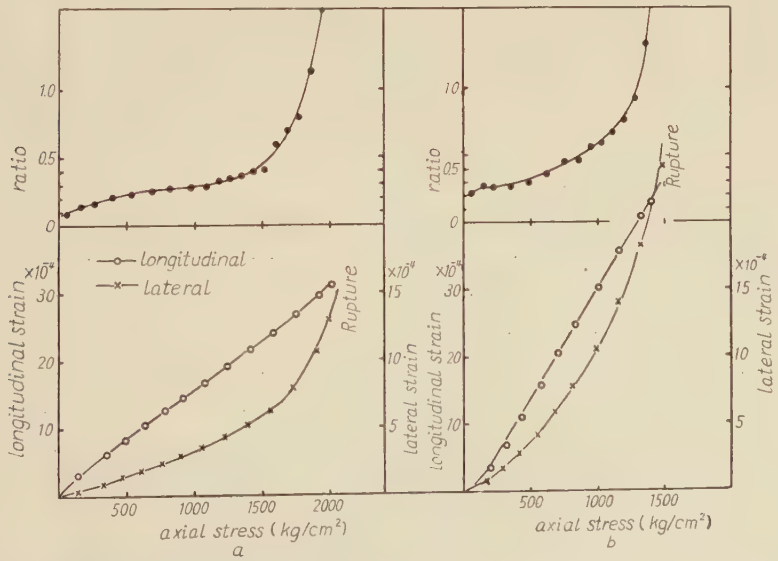

Fig. 1. Stress-strain curves and variation of Poisson's ratio with stress, (a) Aokiko-Nagano quartz monzonite, (b) Yakuno-Kyoto olivine basalt.

According to the above consideration, the measurements of stress-strain relations of the several sorts of igneous rocks both in the longitudinal and in the lateral directions were carried out up to the rupture point, and the ratio of the lateral to the longitudinal strain was calculated. The rock specimens used for these experiments are 30 mm. in diameter and 60 mm. long.

The longitudinal strain of each specimen varied almost linearly with stress up to the rupture as above mentioned. As shown in Fig. 1, however, it was found that the rate of increase of the lateral strain increased gradually with stress, and in the fracture range the increase of the lateral strain becomes much larger than the longitudinal one. At the first stage, the Poisson's ratio gives the less value compared with the other materials, and with the increasing load it reaches at the ordinaly value, about 0.3. When the rock specimen begins to show the aspect of failure, the ratio increases beyond 0.5, and finally it shows the extraordinaly high value at the rupture stage. This suggests the effect of volume expansion in the fracture or the plastic stage, which was found by P. W. Bridgman in his volumetric tests[2]. It is supposed that this effect involves in itself the fundamental meaning for the rupture mechanism of rocks.

3. When the stress-strain relation was observed in the fracture range, it was clearly indicated that all the abrupt increase of lateral strain was not produced instantaneously at the moment of loading, but the flow strain after loading had the close connection with such abrupt increase of strain. Then it may be interesting to observe the amount of flow along the lateral direction compared with the one along the longitudinal direction during the moderate period at the fracture stage.

To avoid the reasonable suspicion on the barrel shape deformation of the specimen, the lateral strain was measured at the ending portion of them. The other conditions were kept the same as the previous experiments. As an example, the results of strain-time relations for a Kitashirakawa biotite granite under various stresses are shown in Fig. 2, where (a) denotes the longitudinal direction and (b) the lateral direction. The results of the others were almost the same as the above. The normal strength of this granite is 1400 kg/cm^2, then it will be seen that the lateral flow is hardly perceptible below the stress of one third of the normal strength. Beyond the stress of a half of the normal strength, however, the lateral flow becomes larger than that of the longitudinal one, and it surpasses the later

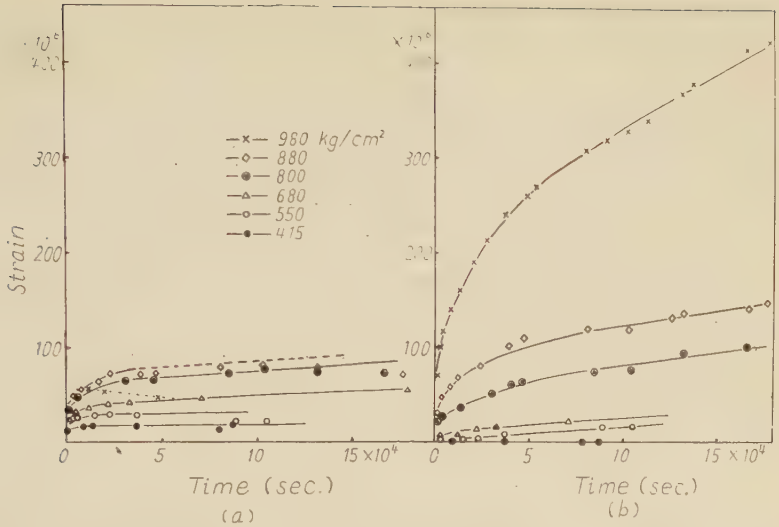

Fig. 2. Strain-time curves for Kitashirakawa biotite granite under various loads, (a), longitudinal direction, (b) lateral direction.

by far in the fracture range, in which the microscopic failure will rapidly occur.

Thus the deformation process of rocks can be divided into three stages, that is, the first stage in which the pores are closed, the second stage in which the material behaves almost perfectly elastic, and the final and fracture stage in which the lateral strain shows a distinctive increase.

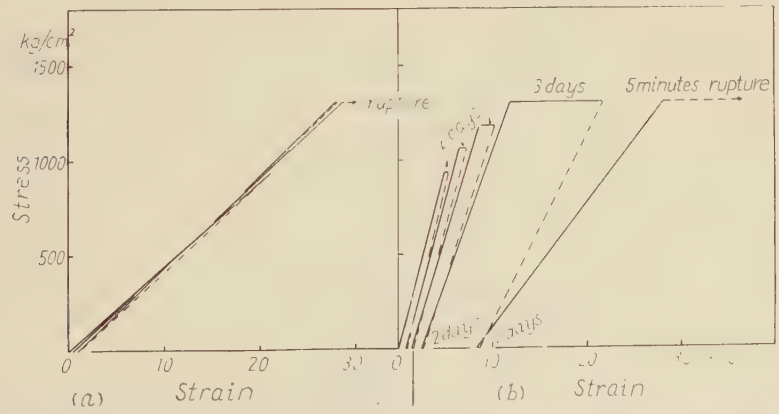

Fig. 3. Stress-strain relations, which involve the flow and recovery, for Kitashira biotite granite, (a) longitudinal direction, (b) lateral direction.

In these observations, the elastic recovery was measured after each test. Fig. 3 shows the stress-strain-time relation given from the successive test for flow and recovery. In the longitudinal direction, the strain caused by the creep almost returned, but the lateral creep strain scarcely returned at the removal of the load. Then the large amount of permanent set, the amount of which will be closely related with the duration of loading, was observed in the lateral direction. It may be said that the rocks have the unusual properties, elastic in the direction of compression and plastic in the direction transverse to it.

4. Many measurements have been reported on the creep of rocks, and the experimental equation of the results has been given in the form of

$$S = A + B \log t + Ct,$$

where S denotes the flow strain, t the time and A, B, C the constants.

In this section, the experimental formula of the creep for granite is estimated. The specimens used in this experiments are Shodoshima biotite granite, 30 mm. in diameter and 60 mm. long. The measurements were done in two stages, the one was in the short period 1 to 10^2 second, and the other was in the long period 10^2 to 10^6 seconds. The creep of long period was measured by the unbonded-type strain gauge. This sensitivity is a quarter of 10^{-6} in the axial direction and 10^{-6} in the transverse direction. The error of the observed value was within 3×10^{-6}, during the all period of the observation. The change of the room temperature, by which the

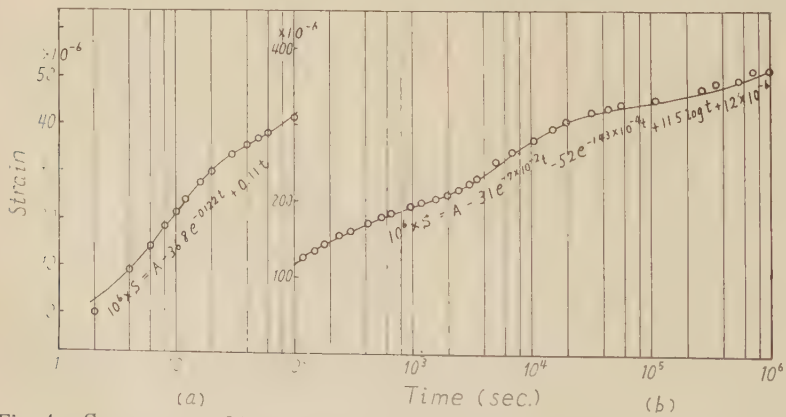

Fig. 4. Creep curves of longitudinal direction for biotite granite, (a) short period test for Kitashirakawa granite under load of 945 kg/cm², (b) long period test for Shodoshima granite under load of 1170 kg/cm².

observed values are materially affected, was kept within $\pm 0.2^{\circ}C$ in the axial direction and $\pm 0.5^{\circ}C$ in the transverse direction. The results are described separately in two directions.

In Fig. 4(a) and (b) show the creep curves for the longitudinal direction in two periods plotted on semilogarithmic papers, respectively. The empirical formulae derived from these two curves are

$$S = A + A'e^{-\alpha t} + Ct,$$
$$S = A_0 + A_1 e^{-\alpha_1 t} + A_2 e^{-\alpha_2 t} + B \log t + Ct.$$

Let us assume that the term Ct of the former equation can be replaced by the second and later terms of the later equation, as it was determined in the short period 1 to 10^2 seconds. Then the full equation can be described in the form

$$S = A_0 + A_1 e^{-\alpha_1 t} + A_2 e^{-\alpha_2 t} + A_3 e^{-\alpha_3 t} + B \log t + Ct$$

putting together, where the reciprocals of α_1, α_2, α_3 express the retardation times of Kelvin's model of the order of 10, 10^2, 10^4 seconds respectively.

The results of lateral direction in short and long periods are shown in Fig. 5. These formulae are

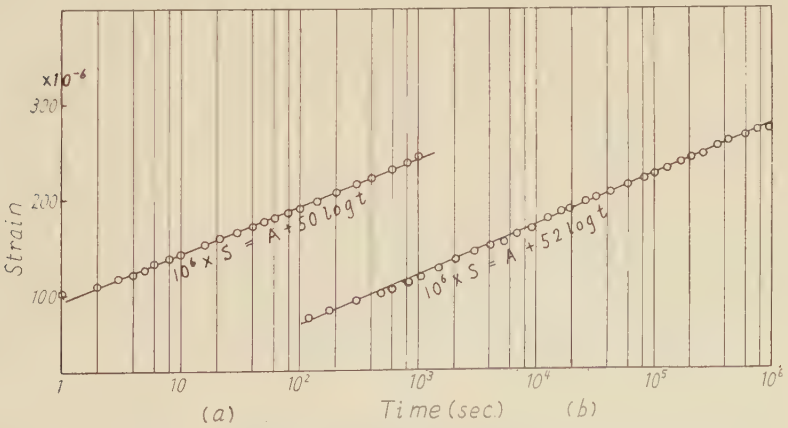

Fig. 5. Creep curves of lateral direction for Shōdoshima biotite granite under load of 1170 kg/cm², (a) short period test, (b) long period test.

$$S = A + B \log t,$$
$$S = A + B \log t + Ct,$$

respectively. Putting together, the empirical formula of the creep for the

direction perpendicular to the applied force is given as follows

$$S = A + B \log t + Ct.$$

This formula entirely coincides with the formula given by Griggs and others[3]. The formula for the longitudinal direction, does not concur with theirs, but has the different expression with the lateral one. While the curves shown in Fig. 5 are approximately linear, the ones in Fig. 4 somewhat indicate the unduration.

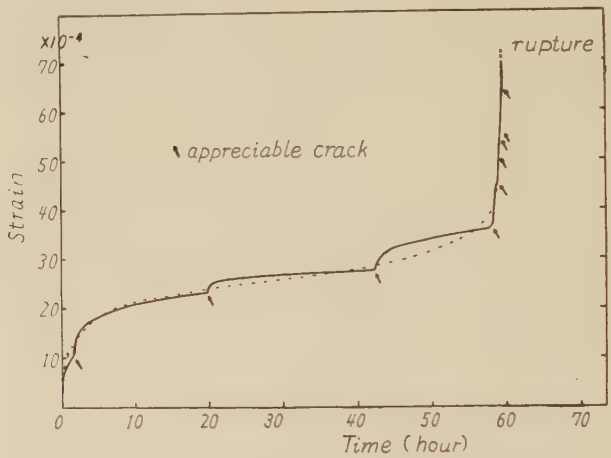

Fig. 6. Creep and rupture for Shodoshima biotite granite, observed in lateral direction. Solid line denotes the observed value, and the dotted line denotes the normal creep curve.

An example of rupture caused by creep is shown in Fig. 6. This curve has the same three stages as the metals and other materials have. However, it was observed that the deformation did not continue smoothly, but the appreciable cracks occurred in succession on the way of creep, and finally reached to rupture with continual crack.

ACKNOWLEDGEMENT

The writer wishes to express his sincere thanks to Prof. K. Sassa of the Geophysical Institute, Kyoto University, for his cordinal instructions and encouragements.

REFERENCES

1) Zisman W. A., "Yong's modulus and Poisson's ratio with reference to geophysical applications." Proc. Nat. Acad. Sci., **19** (1933) 653.

2) Bridgman P. W., "Volume change in the plastic stages of simple compression." J. App. Phys., **20** (1949) 1241.

3) Griggs D. T., "Creep of rocks." J. Geol., **47** (1939) 225.
Lomnitz C., "Creep measurements in igneous rocks." J. Geol., **64** (1956) 473.

DISASTER PREVENTION RESEARCH INSTITUTE
KYOTO UNIVERSITY
BULLETIN

Bulletin No. 43 February, 1961

On the Strength Distribution of the Earth's Crust and the Upper Mantle, and the Distribution of the Great Earthquakes with Depth

By

Shogo MATSUSHIMA

Geophysical Institute, Faculty of Science, Kyoto University
(Communicated By Prof. K. Sassa)

On the Strength Distribution of the Earth's Crust and the Upper Mantle, and the Distribution of the Great Earthquakes with Depth

By

Shogo MATSUSHIMA

Geophysical Institute, Faculty of Science, Kyoto University
(Communicated By Prof. K. Sassa)

Abstract

It seems that the strength of the earth's crust and upper mantle has some relation with the magnitude of the earthquakes. In this paper, we try to estimate the strength distribution of the earth's crust and upper mantle from the experimental results carried out under high pressure and temperature.

We compare the above result with the distribution of the great earthquakes with depth, which occurred in and near Japan in 1926–1956. It seems that the both are fairly resemble each other in tendency.

Introduction

The geographycal distribution of the earthquakes has been studied in detail and well known as the seismic zone. On the other hand, noticing the distribution with depth, it will be seen that the distribution of the hypocentres of the great earthquakes with depth has the considerably conspicious feature, even of the shallow focus earthquakes within the depth of 100 k.m..

The abundant problems pertaining to the mechanism of the earthquakes will not be able to be proved till we get the sufficient knowledges for the time and space distribution of the forces in the crust and upper mantle, and for the constitution of there. Nevertheless, it will be the reasonable inference that the magnitude of the earthquakes will depend on the mechanical strength of the hypocentre, and it will not be the futile attempt to estimate the strength of the crust and upper mantle.

Because the large amount of energy should be stored in the region where the strength is large, and the less do in the region of the small strength.

In this paper, we try to estimate the distribution of the strength of the crust and upper mantle with depth by the experimental results on the strength of rocks under high pressure and temperature. Then we consider the distribution of the great earthquakes with depth, which occurred in and near Japan, with references to the above estimated results.

Pressure, Temperature and Constituents of the Crust and Upper Mantle

The strength of rocks is strongly affected by confining pressure and temperature, and these effects are different for rocks of different types. Then we must know the pressure and temperature distributions and the constituent rocks of the crust and upper mantle to evaluate the strength there.

Of the pressure distribution, we have had the sufficient knowledge for our purposes[1]. This is shown in Fig. 1.

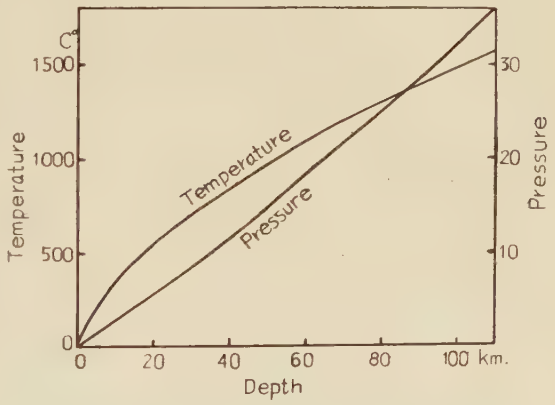

Fig. 1. Pressure and temperature distribution in the earth's crust and the upper mantle.

Of the temperature distribution, on the other hand, the various estimations have been presented by many authors[1] and we have had no definitive distribution. These distribution curves, however, are approximately coincident in tendeny and magnitude one another. So we will take the average of these curves as the temperature distribution of the crust and upper mantle. This curve is shown in Fig. 1, which will not give so large error for the temperature within the superfiical layers of the earth.

Next we consider the constituent rocks of the crust and upper mantle. The boundary between the crust and the upper mantle shows very re-

markable discontinuity and has been well known as Mohorovicic discontinuity. From the seismological and geological evidences, it has been clarified that the crust is composed of relatively acidic rocks such as granite and that the upper mantle is done of basic rocks such as dunite or so. In the following discussions, we assume the simplest model of the crust and upper mantle, that is, the crust is composed of granite and the main constituent rocks of the upper mantle are dunite or similar rocks.

Variation of the Strength of Rocks with Confining Pressure

In the previous paper[2], we studied the variation of strength with various confining pressures for Kitashirakawa granite. This and subsequently obtained results are shown in Fig. 2. The empirical formula of the strength versus pressure for this rock is given

$$P_p^* = P_0^* (k \cdot p + 1)^{1/2},$$

where P_0^*, P_p^* are the strength at an atmospheric pressure and confining pressure of p k.b., respectively, and k is the characteristic constant for the rock.

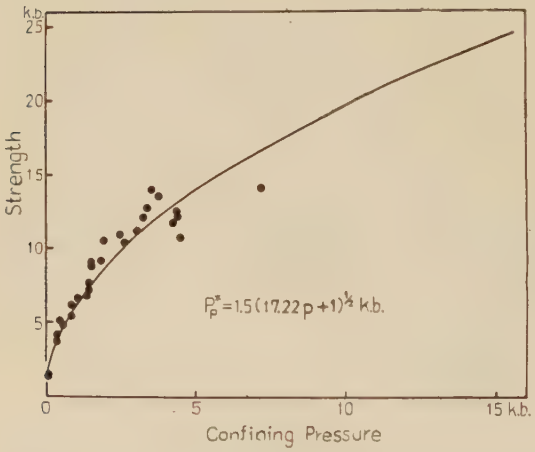

Fig. 2. Variation of strength of granite with confining pressure at room temperature.

Here we assume that the above formula holds in all types of silicate rocks, though we can not assert strongly this assumption for the accumulation of the experimental results are not sufficient to determine the plausible formula.

As k and P_0^* for granite, we use the experimentally derived values for Kitashirakawa granite, that is, $k=17.22$ (k.b.)$^{-1}$ and $P_0^*=1.5$ k.b.. The average value of P_0^*, listed in "Handbook of Physical Constants[3]", is 1.48 k.b., so that the above value seems to be appropriate.

Next, we must find the values of k and P_0^* for dunitic rocks. There has been no experimentally derived value of k for this sort of rocks, so we will determine this value from the values of P_0^* and P_p^* (strength under certain confining pressure). In "Handbook of Physical Constants", average value of P_0^* for gabbro, diabase, etc. is listed. This is 1.8 k.b.. The strength of gabbro, basalt and diabase, which we obtained, was about 2.0 k.b.. Then we put $P_0^*=2.0$ k.b. for dunitic rocks as the approximate value. D. T. Griggs et al.[4] has observed the stress-strain relations for dunite under 5.0 k.b. confining pressure. In their report, the strength of dunite at room temperature is shown as about 21 k.b.. From the values of P_0^* and P_5^*, we can obtain the value of $k=22.0$ (k.b.)$^{-1}$ for dunitic rocks.

In Table 1, the strength of granitic and dunitic rocks under pressures corresponding to the various depths from the earth's surface, which is calculated by the above mentioned way, is listed.

Table 1. Strength of granite and dunitic rocks under pressures corresponding to the depths from the earth's surface.

Depth	Pressure	Strength	
		Granite	Dunitic rocks
k.m.	k.b.	k.b.	k.b.
0	0	1.5	2.0
5	1.3	7.3	10.9
10	2.7	10.3	15.5
20	5.5	14.7	22.1
30	8.5	18.2	27.4
40	11.5	21.2	31.9
50	15.0	24.2	36.4
60	18.5	26.8	40.4
80	25.5	31.5	47.4
100	32.0	35.3	53.1

Reduction of the Strength caused by the Elevated Temperature

It has been currently accepted that the strength of rocks is considerably reduced by the elevated temperature, but it has not been made clear quantitatively how much amount of reduction is brought about.

Recently, D. T. Griggs et al., as above mentioned, has experimentally investigated the stress-strain relations for various sorts of rocks at the temperatures up to 800°C and pressures of 5.0 k.b..

We will quote their results and picture again the temperature-strength relations for granite and dunite. This is shown in Fig. 3. As seen in this figure, it seems that the linear relation exists between the strength and temperature for granite, and exponentially decreasing relation for dunite. Here we assume that the following formula can be adopted for granite as the empirical one and that this formula is held all over the pressure range, that is,

$$ {}_{T}P_{p}^{*} = {}_{0}P_{p}^{*}(1 - T/1100), $$

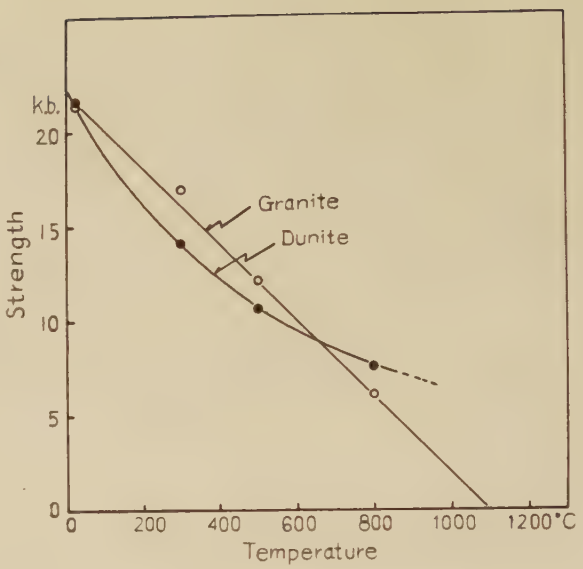

Fig. 3. Variation of strength of granite and dunite with temperature, at 5.0 k.b confining pressure (after D. T. Griggs et al.).

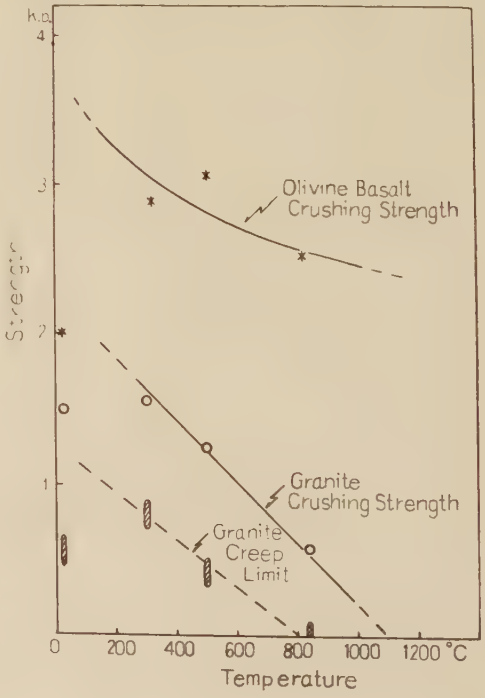

Fig. 4. Variation of strength of granite and olivine basalt with temperature, at an atmospheric pressure. The upper and lower solid curves show the crushing strength of olivine basalt and granite respectively, and the dotted curve shows the estimated creep limit of granite.

where ${}_TP_p^*$, ${}_0P_p^*$ are the strength at temperatures of T°C and 0°C under confining pressure p k.b., respectively.

The temperature-strength relation for dunite is not given in such a simple form as for granite, then we evaluate the strength reduction graphycally from the curve in Fig. 3. That is, the strength at T°C, p k.b. is given as the product of the strength at 0°C, p k.b., which was estimated in the former section, by the ratio of strength at T°C and 0°C under 5 k.b.. This is given formally as follows,

$$ {}_TP_p^* = {}_0P_p^* ({}_TP_5^* / {}_0P_5^*). $$

In addition to the above argument, we refer to the temperature de-

Fig. 5. Strength distribution in the earth's crust and the upper mantle.

Table 2. Strength of the earth's crust and the upper mantle taking account of the temperature and pressure.

Depth	Pressure	Temperature	Strength	
			Granite	Dunitic rocks
k.m.	k.b.	°C	k.b.	k.b.
0	0	0	1.5	2.0
5	1.3	200	5.95	8.0
10	2.7	350	7.05	9.15
20	5.5	550	7.35	10.15
30	8.5	700	6.6	10.6
40	11.5	850	4.8	10.15
50	15.0	980	2.6	9.9
60	18.5	1100	0.0	9.55
80	25.5	1300		8.2
100	32.0	1500		6.3

pendence of strength of granite and olivine basalt in our experiments at an atmospheric pressure[5]. This is shown in Fig. 4. This results will suggest that the above treatment is not so unreasonable.

Thus we can estimate the strength distribution within the earth's crust and upper mantle taking account of the temperature and pressure of there. This is shown in Table 2 and Fig. 5.

Creep Limit of the Earth's Crust

If the earthquakes are caused by forces generated suddenly[6], the crushing (or yield) strength obtained in the foregoing sections should give the actual one in the crust and upper mantle. On the other hand, if the earthquakes are caused by forces accumulated gradually, the above obtained strength does not give the real strength. The stress is released constantly by the flow or the creep in such a rather static process, and rupture must be occurred by further lower stress than the crushing strength. Then we must estimate the creep limit in the crust and upper mantle.

For this problem, we scarcely have any experimental data to be available. Nevertheless, we will try to estimate the rather qualititative distribution of the creep limit within the earth's crust, using the very rough-and-ready presumptions. Creep limit can be obtained only by the very long period tests, but such experiments are considerably difficult to be carried out sufficiently, especially at high pressure and temperature. Thus we assume that the creep limit corresponds to the point at which the curve of the rate of creep versus stress comes in contact asymptotically with the stress axis.

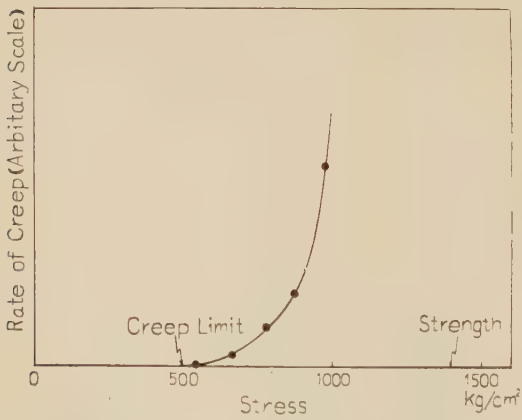

Fig. 6. Relation between the rate of creep and stress, and the estimated creep limit for Kitashirakawa granite, at an atmospheric pressure and room temperature.

In Fig. 6, the curve of the rate of creep versus stress for Kitashirakawa granite at an atmospheric pressure and room temperature is shown. Fig. 7 shows the variation of creep limit with confining pressures for Kitashirakawa granite obtained by the above method. The dotted line in Fig. 4 shows the relation between creep limit and temperature at an atmospheric pressure for this granite.

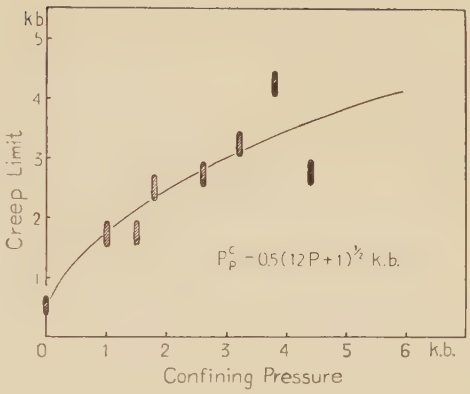

Fig. 7. Variation of the estimated creep limit with confining pressure for Kitashrakawa granite, at room temperature.

It will be seen from the figures that the empirical formulas of the variation of creep limit with confining pressure and temperature have the same form as the one of crushing (or yield) strength. That is,

$$P_p^c = P_0^c (k \cdot p + 1)^{1/2},$$

and

$${}_T P_p^c = {}_0 P_p^c (1 - T/800),$$

where the index c instead of * appeared in crushing (or yield) strength denotes the creep limit.

Using the results shown in Fig. 7 and Fig. 4, we can roughly estimate the creep limit of the earth's crust. The result is shown in Fig. 8. Of course, the quantitatively plausible result must be recomputed after the accurate tests of creep under high pressure and temperature.

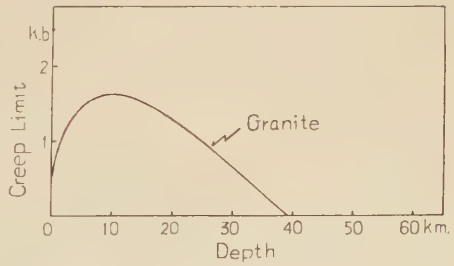

Fig. 8. Distribution of the creep limit with depth in the crust.

Distribution of the Great Earthquakes with Depth

Let us consider the distribution of hypocentres of the great earthquakes with depth. We pick up the shallow focus earthquakes, the magnitudes of which are larger than 6.3, which occurred in and near

Japan from 1926 to 1956. The data are listed in "The Seismological Bulletin of the Japan Meteorological Agency, Supplementary Volume No. 1[7]".

We consider the seimic zone in Japan dividing into two parts by Fuji Volcanic Belt. In North-eastern Japan, the earthquakes have occurred mainly under the Pacific Ocean along the coast and these hypocentres are rather deep in general. On the other hand, in South-western Japan, the earthquakes have occurred mainly under the land and the depth of hypocentres is shallow. This means, that is to say, that the earthquakes have occurred in the upper mantle in North-eastern Japan and in the

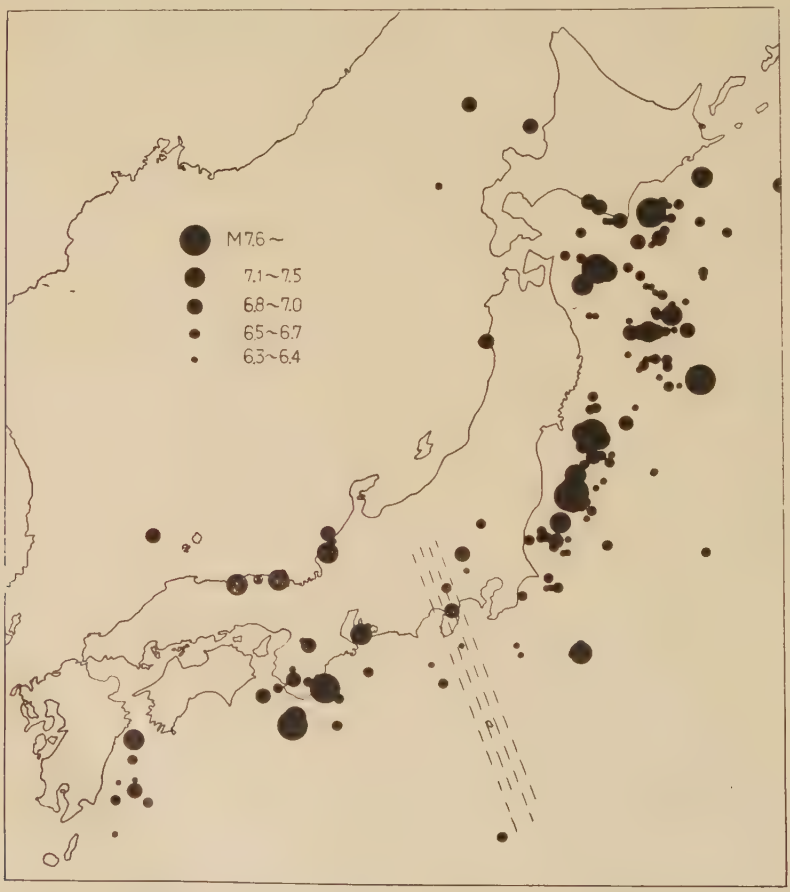

Fig. 9. Geographycal distribution of the great earthquakes which occurred in and near Japan in 1926-1956.

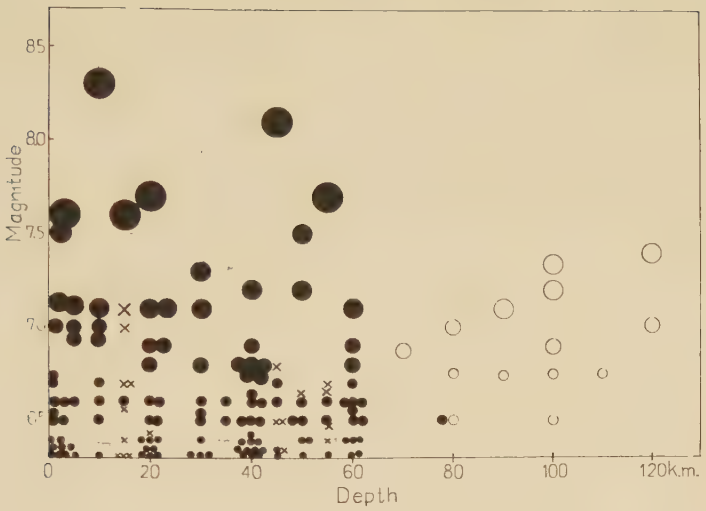

Fig. 10(a).

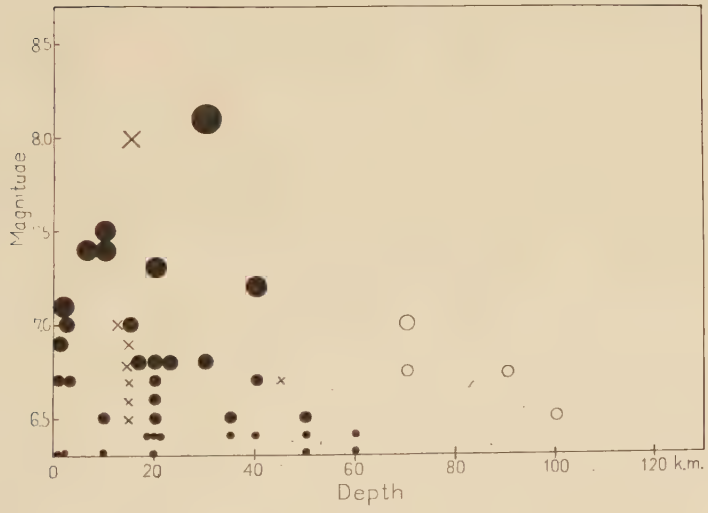

Fig. 10(b).

Fig. 10. Distribution of the great earthquakes with depth, which occurred in and near Japth, in 1926–1956. (a) In North-eastern Japan, and (b) in South-western Japan. The full circles and empty circles express th magnitudes determined by the Japan Meteor. Agency and by B. Gutenberg respectively, and the X marks express the earthquakes, the depths of which are not determined definitely.

crust in South-western Japan. Fig. 9 shows the geographycal distribution of epicentres in and near Japan. Fig. 10(a), (b) show the distributions of hypocentres in North-eastern and South-western Japan respectively.

Comparing Fig. 10 with Fig. 5, it seems that the tendencies of both distributions with depth are fairly alike to each other. Fig. 10(a) corresponds to the upper curve in Fig. 5, strength of dunitic rocks, and Fig. 10(b) to the lower curve, strength of granite.

If the energy of earthquake is chosen as the vertical coordinate, the curves in Fig. 10 show the rather sharp maximum. This will mean that the concept of the "earthquake volume[8]" is very available, because the earthquake which occurs in the region with great strength should have the much larger volume than the one which occurs in the region with less strength.

Acknowledgement

The writer wishes to express his sincere thanks to Prof. K. Sassa of the Geophysical Institute, Kyoto University, for his continual encouragements.

References

1) B. Gutenberg, "Internal constitution of the Earth.", (1949).
2) S. Matsushima, "On the deformation and fracture of granite under high confining pressure.", Disaster Prevention Research Inst. Bull. Kyoto Univ. No. **36** (1960).
3) F. Birch, "Handbook of Physical Constants.", Geol. Soc. Amer. Sp. No. **36** (1942).
4) D. T. Griggs et. al., "Deformation of rocks at 500° to 800°C.", Geol. Soc. Amer. Mem. **79**, 39–104 (1960).
5) S. Matsushima, unpublished.
6) T. Matsuzawa, "Feldtheorie der Erdbeben." Bull. Earthquake Res. Inst. Tokyo Univ. **31**, 179–201 (1953).
7) Japan Meteorological Agency, "Catalogue of major earthquakes which occurred in and near Japan.", Seism. Bull. Jap. Meteor. Agency Supple. Vol. No. **1** (1958).
8) C. Tsuboi, "On seismic activities in and near Japan.", Contributions in Geophysics 87–112 (1958).

DISASTER PREVENTION RESEARCH INSTITUTE
KYOTO UNIVERSITY
BULLETINS

Bulletin No. 44 February, 1961

Observational Study on Microseisms (Part 1)

By

Kennosuke OKANO

Abuyama Seismological Observatory, Faculty of Science, Kyoto University
(Communicated by Prof. K. Sassa)

Observational Study on Microseisms (Part 1)

By

Kennosuke Okano

Abuyama Seismological Observatory, Faculty of Science, Kyoto University
(Communicated by Prof. K. Sassa)

1. Introduction

For many years microseisms have been investigated by numerous scholars. But there is still lack of general agreement about the origin, the mechanism of generation and the other properties of microseisms. It is the object of this paper to solve these problems.

It has been well known that microseismic storms appear on seismograms during the passage of typhoons or cyclones. The view has often been expressed that microseisms are associated with atmospheric depressions, but recently most of investigators support the opinion that sea waves generate microseismic waves in the solid crust.

Bernard (1937) et al. found that the period of microseismic waves is about half that of the generating sea waves. Longuet-Higgins (1950) presented a significant theory for the effect at the ocean bottom of standing sea waves produced by the interference between two similar wave trains travelling in opposit directions. Such a condition as Longuet-Higgins pointed out is expected to be attained at the neighbourhood of the atmospheric low pressure center or the coast, and hence the opinion on the location of the origin of microseisms is divided into two. Although at present his theory seems most attractive, no evidence of existence of standing sea waves is observed.

From the case studies of microseismic storms, it is known that the occurrence of the peak in microseismic activity observed at an observing station does not coincide with the moment when a typhoon or cyclon approaches to the station as closely as possible, but rather is delayed, and also the occurrence of the maximum amplitude at each station seems to propagate with the velocity similar to that of progress of the typhoon

or cyclone. To explain the phenomenon some of seismologists considered that the generation of microseisms is due to the swells propagated from a storm area to the coasts, and they investigated the relation between microseisms and swells. Sakata (1940) presented an excellent paper on this subject. Wadati et al. also were led to the same consideration from the existence of close relation between microseisms and swells, as observed at some stations in Japan. Santo (1959) also investigated in detail the problem by the observational data obtained at many stations in Japan during I.G.Y. period and confirmed that consideration.

One of the most effective means to investigate the origin of microseisms is a determination of arrival directions of microseismic waves. In spite of a great deal of efforts of seismologists, they did not reach the satisfactory conclusion to that investigation because of their unsuitable methods. Therefore the writer did not follow their methods, namely, the tripartite and the Lee's method, and he studied the arrival directions from the analysis of orbital motions of the earth's particles by means of vector seismographs. It became evident from these observations that the arrival directions of microseismic waves are associated with not the positions of atmospheric low pressure centers, but the coasts near the observing station. And a comprehension of the other properties of microseisms was also considerably gained, and these results appear to support the above-mentioned consideration as already pointed by the writer (1959) and (1960).

2. General features of microseismic waves observed at the Abuyama Seismological Observatory

The writer will at first refer to the general features of microseismic waves at the Observatory based upon the information deduced from the data on the waves by the precise observation during I.G.Y. period. The Abuyama Seismological Observatory is located at the position with coordinates : 34°52′N and 135°34′E, and founded on palaeozoic system.

Good care was taken in making selection of the constants of seismographs. With due consideration for ground movements with periods of 2 to 8 sec. and with amplitudes up to 7 microns, the constants of seismographs were arranged as follows.

Constants of seismographs.

Component	T_1 (sec)	T_2 (sec)	h_1	h_2	$V_{max.}$
UD	4.00	10.00	0.75	1.00	4,100
NS	4.00	10.00	0.75	1.00	3,500
EW	4.00	10.00	0.75	1.00	3,400

T_1 : Period of pendulum
T_2 : Period of galvanometer
h_1 : Damping constant of pendulum
h_2 : Damping constant of galvanometer
$V_{max.}$: Maximum magnification

Wave type

From most observations hitherto made in the world it was reported that the three components of microseismic waves possess nearly same amplitudes, and hence it has been widely accepted that microseismic waves are the Rayleigh waves. Some of seismologists, however, have considered them to be of the Love type, the Rayleigh type combined with the Love type or the Rayleigh type combined with the standing wave. The micro-

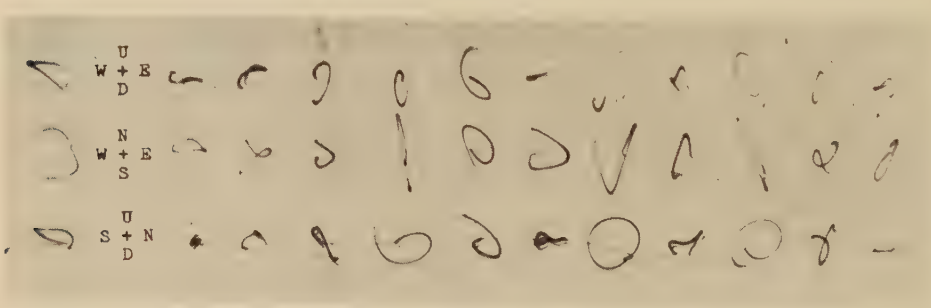

Fig. 1(1).

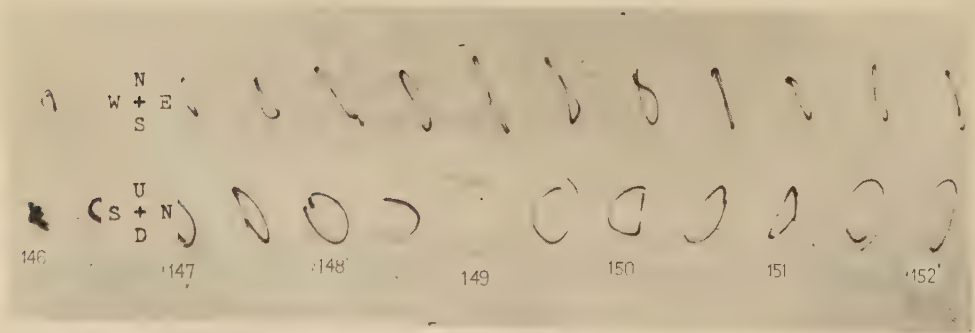

Fig. 1(2).

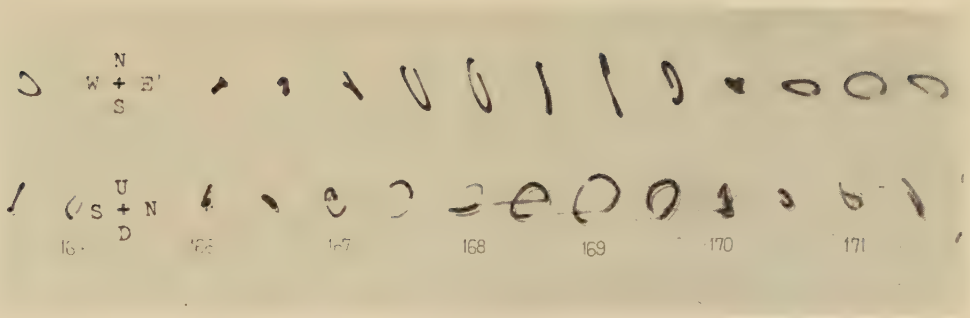

Fig. 1(3).
Fig. 1. Examples of seismograms.

seismic waves observed at the Abuyama Seismological Observatory appear to be of the Rayleigh type, as shown in Fig. 1, which is the example of seismograms obtained by the vector seismographs. In fact the vector seismographs recorded frequently the waves of the typical Rayleigh type, but on the other hand, recorded little the Love or standing waves, apart from a few waves regarded as apparent Love waves or standing waves produced by superposition of several waves propagated from various directions.

Amplitude

The ground amplitude and the wave period by which the writer will investigate microseisms in following pages were measured according to the Instruction Manual of Seismology for I.G.Y.

Fig. 2 shows the frequency distributions of ground amplitudes in

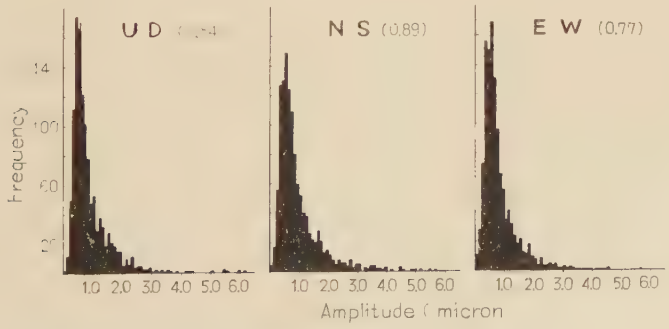

Fig. 2. Frequency distributions of the amplitude of microseismic waves. The numerals show mean values of amplitudes in each component.

three components. The numerals in the figures give the mean values of amplitudes in each component. The value in vertical component is similar to that in NS-component, whereas the value in EW-component is somewhat less than in NS-component. This tendency of amplitude is observable also on the other seismographs of the Observatory. If the microseismic waves are of the Rayleigh type and come from the coasts near the Observatory, this tendency should be natural and resanable, as there is no coast close to the Observatory in its easterly and westerly regions, but in the northerly region the Sea of Japan and in the southerly region the Pacific Ocean are comparatively close to the Observatory.

Period

Frequency distributions of wave periods are shown in Fig. 3. The numerals in the figures give the mean values of periods in each component. They are approximately equal to half the mean period (8.2 sec.) of about four thousand sea waves in the westerly Pacific Ocean observed by L. Paris. There are two groups with the respective maximum of frequency in the distributions. The group whose peak is at the period of 4 sec. is what you call microseisms. Another group with the peak of 2 sec. has been observed at various stations during the passage of cold fronts. Lynch (1952) studied this 2-second microseisms observed at New York by using the tripartite observation. The results obtained by his investigation indicate that the Great Lake is probably the source of generation of the 2-second microseisms. This sort of microseisms will be referred afterwards.

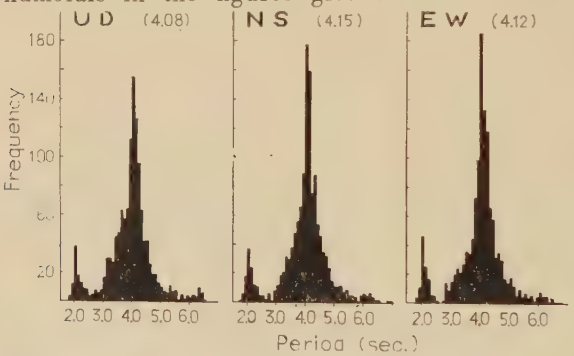

Fig. 3. Frequency distributions of the period of microseismic waves. The numerals show mean values of periods in each component.

3. Variation of the amplitude and the period of microseismic waves during microseismic storms

When typhoons or cyclones are passing near an observatory, micro-

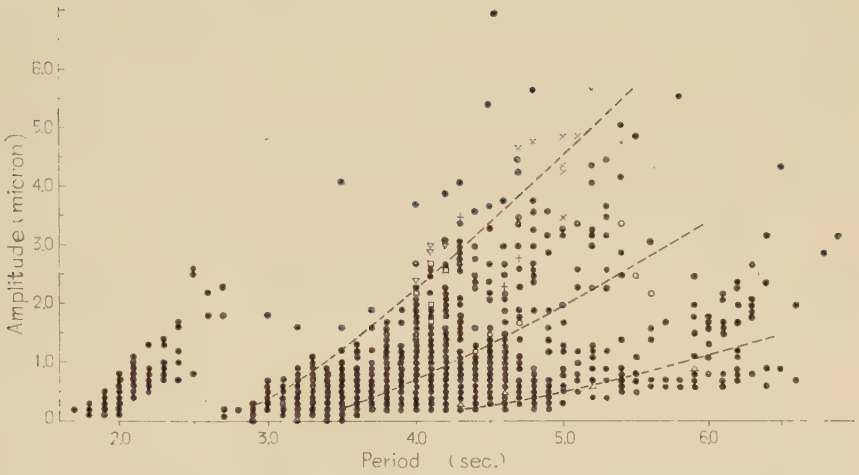

Fig. 4. Ralation between amplitudes and periods of microseismic waves.

seismic waves grow in amplitude and their period changes in the wide range. There are many reports of these variations, but they gave the explanation only for the case of the individual storm. The writer studied these variation in detail during I.G.Y. period and could give the plausible explanation of them. Since microseismic waves resemble in appearance in three components, hereafter they will be stated only in NS-component. Fig. 4 shows the relation between ground amplitudes and wave periods of microseisms. The points are scattered, but they have the tendency that the amplitude is larger for a longer period as pointed out by most of seismologists. To investigate this problem more precisely than made hitherto, the writer gave attention for the case of the individual storms. The symboles excepting the solid circles in Fig. 4 show the waves whose forms are remarkably regular in appearance in all seismogrms. They fall into three groups as indicated by the broken curves, that is, the group laid along the abscissa (A), near the middle region (B) and near the upper limit of the scattered points (C). Then the writer made a comparison between those three groups and the meteorological conditions corresponding to the times when the three groups were observed. Fig. 5, 6 and 7 are the weather charts corresponding to the times when the waves expressed by the symbols of open triangles (△), open circles and crosses were observ-

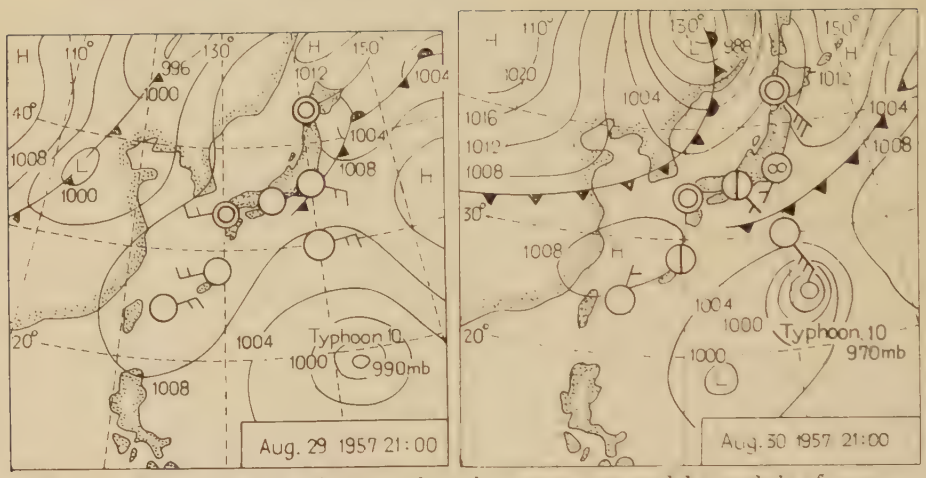

Fig. 5. Weather charts at the time when the waves expressed by symbols of open triangles (△) in Fig. 4 were observed.

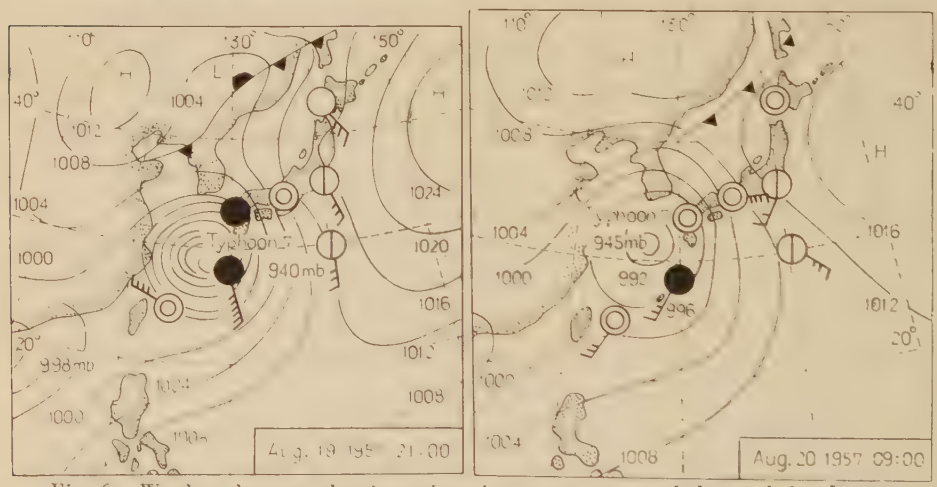

Fig. 6. Weather charts at the time when the waves expressed by symbols of open circles in Fig. 4 were observed.

ed respectively.

The first group (Fig. 5) was observed at the time when the typhoon was far distant from the Observatory, the second (Fig. 6) during its presence at a moderate distance and the third (Fig. 7) on its passing near the Observatory. From this fact the following inference may be drawn. Sea waves generated in a typhoon area have the wave height and period depending on the scale of typhoon. After leaving the generating area they

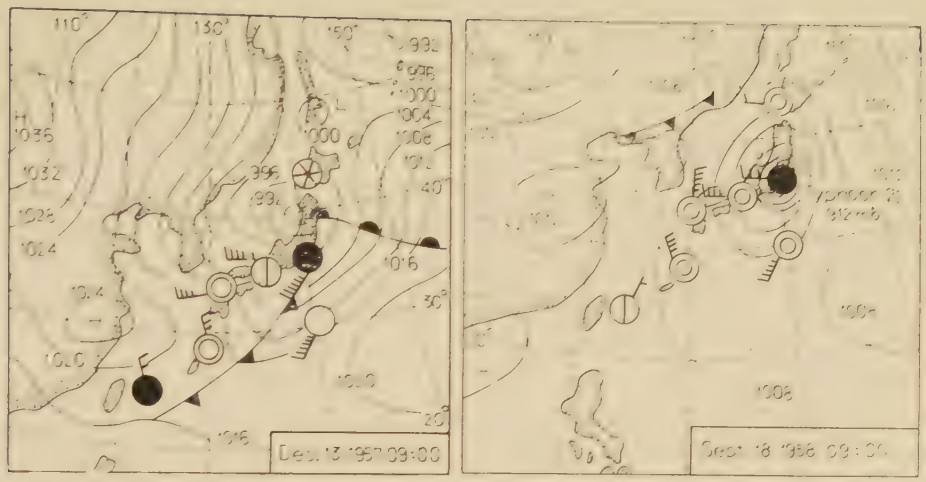

Fig. 7. Weather charts at the time when the waves expressed by symbols of crosses in Fig. 4 were observed.

propagate through the open sea to the coasts as the swell, and generate the microseismic waves in the neighbourhood of the coasts. The oceanography suggests that the swell decreases in height and its period becomes long with propagating of the swell. Therefore the amplitude and the period of microseismic waves depend on the scale of typhoon and the distance of propagation of the swell.

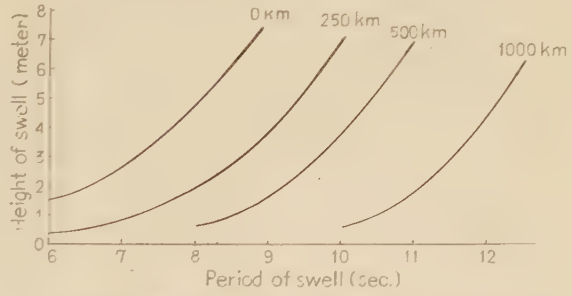

Fig. 8. Distance (km) from which swell comes as functions of height and period of swell at end of distance of decay.

Fig. 8 shows the relation between the wave height and the period of swells at the end of distance of decay given by Sverdrup and Munk (1947). A similarity between Fig. 4 and 8 is very noticeable and this is one of the probable proofs that the microseismic waves may be generated by the swell propagated from a typhoon area to the coasts. Accordingly the scale of typhoon (wind velocity in generating area, duration of wind and so on) and the decay distance of the swell, that is, the distance from the typhoon

to the coast near the station, may be estimated by using Fig. 4 from the amplitude and the period of the microseismic waves at the Observatory. There is another group of waves with the period of 2 sec. in Fig. 4. This group also has the tendency growing in amplitude with an increase of the wave period and the slopes by which those two groups are enveloped resemble closely. But the group with the period of 2 sec. is lacking in points along the abscissa. Accordingly it is supposed, that the 2-second microseisms are probably generated by the sea waves that the local winds due to the cold front produce in the neighbourhood of coasts, while the 4-second microseisms are generated by the swell propagated from the disturbance source far away from coasts.

Apart from the general discussion of the amplitude and the period of microseismic waves as described above, the writer will turn to the discussion on the individual character of them referred to the two kinds of storms, e.g., the cyclone in winter season and the typhoon in summer season.

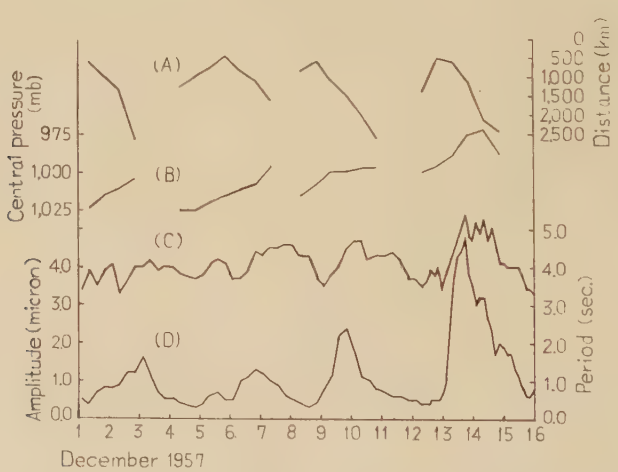

Fig. 9. Variations of distance from the Observatory to center of depression (A), central pressure of depression (B), periods (C) and amplitudes (D) of microseismic waves.

Fig. 9 shows the variation of the amplitude and the period of microseismic waves generated by cyclones in winter season, the central pressure of depression and the distance from the Observatory to the center of depression. And Fig. 10 shows the variation of microseismic waves

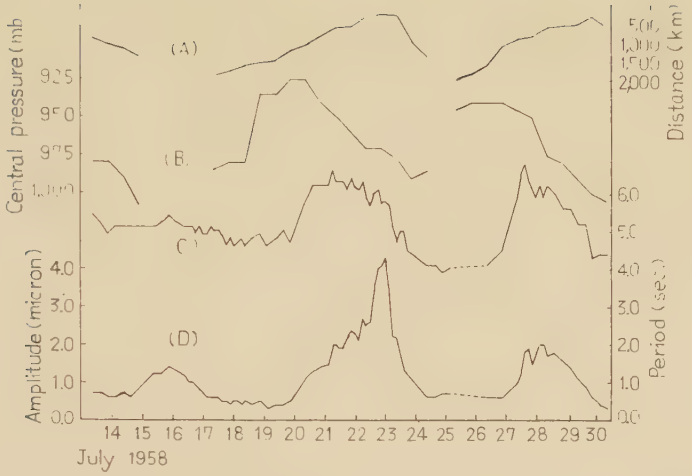

Fig. 10. Variations of distance from the Observatory to center of typhoon (A), central pressure of typhoon (B), periods (C) and amplitudes (D) of microseismic waves.

generated by typhoons in summer season, the central pressure of typhoon and the distance from the Observatory to the center of typhoon. It is marked by three noticeable differences between those two variations. The first is that the wave period in winter is shorter than in summer, that is to say, in winter the period variates centering around about four seconds, and in summer around about five seconds. The second is the marked growth of the amplitude against the gradual growth of the period in winter, while in summer the growth of the amplitude is similar to that of the period. The third is that the fall of growth of the amplitude is earlier than that of the period in winter and it is the opposite in summer. Since the seasonal wind stirs mainly the Sea of Japan in winter and the typhoon carries swells from a distance to the Pacific coasts in summer, the disturbance source in winter is not so far as the occasion of the typhoon. Accordingly the wave period in winter is shorter than in summer when the microseismic waves are produced by the swell with a longer distance of propagation, and it rises not frequently above five seconds. In winter season a low pressure produced in the south-westerly ocean off Japan passes over the Sea of Japan with developing its energy, as the variations of the central pressure of depressions and the distance from the Observatory to the center of depressions are indicated in Fig. 9, and hence

the microseismic amplitude increases rapidly and its period increases moderately by the decrease of the distance of propagation of swells and the development of the storm energy. When the disturbance source is going away, the amplitude decreases by the increase of the distance of propagation of swells and the period increases furthermore by the development of the storm energy and the increase of the distance of propagation of swells.

On the other hand the energy of a typhoon produced on the southerly Pacific Ocean far off Japan at first increases with the northward approaching of the typhoon as shown in Fig. 10. Therefore the microseismic waves generated by the typhoon grow gradually in amplitude and period owing to the increase of the storm energy which is expected to be powerfull enough to exceed the opposite effect due to the decrease of the distance of propagation of swells. As the typhoon approaches considerably near Japan, the energy begins to decrease. Then the wave period of microseisms also begins to decrease owing to the decrease of the energy of typhoon and the diminishing of the distance of propagation of swells, wherease the amplitude rises still owing to the diminishing of the distance of propagation of swells. It has been hitherto considered that the wave period of microseisms should be associated with the depth of the ocean where a disturbance source exists. But this offers a striking contrast with the result, as above mentioned, that the dependency of the wave period on the energy scale of the disturbance source and the distance from the disturbance source to the coast near the observation point is obviously proved from the writer's observation. As seen on the figures of Santo's paper (1959), the variations of the amplitude and the period of microseismic waves depend a little on the location of the observing station, though the amplitude is influenced by the vibrational properties of the ground and the period by the instrumental constants of seismographs. From this fact, it may be accepted that the observational data of most of stations located at least in Japan may yield the same results as the above one deduced from the observation of the Abuyama Seismological Observatory alone. The wave period of about 4 sec. which predominates in microseisms observed in most of stations of the world, has been frequently regarded as being due to the vibrational properties of the ground. However, if it is so, the fact that there is no maximum peak

of the amplitude corresponding to the period of 4 sec. can not be accepted without contradication (see Fig. 4).

4. Tripartite observation

The tripartite observation also was carried out during I.G.Y. period, but the satisfactory result was not brought. The positions of three points of observation are shown by A, B and C in Fig. 11. The instruments used in this observation are the vertical electromagnetic seismographs which were adjusted to the following constants : the period and the damping constant of pendulum are 4.0 sec. and 0.65, the period and the damping constant of galvanometer are 10.00 sec. and 1.00 and the magnification is about 4,000. As the side-lengths of the tripartite net were not sufficiently long notwithstanding the serious attention for the coincidence of constants of the three seismographs, the considerable error was unavoidable. The velocities of propagation and the arrival directions gained by the observation were scattered in the wide range. The relation between velocities and periods is shown in Fig. 12. About half of the numbers of velocities computed are above 3 km/sec, and they are excluded from Fig. 12 because they are of unreliable accuracy. The open circles show the values of the waves which have regular sinusoidal

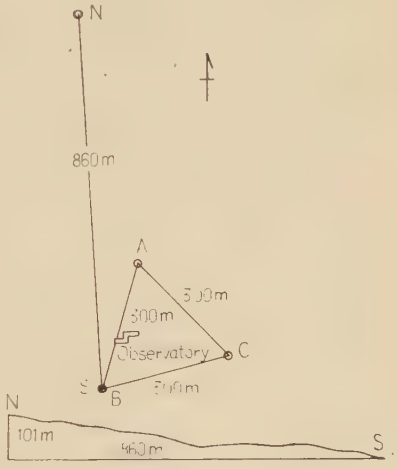

Fig. 11. Positions of observation.

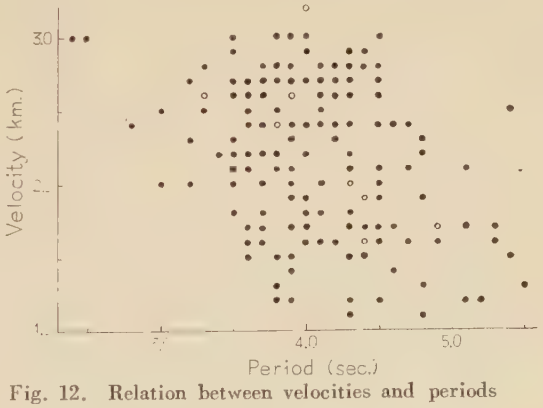

Fig. 12. Relation between velocities and periods of microseismic waves.

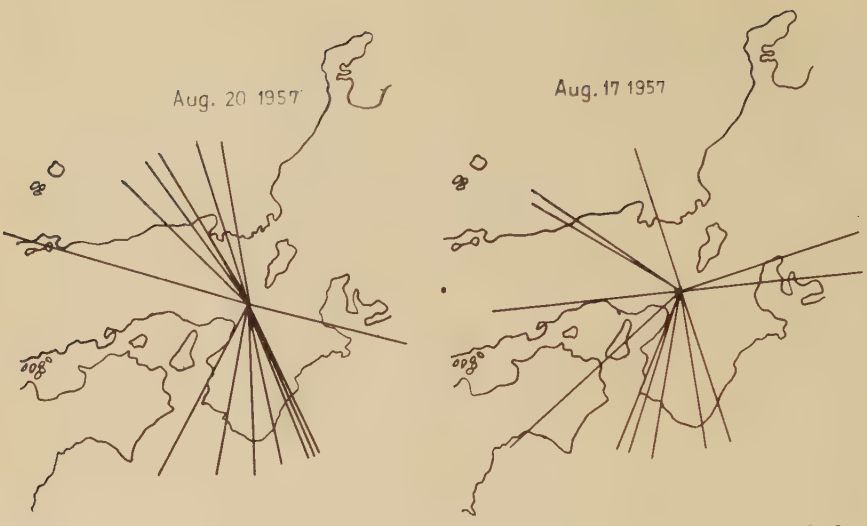

Fig. 13. Arrival directions of microseismic waves measured by tripartite method.

forms and whose periods are identical within 0.1 seonds at three points of observation. The arrival directions of individual waves are shown in Fig. 13. The directions are considerably scattered, but it may be seen that they point toward mainly the Sea of Japan and the Pacific Ocean. And we notice the tendency that the velocity increases with the decrease of the period. Ikegami and Kishinouye (1951) also indicated this tendency in their paper, but the subject does not bear further discussions because of the insufficient accuracy of the observation. As Don Leet (1949) discusses, many microseismic waves coming from various directions are superposed and the each phase of the superposed waves differs at different points of observation. Therefore it stands to reason, that the values of velocities and arrival directions of microseismic waves are scattered in wide range, if they are computed from the phases selected at will in the tripartite method. The writer can hardly avoid the conclusion from his observation that the tripartite measurement is not effective to the determination of the velocity and the arrival direction of microseismic waves.

5. Observation by vector seismographs

From the above mentioned observations it is a natural inference that the microseismic waves are generated by swells propagated from the dis-

turbance source to the coasts near the observing station. But this inference was not drawn from the direct observation of the origin of microseisms. It seems most important to the writer that the arrival direction of microseismic waves is clearly observed, if the best results are to be obtained for the investigation of the origin of microseisms. For this purpose, the writer adopted the analysis of the orbital motions of waves. The orbital motions analyzed hitherto by many seismologists were found to be so complicated that any usefull information might not be deduced. To overcome this difficulty the writer made newly vector seismographs. The seismograms recorded at the Abuyama Seismological Observatory were also considerably complicated, but their orbital motions brought out the various significant facts. The recording system of orbital motions is shown Fig. 14.

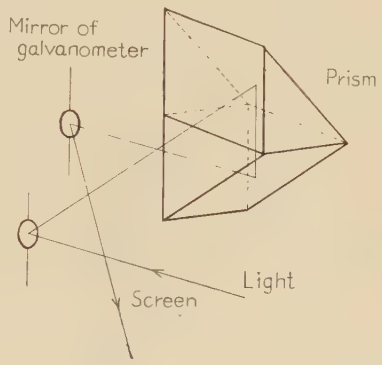

Fig. 14. Recording system of orbital motions.

The seismographs using for the routine observation during I.G.Y. period were turned to immediate account for this purpose, and hence the constants of seismographs are the same as on the occasion of the routine observation. Three orbital motions in UD-EW, UD-NS and EW-NS planes were simultaneously recorded on the same recording paper which runs during 1 sec. and stops during about 4 sec. Examples of the seismograms are shown in Fig. 1. The single wave of the Rayleigh type is frequently observed, but the Love wave or the standing wave is scarcely present. Only a few of the later two wave types may be considered to have been accidentally produced by the superposition of waves coming from various directions. On comparing the seismograms of ordinary seismgraphs with those obtained by vector seismographs, it may be readily understood that even if the vertical amplitude is small and the horizontal amplitude is considerable or even if they are the opposite on the ordinary seismographs, it is in consequence of the superposition of waves. Accordingly the microseismic waves are regarded as the Rayleigh waves in the following discussions.

Frequency distributions of arrival directions

The longer axis of the elliptical orbits of ground particles in the horizontal plane was used for the study on the direction of approach of microseismic waves by Donn (1954), Strobach (1955) and others, but their inferences are insufficient for lack of the records in the vertical component. The writer picked out such waves that their orbits are nearly linear in the horizontal plane and elliptic in the two vertical planes for making the frequency distributions of arrival directions. The distributions were directly drawn on the charts which were divided radially into thirty-six round the Observatory. Fig. 15 shows the distribution on the occasion of the microseisms generated by the typhoon No. 6 in 1959 and the travelling path of the typhoon is shown in Fig. 16.

Fig. 15(a).

Fig. 15(b).

Fig. 15(c).

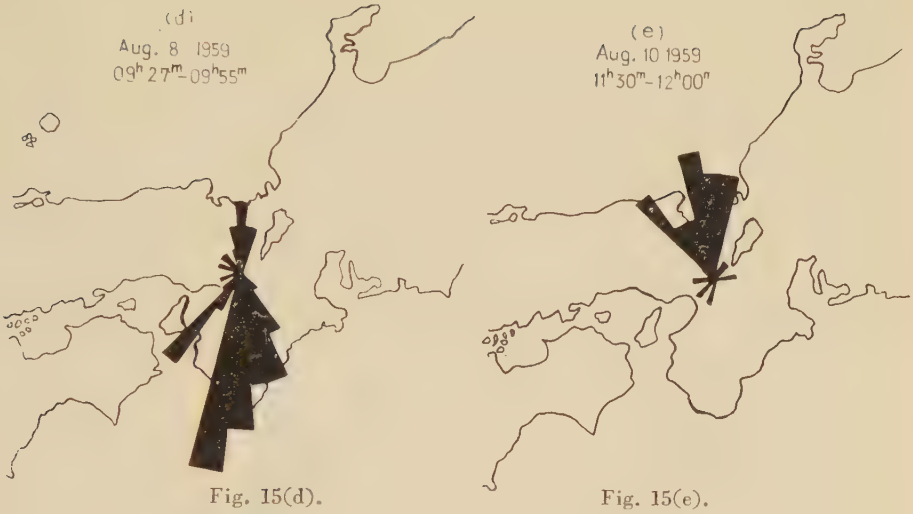

Fig. 15(d). Fig. 15(e).

Fig. 15. Frequency distributions of arrival directions of microseismic waves.

When the center of the typhoon was passing off the south-west coast of Kyushu the microseismic waves come to the Observatory mainly from the Pacific coasts as shown in (a), (b) and (c) of Fig. 15, and their directions of propagation do not point toward the center of the typhoon. As the typhoon did not yet stir up the Sea of Japan, the waves appearing to come from the coasts of the Sea of Japan are scarcely found. When the typhoon passed through Kyushu and went on off the east coast of Kyushu, the distribution is (d)

Fig. 16. Travelling path of the typhoon No. 6 in 1959.

of Fig. 15. It is similar in appearance to (a), (b) and (c), and the arrival directions do not point toward the center of the typhoon. When the center of the typhoon went on into the Pacific Ocean on Aug. 10, the distribution is shown in (e) of Fig. 15. In this case the Sea of Japan was stirred up and in the southern ocean off the Kii Peninsula swells went down considerably, and hence most of the arrival directions point toward the Sea of Japan. In winter season the seasonal winds blow hardly over the Sea of Japan and the surge is raised, whereas the Pacific Ocean remains comparatively calm. Therefore the frequency distributions of the propagating direction of microseismic waves pointed mostly toward

Fig. 17. Frequency distributions of arrival directions of microseismic waves.

the coasts of the Sea of Japan as shown in Fig. 17. When the disturbance sources are in the Sea of Japan, the prevailing direction of propagation is somewhat westerly shifted from the due north direction having the shortest distance of the wave propagation, and the frequency distribution is roughly in inverse proportion to the distance from the Observatory to the land shelf. When the disturbance sources exist in the Pacific Ocean, the prevailing direction is southerly, in whose direction the distance of propagation is longest, and the frequency has the tendency to decrease in proportion to the distance from the Observatory to the coast. This is

probably due to the position of the typhoon where the typhoon does not send swells to the south-easterly coast of the Kii Peninsula. The frequency distribution is found to be rather dense in the direction of Osaka Bay. These waves coming from that direction may be not considered to be generated at Osaka Bay separated almost from the open sea. They are supposed to be the waves propagated from Tosa Bay, because their periods are similar to that of the waves coming from the other directions. In the direction of Wakayama the frequency is minimum without any exception in all distributions. This is the most interesting fact, and if we take up a pursuit of this fact, the origin of microseisms may be found soon unexpectedly. The frequency distribution shown in Fig. 18 was obtained on the waves of the typical Rayleigh form selected among the all waves observed by vector seismographs. This figure also shows that all directions point toward the coasts with two exceptions and the frequency is minimum in the direction of Wakayama district.

Fig. 18. Frequency distribution of arrival directions of microseismic waves having the pure Rayleigh type.

6. Progression of microseismic waves and their wave velocity

For the purpose of investigating whether the waves of the Rayleigh type selected to make the frequency distributions are progressive or not, the observation by ordinary seismographs at the two points were carried out simultaneously with the observation by vector seismographs. The positions of the two points are shown by N and S in Fig. 11, and the instruments used for this purpose are NS-component seismgraphs with the same constants as those of the vector seismographs. The arrival directions were measured on the vector seismographs and the differences

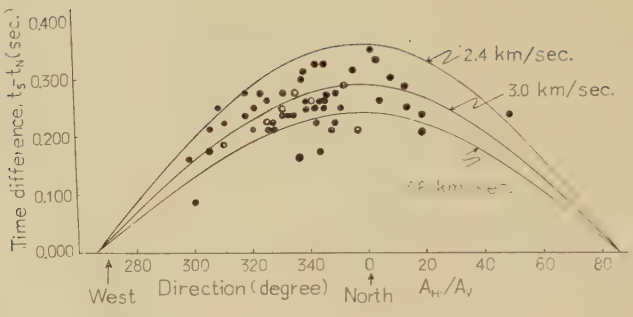

Fig. 19. Differences of the arrival times of microseismic waves at the two points of observation versus the arrival directions.

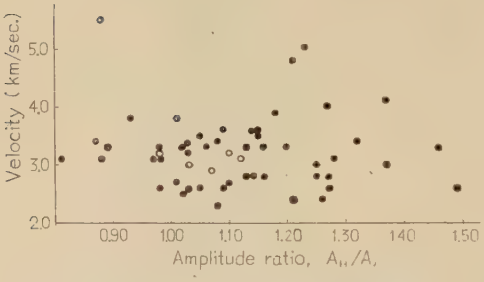

Fig. 20. Wave velocity as a function of the amplitude ratio of horizontal to vertical component.

of the arrival times of microseismic waves were read from the seismographs of the two points of observation. These relations are plotted in Fig. 19. The three sinusoidal curves in the figure show the relations between the arrival directions and the differences of arrival times at the two points computed for the waves of the velocities of 3.6 km/sec, 3.0 km/sec and 2.4 km/sec. The points are scattered. But they are on the whole distributed between the two curves showing the velocities of 2.4 km/sec and 3.6 km/sec, while the velocities observed by tripartite measurements are widely scattered. The open circles in the figure show only the waves with the orbital motions of the typical Rayleigh form. These points are plotted along the curve of 3.0 km/sec. Fig. 20 shows the wave velocity as a function of the amplitude ratio of horizontal to vertical component, which was deduced from the analysis of orbital motions. The wave velocity, especially for the waves of the typical Rayleigh form, is not scattered so much within the range of the ratio of 0.8 to 1.2. Accordingly the wave of the typical Rayleigh form may be considered to be the single wave, and there is little doubt that they progress with the velocity of about 3 km/sec.

7. Summary

1) The microseismic waves are undoubtedly of the Rayleigh type. Even though vertical ground motions are small as compared with horizontal motions, it is in consequence of superposition of waves coming from various directions.

2) Vertical ground motions are nearly equal in mean amplitude to horizontal motions. The mean amplitude in NS component is slightly larger than in EW component, because the Rayleigh waves approach from the northerly or southerly directions in which the origins of generation of microseisms exist.

3) The mean period of microseismic waves is nearly equal in each component, and it is about 4.1 sec. This period is approximately equal to half the mean period of swells in the westerly Pacific Ocean.

4) There are the predominant period of 2 sec. beside of 4 sec. in the frequency distribution of the period. The 2-second microseisms are associated with the local wind blowing at the time of the passage of cold fronts.

5) The amplitude and the period of microseismic waves depend on the scale of the disturbance source and the distance of propagation of swells from the disturbance source to the coast near the station.

6) The tripartite observation does not give the satisfactory results.

7) The wave velocity is about 3.0 km/sec.

8) The arrival directions observed by the vector seismgraphs indicate decidedly that the microseismic waves propagate from the coasts. The observation by vector seismographs is one of the most effective means to investigate the microseisms.

9) All results of the writer's investigations show that microseisms are generated by swells propagated from the disturbance source to the coasts near the observatory.

8. Acknowledgment

The writer wishes to express his gratitude to Professor Kenzo Sassa of Kyoto University for his invaluable advice and encouragement. The writer thanks Professor Haruo Miki of Kyoto University for his generous help.

References

1) Bernard, P. : Relations entre la houle sur la Côte du Moroc et l'agitation microseismique en Europe Occientale, C. R. Acad. Sci. Paris, 205 (1937), 163–165.
2) Donn, W. L. : Direction studies using microseisms ground-particle motion, Trans. Amer. Geophys. Union, 35 (1954), 821–832.
3) Ikegami, R. and F. Kishinouye : A study on the propagation of microseismic waves (Part 4), Bull. Earthq. Res. Inst., 29 (1951), 313–325.
4) Leet, L. Don : Discussion of tripartite microseismic measurements, Bull. Seis. Soc. Amer., 39 (1949), 249–255.
5) Longuet-Higgins, M. S. : A theory of the origin of microseisms, Phil. Trans. Roy. Soc. London, A257 (1950), 1–35.
6) Lynch, J. Joseph : The Great Lakes, a source of 2-second period microseisms, Trans. Amer. Geophys. Union, 33 (1952), 432–434.
7) Okano, K. : Microseisms observed at Abuyama Seismological Observatory (in Japanese), J. Seis. Soc. Japan, ser. 2, 12 (1959), 182–190.
8) Okano, K. : Direction of approach of microseisms observed by vector seismographs (in Japanese), J. Seis. Soc. Japan, ser. 2 (1960), 37–42.
9) Sakata, K. : Study on microseisms (in Japanese), Quart, J. Seismology, 10 (1940), 473–493.
10) Santo, T. A. : Investigations into microseisms using the observational data of many stations in Japan (Part 1), Bull. Earthq. Res. Inst., 37 (1959), 307–325.
11) Santo, T. A. : Investigations into microseisms by the observational data of many stations (Part 2), Bull. Earthq. Res. Inst., 37 (1959), 483–494.
12) Strobach, K. : Zum Studium der mikroseismischen Bodenunruhe in Hamburg, Z. f. Geophys., 21 (1955), 190–214.
13) Sverdrup H. U. and W. H. Munk : Wind, sea and swell : theory of relations for forecasting, Publ. Hydrog. Office, Wash., No. 601 (1947).
14) Wadati, K., U. Inoue and T. Hirono : The relationship between typhoon and microseiseisms (in Japanese), Quart. J. Seismology, 21 (1956), 3–11.

Publications of the Disaster Prevention Research Institute

The Disaster Prevention Research Institute publishes reports of the research results in the form of bulletins. Publications not out of print may be obtained free of charge upon request to the Director, Disaster Prevention Research Institute, Kyoto University, Kyoto, Japan.

Bulletins :

No. 1 On the Propagation of Flood Waves by Shoitiro Hayami, 1951.
No. 2 On the Effect of Sand Storm in Controlling the Mouth of the Kiku River by Tojiro Ishihara and Yuichi Iwagaki, 1952.
No. 3 Observation of Tidal Strain of the Earth (Part I) by Kenzo Sassa, Izuo Ozawa and Soji Yoshikawa. And Observation of Tidal Strain of the Earth by the Extensometer (Part II) by Izuo Ozawa, 1952.
No. 4 Earthquake Damages and Elastic Properties of the Ground by Ryo Tanabashi and Hatsuo Ishizaki, 1953.
No. 5 Some Studies on Beach Erosions by Shoitiro Hayami, Tojiro Ishihara and Yuichi Iwagaki, 1953.
No. 6 Study on Some Phenomena Foretelling the Occurrence of Destructive Earthquakes by Eiichi Nishimura, 1953.
No. 7 Vibration Problems of Skyscraper. Destructive Element of Seismic Waves for Structures by Ryo Tanabashi, Takuzi Kobori and Kiyoshi Kaneta, 1954.
No. 8 Studies on the Failure and the Settlement of Foundations by Sakurō Murayama, 1954.
No. 9 Experimental Studies on Meteorological Tsunamis Traveling up the Rivers and Canals in Osaka City by Shoitiro Hayami, Katsumasa Yano, Shohei Adachi and Hideaki Kunishi, 1955.
No.10 Fundamental Studies on the Runoff Analysis by Characteristics by Yuichi Iwagaki, 1955.
No.11 Fundamental Considerations on the Earthquake Resistant Properties of the Earth Dam by Motohiro Hatanaka, 1955.
No.12 The Effect of the Moisture Content on the Strength of an Alluvial Clay by Sakurō Murayama, Kōichi Akai and Tōru Shibata, 1955.
No.13 On Phenomena Forerunning Earthquakes by Kenzo Sassa and Eiichi Nishimura, 1956.
No.14 A Theoretical Study on Differential Settlements of Structures by Yoshitsura Yokoo and Kunio Yamagata, 1956.
No.15 Study on Elastic Strain of the Ground in Earth Tides by Izuo Ozawa, 1957.
No.16 Consideration on the Mechanism of Structural Cracking of Reinforced Concrete Buildings Due to Concrete Shrinkage by Yoshitsura Yokoo and S. Tsunoda. 1957.
No.17 On the Stress Analysis and the Stability Computation of Earth Embankments by Kōichi Akai, 1957.
No.18 On the Numerical Solutions of Harmonic, Biharmonic and Similar Equations by the Difference Method Not through Successive Approximations by Hatsuo Ishizaki, 1957.
No.19 On the Application of the Unit Hydrograph Method to Runoff Analysis for Rivers in Japan by Tojiro Ishihara and Akiharu Kanamaru, 1958.
No.20 Analysis of Statically Indeterminate Structures in the Ultimate State by Ryo Tanabashi, 1958.
No.21 The Propagation of Waves near Explosion and Fracture of Rock (I) by Soji Yoshikawa, 1958.
No.22 On the Second Volcanic Micro-Tremor at the Volcano Aso by Michiyasu Shima, 1958.
No.23 On the Observation of the Crustal Deformation and Meteorological Effect on It at Ide Observatory and On the Crustal Deformation Due to Full Water and Accumulating Sand in the Sabo-Dam by Michio Takada, 1958.
No.24 On the Character of Seepage Water and Their Effect on the Stability of Earth Embankments by Kōichi Akai, 1958.
No.25 On the Thermoelasticity in the Semi-infinite Elastic Soid by Michiyasu Shima, 1958.
No.26 On the Rheological Characters of Clay (Part 1) by Sakurō Murayama and Tōru

Shibata, 1958.

No.27 On the Observing Instruments and Tele-metrical Devices of Extensometers and Tiltmeters at Ide Observatory and On the Crustal Strain Accompanied by a Great Earthquake by Michio Takada, 1959.

No.28 On the Sensitivity of Clay by Shinichi Yamaguchi, 1959.

No.29 An Analysis of the Stable Cross Section of a Stream Channel by Yuichi Iwagaki and Yoshito Tsuchiya, 1959.

No.30 Variations of Wind Pressure against Structures in the Event of Typhoons by Hatsuo Ishizaki, 1959.

No.31 On the Possibility of the Metallic Transition of MgO Crystal at the Boundary of the Earth's Core by Tatsuhiko Wada, 1960.

No.32 Variation of the Elastic Wave Velocities of Rocks in the Process of Deformation and Fracture under High Pressure by Shogo Matsushima, 1960.

No.33 Basic Studies on Hydraulic Performances of Overflow Spillways and Diversion Weirs by Tojiro Ishihara, Yoshiaki Iwasa and Kazune Ihda, 1960.

No.34 Volcanic Micro-tremors at the Volcano Aso by Michiyasu Shima, 1960.

No.35 On the Safety of Structures Against Earthquakes by Ryo Tanabashi, 1960.

No.36 On the Flow and Fracture of Igneous Rocks and On the Deformation and Fracture of Granite under High Confining Pressure by Shogo Matsushima, 1960.

No.37 On the physical properties within the B-layer deduced from olivine-model and on the possibility of polymorphic transition from olivine to spinel at the 20° Discontinuity by Tatsuhiko Wada, 1960.

No.38 On Origins of the Region C and the Core of the Earth ——Ionic-Intermetallic-Metallic Transition Hypothesis—— by Tatsuhiko Wada, 1960.

No.39 Crustal Stucture in Wakayama District as Deduced from Local and Near Earthquake Observations by Takeshi Mikumo, 1960.

No.40 Earthquake Resistance of Traditional Japanese Wooden Structures by Ryo Tanabashi, 1960.

No.41 Analysis With an Application to Aseismic Design of Bridge Piers by Hisao Goto and Kiyoshi Kaneta, 1960.

No.42 Tilting Motion of the Ground as Related to the Volcanic Activity of Mt. Aso and Micro-Process of the Tilting Motion of Ground and Structure by Yoshiro Itō, 1961.

No.43 On the Strength Distribution of the Earth's Crust and the Upper Mantle, and the Distribution of the Great Earthquakes with Depth by Shogo Matsushima, 1961.

No.44. Observational Study on Microseisms (Part 1) by Kennosuke Okano, 1961.

Bulletin No. 44 Published February, 1961

昭和 36 年 2 月 22 日 印 刷
昭和 36 年 2 月 28 日 発 行
編輯兼発行者 京都大学防災研究所
印刷者 山 代 多 三 郎
京都市上京区寺之内通小川西入
印刷所 山代印刷株式会社

[From Proceedings of the Japan Academy, Vol. 37, No. 1 (1961)]

10. *Free Oscillations of the Earth*

By Hitoshi Takeuchi and Masanori Saito
Geophysical Institute, Tokyo University
(Comm. by C. Tsuboi, M.J.A., Jan. 12, 1961)

In view of recent progress in seismometrical instruments, it is of interest to calculate theoretically the periods of the earth's free oscillations. This is a report of our study in this direction.

Assuming that the density ρ and elastic constants λ and μ of the earth are given functions of distance r from its center and denoting the (r, θ, φ) components of displacement u and an additional potential P due to the earth's deformation respectively by

$$\begin{aligned} u_r &= U(r)S_n(\theta, \varphi), & u_\theta &= V(r)\frac{\partial S_n(\theta, \varphi)}{\partial \theta}, \\ u_\varphi &= \frac{V(r)}{\sin\theta}\frac{\partial S_n(\theta, \varphi)}{\partial \varphi}, & P &= P(r)S_n(\theta, \varphi), \end{aligned} \tag{1}$$

where a common time factor $e^{i\sigma t}$ is omitted and $S_n(\theta, \varphi)$ is a spherical harmonic of order n, we can study the problem of the earth's free spheroidal oscillations by solving three simultaneous differential equations among $U(r)$, $V(r)$ and $P(r)$. These three equations with homogeneous boundary conditions to be satisfied at the free surface and at several discontinuity surfaces within the earth will determine the period $T=2\pi/\sigma$ of its free oscillation as a function of the azimuthal wave number n. Making use of the earth model by Jeffreys and Bullen,[1] Alterman, Jarosch and Pekeris[2] calculated T for $n=0, 2, 3$ and 4.

By using numerical integrations, we extended the calculation for the same model up to $n=5, 6, 8, 10, 16, 24, 38$ and 96. As is well known from previous studies,[3,4] the Jeffreys-Bullen model is not a very accurate approximation to the physical structure of the upper mantle. In view of this, we also calculated T for the Gutenberg model.[5] Since the main difference between the Jeffreys-Bullen and Gutenberg model of the earth is the existence of a low velocity zone around 150 Km depth in the latter, we may expect that a significant difference for the two models will be seen in T values for larger n. Thus the calculation for the Gutenberg model is made only for $n=16, 24, 38$ and 96. In making the calculations for $n=16$, 24, 38 and 96, we put a homogeneous crust of thickness 35 Km, density 2.8 g/cm^3, compressional wave velocity 6.10 Km/sec and distortional wave velocity 3.535 Km/sec on both of the models, whereas we assume no crust in the calculations for $n=0$ to 16. For both of the models, the values of T for $n=16$

with and without the crust agree to the third significant figure, justifying the above way of handling the crust. The values of T thus calculated are shown in Table I. In Table I are shown also the values of T obtained by Benioff, Press and Smith[6] from spectrum analysis of records of the Chilean earthquake of May 22, 1960.

In 1959, by using variational calculus, Takeuchi[7] calculated free periods of the earth's torsional oscillations for the Jeffreys-Bullen model. Extending the calculation, we get T given in Table II. In Table II, are shown also the observed T by Benioff and others.[6]

Table I. Periods of the earth's free spheroidal oscillations

n	calculated T: min		observed T: min
2	53.7		54.7 and 53.1
3	35.5		35.9 and 35.2
4	25.7		25.8
5	19.8		19.8
6	15.9		16.0
8	11.68		11.81
10	9.68		9.66
	Jeffreys-Bullen	Gutenberg	
16	6.74	6.74	6.78
24	5.05	5.06	5.10
38	3.62	3.65	3.66
96	1.658	1.679	—

Table II. Periods of the earth's free torsional oscillations

n	calculated T: min	observed T: min
2	43.4	42.3
3	28.1	28.6
4	21.5	21.8
5	17.1	17.9
6	15.3	15.5
7	13.5	13.5
8	12.1	12.3
9	11.04	11.21
10	10.17	10.33
11	9.43	9.60

From Tables I and II, we see that the calculated periods agree well with the observed values. Thus it is evident that the models used are good ones for representing the internal constitution of the earth.

Furthermore, by comparing the calculated results with the observations of mantle Rayleigh waves, we may see which of the Gutenberg's model and the Jeffreys-Bullen's is a better representation of

the earth. Calculating the phase velocity C of the mantle Rayleigh waves by means of the formula

$$C = \frac{2\pi a}{(n+0.5)\,T}, \tag{2}$$

where a is the radius of the earth, we get the relations between T and C of the waves shown in Table III.

Table III. Relations between T and C for the two earth models

Gutenberg		Jeffreys-Bullen	
T: sec	C: Km/sec	T: sec	C: Km/sec
100.7	4.118	99.5	4.168
218.9	4.749	217.1	4.789
303.8	5.378	303.3	5.387
404	6.00	404	6.00

The group velocity U as a function of T as experimentally determined by Ewing and Press[2] is shown in Table IV. With assumed initial values $C=4.00$, 4.10 and 4.20 Km/sec for $T=100$ sec, the equation

$$\frac{dC}{dT} = \frac{C(C-U)}{UT} \tag{3}$$

is numerically integrated and the results are shown in Table IV.

Table IV. Experimentally determined U and C

T: sec	U: Km/sec	C: Km/sec		
100	3.76	4.00	4.10	4.20
150	3.66	4.159	4.324	4.493
200	3.59	4.374	4.621	4.883
250	3.58	4.631	4.984	5.372
300	3.73	4.902	5.385	5.943
350	4.00	5.135	5.766	
400	4.10	5.335	6.127	

In Table III, both Gutenberg and Jeffreys-Bullen models are seen to give $C=6.00$ and 5.38 Km/sec for T around 400 and 300 sec. Table IV gives C around 4.10 Km/sec as the initial value at $T=100$ sec which is compatible with the above C's around $T=300$ and 400 sec. Thus in this respect the Gutenberg model, which gives C around 4.10 Km/sec at T 100 sec, appears to be better than the Jeffreys-Bullen's.

References

1) E. C. Bullard: The Earth as a Planet, Univ. of Chicago Press, 96 (1953).
2) Z. Alterman, H. Jarosch, and C. L. Pekeris: Proc. Roy. Soc., A, **252**, 80–95 (1959).

3) H. Takeuchi, F. Press, and N. Kobayashi: Bull. Seism. Soc. Amer., **49**, 355–364 (1959).
4) J. Dorman, M. Ewing, and J. Oliver: Bull. Seism. Soc. Amer., **50**, 87–115 (1960).
5) E. C. Bullard: Verhandelingen van het Koninklijk Nederlandsch Geologisch-Mijnbouwkundig Genootschap, Geologische Serie, Deel 18, Gedenkboek F. A. Vening Meinesz. (1957).
6) In press.
7) H. Takeuchi: Geophys. Jour., **2**, 89–100 (1959).
8) M. Ewing and F. Press: Bull. Seism. Soc. Amer., **44**, 127–147 (1954).

Love Waves in case the Surface Layer is Variable in Thickness

By

Ryōsuke SATŌ

Geophysical Institute, Faculty of Science, The University of Tokyo

1. Introduction

Recently, the seismic model study has made remarkable progress and wave characteristics of various complicated structures have been studied experimentally by many authors. F. PRESS (1957) investigated flexural waves, which are easily excited and propagated in plates having various shapes (thickness change, lithology change, fault and scarp). A. TAKAGI (1959) studied Rayleigh waves along the surface of a layered structure of variable thickness and reported many interesting properties of the waves, for example, that when Rayleigh waves are incident from the side of thicker surface layer to that of thinner surface layer, the transmitted Rayleigh waves characteristic for the thinner layer can be easily observed even at points close to the transitional zone, but that when Rayleigh waves are incident from the thinner layer side, the transmitted Rayleigh waves maintain characteristics for the thinner layer even at points distant from the transitional zone.

It is important to treat such problems theoretically. In this paper, Love waves propagated in layered media of which the surface layer is of variable thickness are investigated by means of the method developed by D. S. JONES (1952) for some diffraction problems.

§ 2. The case that Love waves are incident from the side of thicker surface layer to that of thinner surface layer

We consider a layered structure with a surface layer of which the thickness is H for the range $x>0$ and $h(=H-\delta)$ for the range $x<0$ with the origin of coordinates taken along the interface between two media, with the z-axis vertically downward (Fig. 1).

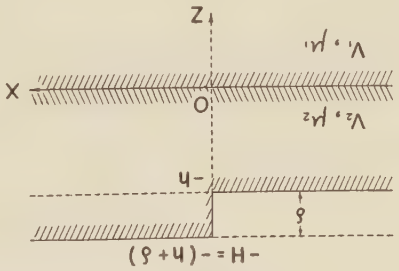

Fig. 1.

Velocities of shear waves and rigidities are taken V_1, μ_1 in the substratum and $V_2(<V_1)$, $\mu_2(<\mu_1)$ in the surface layer, respectively.

Let us express incident Love waves, omitting the time factor $e^{-i\omega t}$, as follows;

$$\left.\begin{aligned} v_{0,1}&=A\cos\tilde{\beta}_{2,N}H\cdot\exp\{-\tilde{\beta}_{1,N}z-i\kappa_{1,N}(x-x_0)\}\,, \quad z\geqslant 0,\\ v_{0,2}&=A\cos\tilde{\beta}_{2,N}(z+H)\cdot\exp\{-i\kappa_{1,N}(x-x_0)\}\,, \quad 0\geqslant z\geqslant -H,\end{aligned}\right\} \quad \infty>x>-\infty\,, \tag{1}$$

where

$$\tilde{\beta}_{1,N}=\sqrt{\kappa_{1,N}^2-k_1^2}\,, \qquad \tilde{\beta}_{2,N}=\sqrt{k_2^2-\kappa_{1,N}^2}\,, \qquad k_1=\omega/V_1\,, \qquad k_2=\omega/V_2\,, \tag{2}$$

and $\kappa_{1,N}$ is a root of the equation

$$\tan\tilde{\beta}_{2,N}H=\gamma\frac{\tilde{\beta}_{1,N}}{\tilde{\beta}_{2,N}}\,, \qquad \gamma=\frac{\mu_1}{\mu_2}\,, \tag{3}$$

and if we write $\kappa_{1,N}=\omega/C_{1,N}$, $C_{1,N}$ represents the phase velocity of Love waves of the N-th mode in a layered structure with a surface layer having the thickness H.

Denote the total displacements by

$$v=v_{0,1}+v_1\,,\qquad z\geqslant 0\,;\qquad \infty>x>-\infty\,, \tag{4a}$$

$$v=v_{0,2}+v_2\,,\qquad 0\geqslant z\geqslant -h\,,\qquad \infty>x>-\infty\,, \tag{4b}$$

$$v=v_{0,2}+v_3\,,\qquad -h\geqslant z\geqslant -H\,,\qquad x\geqslant 0\,. \tag{4c}$$

Then boundary conditions are given by

(i) $z=0,\ \infty>x>-\infty$;

$$v_1=v_2\,,\qquad \gamma\frac{\partial v_1}{\partial z}=\frac{\partial v_2}{\partial z}\,, \tag{5a}$$

(ii) $z=-h,\ x\geqslant 0$;

$$v_2=v_3\,,\qquad \frac{\partial v_2}{\partial z}=\frac{\partial v_3}{\partial z}\,, \tag{5b}$$

(iii) $z=-h,\ x\leqslant 0$;

$$\frac{\partial v_2}{\partial z}=-\frac{\partial v_{0,2}}{\partial z}=A\tilde{\beta}_{2,N}\sin\tilde{\beta}_{2,N}\delta\cdot\exp\{-i\kappa_{1,N}(x-x_0)\}\,, \tag{5c}$$

(iv) $z=-H,\ x\geqslant 0$;

$$\frac{\partial v_3}{\partial z}=0\,, \tag{5d}$$

(v) $x=0,\ -h\geqslant z\geqslant -H$;

$$\frac{\partial v_3}{\partial x}=-\frac{\partial v_{0,2}}{\partial x}=iA\kappa_{1,N}\cos\tilde{\beta}_{2,N}(z+H)\cdot\exp\{i\kappa_{1,N}x_0\}\,. \tag{5e}$$

v_1 satisfies the equation of motion

$$\frac{\partial^2 v_1}{\partial x^2}+\frac{\partial^2 v_1}{\partial z^2}=\frac{1}{V_1^2}\frac{\partial^2 v_1}{\partial t^2} \tag{6}$$

and v_j $(j=2,3)$ the equation

$$\frac{\partial^2 v_j}{\partial x^2}+\frac{\partial^2 v_j}{\partial z^2}=\frac{1}{V_2^2}\frac{\partial^2 v_j}{\partial t^2}\,. \tag{7}$$

If we introduce a virtual resistance $\varepsilon(\partial v_1/\partial t)$ $(\varepsilon>0)$ to (6) and assume the time factor $e^{-i\omega}$ equation (6) is reduced to

$$\frac{\partial^2 v_1}{\partial x^2}+\frac{\partial^2 v_1}{\partial z^2}+k_1^2 v_1=0\,, \tag{8}$$

where $k_1^2=(\omega^2+i\varepsilon\omega)/V_1^2$, that is, k_1 has a positive imaginary part. Hereafter, we consid that $\mathscr{I}k_1>0$ and $k_1=\omega/V_1$ as the limiting case of $\varepsilon\to 0$. v_2 and v_3 satisfy the equation simil to (8), substituting k_2 in place of k_1, and $\mathscr{I}k_2$ should be positive and $|k_1|<|k_2|$.

If we write

$$V_1(\zeta,z)=\frac{1}{\sqrt{2\pi}}\int_0^\infty v_1 e^{i\zeta x}dx+\frac{1}{\sqrt{2\pi}}\int_{-\infty}^0 v_1 e^{i\zeta x}dx\equiv V_{1+}(\zeta,z)+V_{1-}(\zeta,z)\,,\qquad \zeta=\xi+i\eta\,, \tag{9}$$

then, according to a generalized Fourier's theorem, if $|v_1|\leqslant A\exp(\eta_- x)$ as $x\to+\infty$ a $|v_1|\leqslant B\exp(\eta_+ x)$ as $x\to-\infty$, then $V_{1+}(\zeta,z)$ is analytic for $\eta>\eta_-$, $V_{1-}(\zeta,z)$ is analytic for $\eta<$ and therefore $V_1(\zeta,z)$ is analytic in the strip $\eta_+>\eta>\eta_-$. In our case, since the displacemen

consist of reflected waves at $x=0$, transmitted waves and diffracted waves, we can take $\eta_+=\mathscr{F}k_1$ and $\eta_-=-\mathscr{F}k_1$.

Applying the Fourier transform in x to the partial differential equations for v_1 and v_2 (cf. (8)), we find that

$$\frac{d^2}{dz^2}V_1(\zeta, z)-\beta_1^2 V_1(\zeta, z)=0\,, \qquad \beta_1=\sqrt{\zeta^2-k_1^2}\,, \tag{10}$$

$$\frac{d^2}{dz^2}V_2(\zeta, z)-\beta_2^2 V_2(\zeta, z)=0\,, \qquad \beta_2=\sqrt{\zeta^2-k_2^2}\,. \tag{11}$$

These equations have solutions

$$V_{1+}(\zeta, z)+V_{1-}(\zeta, z)=Be^{-\beta_1 z}\,, \tag{12}$$

$$V_{2+}(\zeta, z)+V_{2-}(\zeta, z)=Ce^{-\beta_2 z}+De^{\beta_2 z}\,, \tag{13}$$

where B, C and D are functions of ζ only. From the boundary condition (5a), we can write

$$C=\frac{\beta_2+\gamma\beta_1}{2\beta_2}B\,, \qquad D=\frac{\beta_2-\gamma\beta_1}{2\beta_2}\,. \tag{14}$$

Hence,

$$V_{2+}(\zeta, z)+V_{2-}(\zeta, z)=\frac{1}{\beta_2}[\beta_2\cosh\beta_2 z-\gamma\beta_1\sinh\beta_2 z]B\,. \tag{15}$$

For brevity, we shall write $V_{1\pm}(\zeta)$, $V_{2\pm}(\zeta)$, etc. instead of $V_{1\pm}(\zeta, -h)$, $V_{2\pm}(\zeta, -h)$, etc. ....

Differentiate (15) with respect to z and put $z=-h$. This gives

$$V_{2+}'(\zeta)+V_{2-}'(\zeta)=-[\beta_2\sinh\beta_2 h+\gamma\beta_1\cosh\beta_2 h]B\,. \tag{16}$$

Eliminating B from (15) and (16), we obtain

$$V_{2+}(\zeta, z)+V_{2-}(\zeta, z)=-\frac{1}{\beta_2}\frac{\beta_2\cosh\beta_2 z-\gamma\beta_1\sinh\beta_2 z}{F_2(\zeta)}[V_{2+}'(\zeta)+V_{2-}'(\zeta)]\,, \tag{17}$$

$$F_2(\zeta)=\beta_2\sinh\beta_2 h+\gamma\beta_1\cosh\beta_2 h\,, \tag{18}$$

or

$$V_{2+}(\zeta)+V_{2-}(\zeta)=-\frac{1}{\beta_2}\frac{\beta_2\cosh\beta_2 h+\gamma\beta_1\sinh\beta_2 h}{F_2(\zeta)}[V_{2+}'(\zeta)+V_{2-}'(\zeta)]\,. \tag{19}$$

Next, we apply an operater $\frac{1}{\sqrt{2\pi}}\int_0^\infty dx e^{i\zeta x}$ to the partial differential equation for v_3. We get

$$\frac{d^2}{dz^2}V_{3+}(\zeta, z)-\beta_2^2 V_{3+}(\zeta, z)=\frac{1}{\sqrt{2\pi}}\left(\frac{\partial v_3}{\partial x}\right)_{x=0}-\frac{i\zeta}{\sqrt{2\pi}}(v_3)_{x=0}\,, \tag{20}$$

where $(\partial v_3/\partial x)_{x=0}$ is given by the boundary condition (5e) but $(v_3)_{x=0}$ is still an unknown function. In order to eliminate the unknown $(v_3)_{x=0}$, changing the sign of ζ and adding the resulting equation to (20), we find

$$\frac{d^2}{dz^2}[V_{3+}(\zeta, z)+V_{3+}(-\zeta, z)]-\beta_2^2[V_{3+}(\zeta, z)+V_{3+}(-\zeta, z)]=\frac{2iA\kappa_{1,N}}{\sqrt{2\pi}}\cdot\cos\tilde{\beta}_{2,N}(z+H)\cdot\exp\{i\kappa_{1,N}x_0\}\,, \tag{21}$$

the solution of which is given, taking into account the boundary condition (5d), by

$$V_{3+}(\zeta, z)+V_{3+}(-\zeta, z)=E\cosh\beta_2(z+H)-\frac{2iA\kappa_{1,N}}{\sqrt{2\pi}}\frac{\cos\tilde{\beta}_{2,N}(z+H)}{\zeta^2-\kappa_{1,N}^2}\exp\{i\kappa_{1,N}x_0\}\ . \tag{22}$$

As before, we differentiate (22) with respect to z and put $z=-h$. Then we have

$$V_{3+}'(\zeta)+V_{3+}'(-\zeta)=E\beta_2\sinh\beta_2\delta+\frac{2iA\kappa_{1,N}\tilde{\beta}_{2,N}}{\sqrt{2\pi}}\frac{\sin\tilde{\beta}_{2,N}\delta}{\zeta^2-\kappa_{1,N}^2}\exp\{i\kappa_{1,N}x_0\}\ . \tag{23}$$

Elimination of E between (22) and (23) gives

$$\begin{aligned}V_{3+}(\zeta, z)+V_{3+}(-\zeta, z)=&\frac{1}{\beta_2}\frac{\cosh\beta_2(z+H)}{\sinh\beta_2\delta}\left[V_{3+}'(\zeta)+V_{3+}'(-\zeta)-\frac{2iA\kappa_{1,N}\tilde{\beta}_{2,N}}{\sqrt{2\pi}}\frac{\sin\tilde{\beta}_{2,N}\delta}{\zeta^2-\kappa_{1,N}^2}\exp\{i\kappa_{1,N}x_0\}\right]\\&-\frac{2iA\kappa_{1,N}}{\sqrt{2\pi}}\frac{\cos\tilde{\beta}_{2,N}(z+H)}{\zeta^2-\kappa_{1,N}^2}\exp\{i\kappa_{1,N}x_0\}\ ,\end{aligned} \tag{24}$$

hence, for $z=-h$,

$$\begin{aligned}V_{3+}(\zeta)+V_{3+}(-\zeta)=&\frac{1}{\beta_2}\coth\beta_2\delta\left[V_{3+}'(\zeta)+V_{3+}'(-\zeta)-\frac{2iA\kappa_{1,N}\tilde{\beta}_{2,N}}{\sqrt{2\pi}}\frac{\sin\tilde{\beta}_{2,N}\delta}{\zeta^2-\kappa_{1,N}^2}\exp\{i\kappa_{1,N}x_0\}\right]\\&-\frac{2iA\kappa_{1,N}}{\sqrt{2\pi}}\frac{\cos\tilde{\beta}_{2,N}\delta}{\zeta^2-\kappa_{1,N}^2}\exp\{i\kappa_{1,N}x_0\}\ .\end{aligned} \tag{25}$$

Now, from the boundary condition (5b), we can take

$$V_{2+}(\zeta)=V_{3+}(\zeta)\ ,\qquad V_{2+}'(\zeta)=V_{3+}'(\zeta)\ , \tag{26}$$

and from the application of an operater $\frac{1}{\sqrt{2\pi}}\int_{-\infty}^{0}dxe^{i\zeta x}$ to (5c), we can get

$$V_{2-}'(\zeta)=-\frac{iA\tilde{\beta}_{2,N}}{\sqrt{2\pi}}\frac{\sin\tilde{\beta}_{2,N}\delta}{\zeta-\kappa_{1,N}}\exp\{i\kappa_{1,N}x_0\}\ ,\qquad \mathcal{I}(\zeta-\kappa_{1,N})<0\ . \tag{27}$$

Using (19) and (25) to (27) and eliminating $V_{3+}(\zeta)$ and $V_{3+}'(\zeta)$, we can obtain the following equation of modified Wiener-Hopf form;

$$\begin{aligned}&\frac{1}{\beta_2}\frac{1}{\sinh\beta_2\delta}\frac{F_1(\zeta)}{F_2(\zeta)}[V_{2+}'(\zeta)+V_{2-}'(\zeta)]+\frac{1}{\beta_2}\coth\beta_2\delta\cdot[V_{2+}'(-\zeta)+V_{2-}'(-\zeta)]\\&+[V_{2-}(\zeta)-V_{3+}(-\zeta)]-\frac{2iA\kappa_{1,N}}{\sqrt{2\pi}}\frac{\cos\tilde{\beta}_{2,N}\delta}{\zeta^2-\kappa_{1,N}^2}\exp\{i\kappa_{1,N}x_0\}=0\ ,\end{aligned} \tag{28}$$

where

$$F_1(\zeta)=\beta_2\sinh\beta_2H+\gamma\beta_1\cosh\beta_2H \tag{29}$$

and $F_2(\zeta)$ is given by (18).

The factorization is made as follows;

$$\frac{\beta_2\delta}{\sinh\beta_2\delta}\frac{F_1(\zeta)}{F_2(\zeta)}=K_+(\zeta)K_-(\zeta)\ , \tag{30}$$

where

$$K_+(\zeta)=K_-(-\zeta)=\frac{L_+(\zeta)}{H_+(\zeta)}\prod_{n=1}^{\infty}\frac{(\zeta+\kappa_{1,n})}{(\zeta+\kappa_{2,n})}\ , \tag{31}$$

$H_+(\zeta)=H_-(-\zeta)$ is given by (A6), $L_+(\zeta)=L_-(-\zeta)$ is given by (A13) in Appendix and $\kappa_{1,n}$ and $\kappa_{2,n}$ are zeros of $F_1(\zeta)$ and $F_2(\zeta)$, respectively. $K_+(\zeta)$ is regular in $\mathscr{I}(\zeta+k_1)>0$ and $K_-(\zeta)$ is regular in $\mathscr{I}(\zeta-k_1)<0$. Furthermore, we decompose $\coth \beta_2\delta/\beta_2$ as

$$\frac{1}{\beta_2}\coth\beta_2\delta=f_+(\zeta)+f_-(\zeta)\,, \tag{32}$$

where

$$f_+(\zeta)=f_-(-\zeta)=-\frac{1}{2k_2\delta}\frac{1}{\zeta+k_2}+\sum_{n=1}^{\infty}\frac{i}{p_n\delta}\frac{1}{\zeta+ip_n} \tag{33}$$

and p_n is given by (A2) in Appendix.

Insert (30) and (32) in (28) and rearrange to find

$$\frac{K_+(\zeta)}{\zeta+k_2}V_2'(\zeta)+\frac{iA\tilde{\beta}_{2,N}}{\sqrt{2\pi}}\frac{K_+(\kappa_{1,N})}{k_2+\kappa_{1,N}}\frac{\sin\tilde{\beta}_{2,N}\delta}{\zeta-\kappa_{1,N}}\exp\{i\kappa_{1,N}x_0\}$$
$$+\frac{1}{\zeta+k_2}\frac{V_2'(k_2)}{K_+(k_2)}-\sum_{n=1}^{\infty}\frac{i}{p_n}\frac{k_2+ip_n}{\zeta+ip_n}\frac{V_2'(ip_n)}{K_+(ip_n)}=P_-(\zeta)\,, \tag{34}$$

in which $V_2'(\zeta)$ $[V_2'(\zeta)=V_{2+}'(\zeta)+V_{2-}'(\zeta)]$ is, of course, a known function and is given by (27). Then, the left-hand side of (34) is regular in the domain $\mathscr{I}(\zeta+k_1)>0$ ($\zeta=\kappa_{1,N}$ is not an irregular point since the left-hand side is zero at this point) and the right-hand side is regular in the domain $\mathscr{I}(\zeta-k_1)<0$ and therefore a function, defined by the left- or right-hand side, is regular in the whole of the ζ-plane, since the above-mentioned two half-planes overlap. Hence, if the left- and right-hand sides tend to zero as ζ tends to infinity in appropriate half-planes, both are zero from Louville's theorem. If we assume $(\partial v_2/\partial z)\to\text{constant}\times x^{-1/2}$ as $x\to+0$ on $z=-h$, then $|V_{2-}'(\zeta)|<\text{constant}\times|\zeta|^{-1/2}$. From this edge condition, we can take that each side of equation (34) is identically zero. This edge condition, which is given by the physics of the problem, plays an important rôle in the solution of this problem since it is concerned with the uniqueness of the result.

Thus we can obtain

$$V_2'(\zeta)=-W\frac{\zeta+k_2}{K_+(\zeta)}\left[\frac{i}{\zeta-\kappa_{1,N}}+\frac{1}{\zeta+k_2}\chi_0-\sum_{n=1}^{\infty}\frac{i}{p_n}\frac{k_2+ip_n}{\zeta+ip_n}\chi_n\right], \tag{35}$$

where

$$W=\frac{A\tilde{\beta}_{2,N}}{\sqrt{2\pi}}\frac{K_+(\kappa_{1,N})}{k_2+\kappa_{1,N}}\sin\tilde{\beta}_{2,N}\delta\cdot\exp\{i\kappa_{1,N}x_0\}\,, \tag{36}$$

$$\chi_0=\frac{1}{W}\frac{V_2'(k_2)}{K_+(k_2)}\,,\qquad \chi_n=\frac{1}{W}\frac{V_2'(ip_n)}{K_+(ip_n)}\,. \tag{37}$$

An infinite set of simultaneous linear algebraic equations for χ_n is obtained by setting $\zeta=ip_m$ $(m=0,1,2,\cdots)$ in (35):

$$[K_+(k_2)]^2\chi_0=i\frac{2k_2}{\kappa_{1,N}-k_2}-\chi_0+i\sum_{n=1}^{\infty}\frac{2k_2}{p_n}\chi_n\,, \tag{38}$$

$$[K_+(ip_m)]^2\chi_m=i\frac{k_2+ip_m}{\kappa_{1,N}-ip_m}-\chi_0+\sum_{n=1}^{\infty}\frac{k_2+ip_m}{p_n}\frac{k_2+ip_n}{p_m+p_n}\chi_n\,. \tag{39}$$

Furthermore, if we set $\zeta=-k_2$ or $-ip_n$, the following relation is easily found

$$V_2'(-k_2)=-V_2'(k_2)\,,\qquad V_2'(-ip_n)=-V_2'(ip_n)\,. \tag{40}$$

We use the Fourier inversion formula to find

$$v_2=\frac{1}{\sqrt{2\pi}}\int_{ic-\infty}^{ic+\infty}V_2(\zeta, z)e^{-i\zeta x}d\zeta\ , \qquad \mathcal{I}k_1>c>-\mathcal{I}k_1\ . \tag{41}$$

Therefore, from (17), we have

$$v_2=-\frac{1}{\sqrt{2\pi}}\int_{ic-\infty}^{ic+\infty}\frac{1}{\beta_2}\frac{\beta_2\cosh\beta_2 z-\gamma\beta_1\sinh\beta_2 z}{F_2(\zeta)}V_2'(\zeta)e^{-i\zeta x}d\zeta\ . \tag{42}$$

Next, v_3 in $x\geqq 0$ is given by

$$v_3=\frac{1}{\sqrt{2\pi}}\int_{ic-\infty}^{ic+\infty}V_{3+}(\zeta, z)e^{-i\zeta x}d\zeta\ , \tag{43}$$

but, since $V_{3+}(-\zeta, z)$ is regular in the lower half-plane,

$$\int_{ic-\infty}^{ic+\infty}V_{3+}(-\zeta, z)e^{-i\zeta x}d\zeta=0\ , \qquad x>0\ ,$$

hence, we can also write as

$$v_3=\frac{1}{\sqrt{2\pi}}\int_{ic-\infty}^{ic+\infty}[V_{3+}(\zeta, z)+V_{3+}(-\zeta, z)]e^{-i\zeta x}d\zeta\ , \qquad x>0\ . \tag{44}$$

From (24) and (27), we find

$$\begin{aligned}V_{3+}(\zeta, z)+V_{3+}(-\zeta, z)=&\frac{1}{\beta_2}\frac{\cosh\beta_2(z+H)}{\sinh\beta_2\delta}[V_2'(\zeta)+V_2'(-\zeta)]\\&-\frac{iA}{\sqrt{2\pi}}\cos\tilde{\beta}_{2,N}(z+H)\left\{\frac{1}{\zeta-\kappa_{1,N}}-\frac{1}{\zeta+\kappa_{1,N}}\right\}\exp\{i\kappa_{1,N}x_0\}\ .\end{aligned} \tag{45}$$

Then v_3 in $x>0$ is given by

$$v_3=\bar{v}_3+A\cos\tilde{\beta}_{2,N}(z+H)\cdot\exp\{i\kappa_{1,N}(x+x_0)\}\ , \qquad x>0\ , \tag{46}$$

$$\bar{v}_3=\frac{1}{\sqrt{2\pi}}\int_{ic-\infty}^{ic+\infty}\frac{1}{\beta_2}\frac{\cosh\beta_2(z+H)}{\sinh\beta_2\delta}[V_2'(\zeta)+V_2'(-\zeta)]e^{-i\zeta x}d\zeta\ . \tag{47}$$

First, we will investigate the transmitted Love waves, i. e. v_2 in $x<0$. In the region $0\geqq z\geqq -h$ and x is large negative, we can close the contour in the upper half-plane. $V_2'(\zeta)$ has only a pole at $\zeta=\kappa_{1,N}$ in the upper half-plane. From (35),

$$[V_2'(\zeta)(\zeta-\kappa_{1,N})]_{\zeta=\kappa_{1,N}}=-\frac{iA\tilde{\beta}_{2,N}}{\sqrt{2\pi}}\sin\tilde{\beta}_{2,N}\delta\cdot\exp\{i\kappa_{1,N}x_0\}\ , \tag{48}$$

then, using the relation (3), it is found that the contribution $v_{2,1}$ from this pole gives

$$\begin{aligned}v_{2,1}=&A\sin\tilde{\beta}_{2,N}\delta\cdot\frac{\tilde{\beta}_{2,N}\cos\tilde{\beta}_{2,N}z-\gamma\tilde{\beta}_{1,N}\sin\tilde{\beta}_{2,N}z}{\tilde{\beta}_{2,N}\sin\tilde{\beta}_{2,N}h-\gamma\tilde{\beta}_{1,N}\cos\tilde{\beta}_{2,N}h}\cdot\exp\{-i\kappa_{1,N}(x-x_0)\}\\=&-A\cos\tilde{\beta}_{2,N}(z+H)\cdot\exp\{-i\kappa_{1,N}(x-x_0)\}\ , \qquad x<0\ ,\end{aligned} \tag{49}$$

which exactly cancels the incident Love wave $v_{0,2}$.

Denoting the zeros of $F_2(\zeta)$ in the upper half-plane by $\kappa_{2,m}$ $(m=1, 2, \cdots)$, these poles give

$$v_{2,2}=-\sqrt{2\pi}i\sum_{m=1}^{\infty}\frac{1}{\hat{\beta}_{2,m}}\frac{\hat{\beta}_{2,m}\cos\hat{\beta}_{2,m}z-\gamma\hat{\beta}_{1,m}\sin\hat{\beta}_{2,m}z}{[dF_2(\zeta)/d\zeta]_{\zeta=\kappa_{2,m}}}V_2'(\kappa_{2,m})\cdot\exp\{-i\kappa_{2,m}x\}$$

$$=-\sqrt{2\pi}i\sum_{m=1}^{\infty}\frac{\kappa_{2,m}}{\hat{\beta}_{2,m}}\left(\frac{C_{2,m}}{U_{2,m}}-1\right)\frac{\cos\hat{\beta}_{2,m}(z+h)}{\hat{\beta}_{2,m}h}V_2'(\kappa_{2,m})\cdot\exp\{-i\kappa_{2,m}x\}\,,\qquad x<0\,,\tag{50}$$

where

$$\left.\begin{aligned}&\hat{\beta}_{1,m}=\sqrt{\kappa_{2,m}^{\,2}-k_1^{\,2}}\,,\qquad \hat{\beta}_{2,m}=\sqrt{k_2^{\,2}-\kappa_{2,m}^{\,2}}\,,\\&C_{2,m}=\omega/\kappa_{2,m}\text{: phase-velocity of Love waves of the } m\text{-th mode propagated in the layered structure with a surface layer having thickness } h,\\&U_{2,m}\text{: group-velocity of Love waves corresponding to the phase-velocity } C_{2,m}.\end{aligned}\right\}\tag{51}$$

These waves represent the transmitted Love waves.

Next, we will evaluate the reflected Love waves, i. e. v_3 in $x>0$ (v_2 for large x is identical to v_3). For the large positive x, we can close the contour in the lower half-plane. In (47), zeros of $\beta_2\sinh\beta_2\delta$ and $\sinh\beta_2\delta$ are given by $\zeta=-k_2$ and $\zeta=-ip_m$ ($m=1,2,\cdots$). At these points, however, $V_2'(\zeta)+V_2'(-\zeta)=0$ as shown in (40). Therefore, these points are not poles. In the upper half-plane, $V_2'(\zeta)$ has poles at $\zeta=-\kappa_{1,m}$ ($m=1,2,\cdots$) and $V_2'(-\zeta)$ has a pole $\zeta=-\kappa_{1,N}$. At $\zeta=-\kappa_{1,N}$,

$$[V_2'(-\zeta)(\zeta+\kappa_{1,N})]_{\zeta=-\kappa_{1,N}}=\frac{iA\tilde{\beta}_{2,N}}{\sqrt{2\pi}}\sin\tilde{\beta}_{2,N}\delta\cdot\exp\{i\kappa_{1,N}x_0\}\,,\tag{52}$$

then, the contribution $\bar{v}_{3,1}$ from this pole is

$$\bar{v}_{3,1}=-A\cos\tilde{\beta}_{2,N}(z+H)\cdot\exp\{i\kappa_{1,N}(x+x_0\}\,,\qquad x>0\,,\tag{53}$$

which cancels the second term in the right-hand side of (46). The contribution $\bar{v}_{3,2}$ from the poles $\zeta=-\kappa_{1,m}$ is easily obtained as

$$\bar{v}_{3,2}=\sqrt{2\pi}i\sum_{m=1}^{\infty}\frac{\cos\tilde{\beta}_{2,m}(z+H)}{\tilde{\beta}_{2,m}\sin\tilde{\beta}_{2,m}\delta}[V_2'(\zeta)(\zeta+\kappa_{1,m})]_{\zeta=-\kappa_{1,m}}\cdot\exp\{i\kappa_{1,m}x\}\,,\qquad x>0\,,\tag{54}$$

which represents the reflected Love waves.

§ 3. The case that Love waves are incident from the side of thinner surface layer to that of thicker surface layer

Write the incident Love waves as

$$\left.\begin{aligned}&v_{0,1}=A\cos\hat{\beta}_{2,N}h\cdot\exp\{-\hat{\beta}_{1,N}z+i\kappa_{2,N}(x+x_0)\}\,,\qquad z\geqq 0\,,\\&v_{0,2}=A\cos\hat{\beta}_{2,N}(z+h)\cdot\exp\{i\kappa_{2,N}(x+x_0)\}\,,\qquad 0\geqq z\geqq -h\,,\end{aligned}\right\}\qquad\infty>x>-\infty\,,\tag{55}$$

where

$$\hat{\beta}_{1,N}=\sqrt{\kappa_{2,N}^{\,2}-k_1^{\,2}}\,,\qquad \hat{\beta}_{2,N}=\sqrt{k_2^{\,2}-\kappa_{2,N}^{\,2}}\,,\tag{56}$$

and $\kappa_{2,N}$ is a root of the equation

$$\tan\hat{\beta}_{2,N}h=\gamma\frac{\hat{\beta}_{1,N}}{\hat{\beta}_{2,N}}\,.\tag{57}$$

Displacements are taken as

$$v=v_{0,1}+v_1\,,\qquad z\geqslant 0\,,\qquad \infty>x>-\infty\,, \tag{58a}$$

$$v=v_{0,2}+v_2\,,\qquad 0\geqslant z\geqslant -h\,,\qquad \infty>x>-\infty\,, \tag{58b}$$

$$v=v_3\,,\qquad -h\geqslant z\geqslant -H\,,\qquad x\geqslant 0\,, \tag{58c}$$

then, the given boundary conditions are

(i) $z=0,\ \infty>x>-\infty$;

$$v_1=v_2\,,\qquad \gamma\frac{\partial v_1}{\partial z}=\frac{\partial v_2}{\partial z}\,, \tag{59a}$$

(ii) $z=-h,\ x\geqslant 0$;

$$v_3-v_2=A\cdot\exp\{i\kappa_{2,N}(x+x_0)\}\,,\qquad \frac{\partial v_2}{\partial z}=\frac{\partial v_3}{\partial z}\,, \tag{59b}$$

(iii) $z=-h,\ x\leqslant 0$;

$$\frac{\partial v_2}{\partial z}=0\,, \tag{59c}$$

(iv) $z=-H,\ x\geqslant 0$;

$$\frac{\partial v_3}{\partial z}=0\,, \tag{59d}$$

(v) $x=0,\ -h\geqslant z\geqslant -H$;

$$\frac{\partial v_3}{\partial x}=0\,. \tag{59e}$$

Proceed in the same way as before up to equation (19). For $V_3(\zeta, z)$, since $(\partial v_3/\partial x)_{x=0}=0$ in this case, we have, instead of (24),

$$V_{3+}(\zeta, z)+V_{3+}(-\zeta, z)=\frac{1}{\beta_2}\frac{\cosh\beta_2(z+H)}{\sinh\beta_2\delta}[V_{3+}'(\zeta)+V_{3+}'(-\zeta)]\,. \tag{60}$$

Hence, at $z=-h$, it is reduced to

$$V_{3+}(\zeta)+V_{3+}(-\zeta)=\frac{1}{\beta_2}\coth\beta_2\delta[V_{3+}'(\zeta)+V_{3+}'(-\zeta)]\,. \tag{61}$$

Use the boundary conditions (59a, c) to find

$$\left.\begin{aligned} &V_{2+}'(\zeta)=V_{3+}'(\zeta)\,,\qquad V_{3+}(\zeta)-V_{2+}(\zeta)=\frac{iA}{\sqrt{2\pi}}\frac{1}{\zeta+\kappa_{2,N}}\exp\{i\kappa_{2,N}x_0\}\,,\qquad \mathscr{I}(\zeta+\kappa_{2,N})>0\,,\\ &V_{2-}'(\zeta)=0\,. \end{aligned}\right\} \tag{62}$$

Thus, from (19) and (61), we obtain the equation, corresponding to (28),

$$\frac{1}{\beta_2}\frac{1}{\sinh\beta_2\delta}\frac{F_1(\zeta)}{F_2(\zeta)}V_{3+}'(\zeta)+\frac{1}{\beta_2}\coth\beta_2\delta\cdot V_{3+}'(-\zeta)+[V_{2-}(\zeta)-V_{3+}(-\zeta)]$$
$$\frac{iA}{\sqrt{2\pi}}\frac{1}{\zeta+\kappa_{2,N}}\exp\{i\kappa_{2,N}x_0\}=0\,. \tag{63}$$

According to the same factorization as before, it is found that

$$\frac{K_+(\zeta)}{\zeta+k_2}V_{3+}'(\zeta)+\frac{iA\delta}{\sqrt{2\pi}}\frac{k_2+\kappa_{2,N}}{K_+(\kappa_{2,N})}\frac{1}{\zeta+\kappa_{2,N}}\exp\{i\kappa_{2,N}x_0\}$$
$$+\frac{1}{\zeta+k_2}\frac{V_{3+}'(k_2)}{K_+(k_2)}-\sum_{n=1}^{\infty}\frac{i}{p_n}\frac{k_2+ip_n}{\zeta+ip_n}\frac{V_{3+}'(ip_n)}{K_+(ip_n)}=P_-(\zeta)\,, \tag{64}$$

and this corresponds to the equation (34). Thus, applying Louville's theorem, we have

$$V_{3+}'(\zeta)=-W\frac{\zeta+k_2}{K_+(\zeta)}\left(\frac{i}{\zeta+\kappa_{2,N}}+\frac{1}{\zeta+k_2}\chi_0-\sum_{n=1}^{\infty}\frac{i}{p_n}\frac{k_2+ip_n}{\zeta+ip_n}\chi_n\right), \tag{65}$$

where, in this case,

$$\left.\begin{aligned} W&=\frac{A\delta}{\sqrt{2\pi}}\frac{k_2+\kappa_{2,N}}{K_+(\kappa_{2,N})}\exp\{i\kappa_{2,N}x_0\}, \\ \chi_0&=\frac{1}{W}\frac{V_{3+}'(k_2)}{K_+(k_2)}, \qquad \chi_n=\frac{1}{W}\frac{V_{3+}'(ip_n)}{K_+(ip_n)}. \end{aligned}\right\} \tag{66}$$

Besides, the relations similar to (40) are also obtained as

$$V_{3+}'(-k_2)=-V_{3+}'(k_2), \qquad V_{3+}'(-ip_n)=-V_{3+}'(ip_n). \tag{67}$$

Now, from (17) and (62), we can write

$$V_2(\zeta,z)=-\frac{1}{\beta_2}\frac{\beta_2\cosh\beta_2 z-\gamma\beta_1\sinh\beta_2 z}{F_2(\zeta)}V_{3+}'(\zeta), \tag{68}$$

hence, the displacement v_2 in $0\geqq z\geqq -h$ is given by the following integral;

$$v_2=-\frac{1}{\sqrt{2\pi}}\int_{ic-\infty}^{ic+\infty}\frac{1}{\beta_2}\frac{\beta_2\cosh\beta_2 z-\gamma\beta_1\sinh\beta_2 z}{F_2(\zeta)}V_{3+}'(\zeta)\cdot e^{-i\zeta x}d\zeta. \tag{69}$$

v_3 in $x>0$ is also given by (44). Using the relation (60), we have

$$v_3=\frac{1}{\sqrt{2\pi}}\int_{ic-\infty}^{ic+\infty}\frac{1}{\beta_2}\frac{\cosh\beta_2(z+H)}{\sinh\beta_2\delta}[V_{3+}'(\zeta)+V_{3+}'(-\zeta)]e^{-i\zeta x}d\zeta, \qquad x>0. \tag{70}$$

The transmitted Love waves can be obtained from the residue of integral in (70). For large positive x, we can complete the contour in the lower half-plane. $\zeta=-k_2$ and $\zeta=-ip_m$ $(m=1,2,\cdots)$ are not poles of the integrand according to the relations given by (67). Poles in the lower half-plane are only $-\kappa_{1,m}(m=1,2,\cdots)$, which are zeros of $K_+(\zeta)$. Thus, the transmitted Love waves are given by

$$\left.\begin{aligned} v_3&=\sqrt{2\pi}i\sum_{m=1}^{\infty}\frac{\cos\tilde{\beta}_{2,m}(z+H)}{\tilde{\beta}_{2,m}\sin\tilde{\beta}_{2,m}\delta}[V_{3+}'(\zeta)(\zeta+\kappa_{1,m})]_{\zeta=-\kappa_{1,m}}\cdot\exp\{i\kappa_{1,m}x\}, \qquad x>0, \\ &\tilde{\beta}_{2,m}=\sqrt{k_2{}^2-\kappa_{1,m}{}^2}, \end{aligned}\right\} \tag{71}$$

which is of the same form as (54). Poles of integrand in (69) are given by $\kappa_{2,m}$ $(m=1,2,\cdots)$, which are zeros of $F_2(\zeta)$, in the upper half-plane. Thus, closing the contour in the upper half-plane, we finally obtain

$$\begin{aligned} v_2&=-\sqrt{2\pi}i\sum_{m=1}^{\infty}\frac{1}{\hat{\beta}_{2,m}}\frac{\hat{\beta}_{2,m}\cos\hat{\beta}_{2,m}z-\gamma\hat{\beta}_{1,m}\sin\hat{\beta}_{2,m}z}{[dF_2(\zeta)/d\zeta]_{\zeta=\kappa_{2,m}}}V_{3+}'(\kappa_{2,m})\cdot\exp\{-i\kappa_{2,m}x\} \\ &=-\sqrt{2\pi}i\sum_{m=1}^{\infty}\frac{\kappa_{2,m}}{\hat{\beta}_{2,m}}\left(\frac{C_{2,m}}{U_{2,m}}-1\right)\frac{\cos\hat{\beta}_{2,m}(z+h)}{\hat{\beta}_{2,m}h}V_{3+}'(\kappa_{2,m})\cdot\exp\{-i\kappa_{2,m}x\}, \qquad x<0, \end{aligned} \tag{72}$$

as reflected Love waves.

§ 4. Approximate solutions for the case of small $k_2\delta$

In order to evaluate the reflected and the transmitted Love waves numerically, we must solve the infinite set of simultaneous linear equations, for example as (38) and (39), and even if we could obtain the solutions of the above linear equations, we must also calculate $K_+(\kappa_{2,m})$ in $V_2'(\kappa_{2,m})$ (see (50)). Besides, to obtain the exact values of $K_+(\kappa_{2,m})$, we must get all zeros of $F_1(\zeta)$ and $F_2(\zeta)$, defined by (29) and (18), for all frequencies ω.

Here, we assume that $k_2\delta=k_2(H-h)$ is very small, i.e., the difference in thickness is very small compared with the wave-length of waves under consideration.

(a) The case when Love waves are incident from the side of thicker surface layer to that of thinner surface layer (**Case I**).

When ζ is real, $H_+(\zeta)$, defined by (A3), can be written as

$$H_+(\zeta)=\left[\frac{\sinh\beta_2\delta}{\beta_2\delta}\right]^{1/2}\exp\left[-\chi(\zeta)+i\sum_{n=1}^{\infty}(\zeta\delta_n-\psi_n)\right],\qquad \psi_n=\tan^{-1}(\zeta/p_n)\,. \tag{73}$$

Hence, if we omit the term of $O(k_2\delta)$ compared with 1, we find

$$H_+(k_2)\approx 1\,, \tag{74}$$

then

$$K_+(k_2)\approx 1\,, \tag{75}$$

to the approximation of the same order.

Next, when $\zeta=ip_m\approx i/\delta_m=i(m\pi/\delta)$, since

$$\chi(ip_m)=\frac{p_m\delta}{\pi}\left(1-C-\ln\frac{ip_m\delta}{\pi}\right)+i\frac{p_m\delta}{2}\approx m(1-C-\ln m) \tag{76}$$

(see A7)), we have

$$H_+(ip_m)=\prod_{n=1}^{\infty}(p_n\delta_n+p_m\delta_m)\exp\{-p_m\delta_n-\chi(ip_m)\}\approx\prod_{n=1}^{\infty}\left(1+\frac{m}{n}\right)e^{-(m/n)-m(1-C-\ln m)}$$

$$=\frac{m^m e^{-m}}{\Gamma(1+m)}\,. \tag{77}$$

The remaining terms of $K_+(ip_m)$ are $1+O(k_2\delta)$. Thus we can write

$$K_+(ip_m)\approx\frac{m^m e^{-m}}{\Gamma(1+m)}\,. \tag{78}$$

When m is very large, $K_+(ip_m)\approx 1/\sqrt{2\pi m}$. Omit the term of $O(k_2\delta)$ in (38), (39) to find

$$\left.\begin{aligned}&[1+\{K_+(k_2)\}^2]\chi_0\approx-\frac{2ik_2}{k_2-\kappa_{1,N}}\,,\\&\{K_+(ip_m)\}^2\chi_m\approx-i-\chi_0-\sum_{n=1}^{\infty}\frac{m}{m+n}\chi_n\,.\end{aligned}\right\} \tag{79}$$

Hence, from the above approximations,

$$\left.\begin{aligned}&\chi_0\approx-\frac{ik_2}{k_2-\kappa_{1,N}}\,,\\&\frac{m^{2m}e^{-2m}}{\{\Gamma(1+m)\}^2}\chi_m\approx\frac{\kappa_{1,N}}{k_2-\kappa_{1,N}}-\sum_{n=1}^{\infty}\frac{m}{m+n}\chi_n\,.\end{aligned}\right\} \tag{80}$$

In order to obtain $V_2'(\zeta)$ given by (35), we must know the value of $K_+(\kappa_{1,N})$. We can easily get $K_+(\kappa_{1,N})\approx 1$ from the same approximation as $K_+(k_2)$, taking into account that $\kappa_{1,N}\delta=(\kappa_{1,N}/k_2)(k_2\delta)<(k_1/k_2)k_2\delta<k_2\delta$. $K_+(\kappa_{2,m})$ nearly equals to 1, too.

Thus, $V_2'(\kappa_{2,m})$ in the right-hand side of equation (50) is given by

$$V_2'(\kappa_{2,m})\approx -\frac{A\tilde{\beta}_{2,N}}{\sqrt{2\pi}}\frac{k_2+\kappa_{2,m}}{k_2+\kappa_{1,N}}\sin\tilde{\beta}_{2,N}\delta\cdot\exp\{i\kappa_{1,N}x_0\}\left[\frac{i}{\kappa_{2,m}-\kappa_{1,N}}+\frac{1}{k_2+\kappa_{2,m}}\chi_0-i\sum_{n=1}^{\infty}\frac{\delta}{n\pi}\chi_n\right], \tag{81}$$

which is of the order $(k_2\delta)$ for $m\neq N$. When $m=N$, i.e., the modes of incident and transmitted Love waves are equal, we can obtain the solution as follows:

Differentiate the equation

$$\tan\sqrt{k_2^2-\kappa^2}\,l=\gamma\frac{\sqrt{\kappa^2-k_1^2}}{\sqrt{k_2^2-\kappa^2}} \tag{82}$$

with respect to l, keeping k_1 and k_2 constant. This gives

$$\frac{d\kappa}{dl}=\frac{\kappa}{l}\left(\frac{C}{U}-1\right), \tag{83}$$

where $C=\omega/\kappa$ and $U=d\omega/d\kappa$. Hence, for the same mode and the same frequency,

$$\kappa_{1,N}-\kappa_{2,N}\approx\frac{\kappa_{2,N}}{h}\left(\frac{C_{2,N}}{U_{2,N}}-1\right)\delta. \tag{84}$$

Inserting this relation to the expression of $V_2'(\kappa_{2,N})$, we find

$$V_2'(\kappa_{2,N})\approx\frac{iA\tilde{\beta}_{2,N}}{\sqrt{2\pi}}\frac{h}{\kappa_{2,N}}\frac{1}{\left(\frac{C_{2,N}}{U_{2,N}}-1\right)}\frac{\sin\tilde{\beta}_{2,N}\delta}{\delta}\exp\{i\kappa_{1,N}x_0\}\,[1+O(k_2\delta)]. \tag{85}$$

Thus, (50) can be finally written as

$$v_{2,2}\approx A\cos\tilde{\beta}_{2,N}(z+h)\exp\{-i\kappa_{2,N}x+i\kappa_{1,N}x_0\}\,[1+O(k_2\delta)]. \tag{86}$$

This is the transmitted Love waves for small $(k_2\delta)$. It must be noted that all the waves with different modes from the incident Love waves are of the order $(k_2\delta)$.

Next, we will estimate the reflected Love waves to the same approximation. From (A17),

$$\frac{K_+(\zeta)}{(\zeta+\kappa_{1,m})}=\frac{L_+(\zeta)}{H_+(\zeta)(\zeta+\kappa_{2,m})}\prod_{n=1}^{\infty}{}'\frac{(\zeta+\kappa_{1,n})}{(\zeta+\kappa_{2,n})}, \tag{87}$$

where Π' means an infinite product except $n=m$. According to the same approximate procedure, we have

$$\left[\frac{K_+(\zeta)}{(\zeta+\kappa_{1,m})}\right]_{\zeta=-\kappa_{1,m}}\approx\frac{1}{\kappa_{2,m}-\kappa_{1,m}}\approx-\frac{H}{\kappa_{1,m}}\frac{1}{\left(\frac{C_{1,m}}{U_{1,m}}-1\right)\delta}. \tag{88}$$

$[V_2'(\zeta)(\zeta+\kappa_{1,m})]_{\zeta=-\kappa_{1,m}}$ in the right-hand side of (54) is found to be

$$[V_2'(\zeta)(\zeta+\kappa_{1,m})]_{\zeta=-\kappa_{1,m}}\approx-i\frac{A}{\sqrt{2\pi}}\frac{\kappa_{1,m}}{\tilde{\beta}_{2,N}H}\frac{k_2^2+\kappa_{1,N}\kappa_{1,m}}{\kappa_{1,N}+\kappa_{1,m}}\left(\frac{C_{1,m}}{U_{1,m}}-1\right)\delta\sin\tilde{\beta}_{2,N}\delta\cdot\exp\{i\kappa_{1,N}x_0\}. \tag{89}$$

Hence, we can obtain, as the reflected Love waves,

$$\bar{v}_{3,2}\approx A\sum_{m=1}^{\infty}\cos\tilde{\beta}_{2,m}(z+H)\frac{\kappa_{1,m}\delta}{\tilde{\beta}_{2,N}\tilde{\beta}_{2,m}H}\frac{k_2^2+\kappa_{1,N}\kappa_{1,m}}{\kappa_{1,N}+\kappa_{1,m}}\left(\frac{C_{1,m}}{U_{1,m}}-1\right)\frac{\sin\tilde{\beta}_{2,N}\delta}{\sin\tilde{\beta}_{2,m}\delta}\exp\{i\kappa_{1,m}x+i\kappa_{1,N}x_0\}\,. \tag{90}$$

When $m=N$, it is reduced to

$$\bar{v}_{3,2}\approx A\cos\tilde{\beta}_{2,N}(z+H)\cdot\frac{\delta}{2H}\frac{k_2^2+\kappa_{1,N}^2}{k_2^2-\kappa_{1,N}^2}\left(\frac{C_{1,N}}{U_{1,N}}-1\right)\exp\{i\kappa_{1,N}(x+x_0)\}\,. \tag{91}$$

(b) The case when Love waves are incident from the side of thinner surface layer to that of thicker surface layer (**Case II**).

We can evaluate the waves for this case by the same procedure. From (65), the equations corresponding to (80) are

$$\left.\begin{aligned}&\chi_0=-\frac{ik_2}{k_2+\kappa_{2,N}}\,,\\&\frac{m^{2m}e^{-2m}}{\{\Gamma(1+m)\}^2}\chi_m\approx-\frac{i\kappa_{2,N}}{k_2+\kappa_{2,N}}-\sum_{n=1}^{\infty}\frac{m}{m+n}\chi_n\,.\end{aligned}\right\} \tag{92}$$

Hence,

$$[V_{3+}'(\zeta)(\zeta+\kappa_{1,m})]_{\zeta=-\kappa_{1,m}}\approx-\frac{iA\delta^2}{\sqrt{2\pi}}\frac{k_2^2-\kappa_{1,m}\kappa_{2,N}}{\kappa_{1,m}-\kappa_{2,N}}\frac{\kappa_{1,m}}{H}\left(\frac{C_{1,m}}{U_{1,m}}-1\right)\exp\{i\kappa_{2,N}x_0\}\,, \tag{93}$$

which is of the order $(k_2\delta)$ only when $m=N$. For $m=N$, (93) can be reduced to

$$[V_{3+}'(\zeta)(\zeta+\kappa_{1,N})]_{\zeta=-\kappa_{1,N}}\approx-\frac{iA\delta}{\sqrt{2\pi}}\tilde{\beta}_{2,N}^2\exp\{i\kappa_{2,N}x_0\}\,. \tag{94}$$

Then, we have, from (71),

$$v_3\approx A\cos\tilde{\beta}_{2,N}(z+H)\cdot\exp\{i\kappa_{1,N}x+i\kappa_{2,N}x_0\}\,. \tag{95}$$

All the waves of other modes are of the order $(k_2\delta)$.

To the same approximation,

$$V_{3+}'(\kappa_{2,m})\approx-\frac{iA\delta}{\sqrt{2\pi}}\frac{k_2^2+\kappa_{2,N}\kappa_{2,m}}{\kappa_{2,N}+\kappa_{2,m}}\exp\{i\kappa_{2,N}x_0\}\,. \tag{96}$$

Putting this into (72), we finally obtain

$$v_2\approx-A\sum_{m=1}^{\infty}\cos\hat{\beta}_{2,m}(z+H)\frac{\kappa_{2,m}\delta}{\hat{\beta}_{2,m}^2h}\frac{k_2^2+\kappa_{2,N}\kappa_{2,m}}{\kappa_{2,N}+\kappa_{2,m}}\left(\frac{C_{2,m}}{U_{2,m}}-1\right)\exp\{-i\kappa_{2,m}x+i\kappa_{2,N}x_0\}\,. \tag{97}$$

When $m=N$,

$$v_2\approx-A\cos\hat{\beta}_{2,N}(z+h)\cdot\frac{\delta}{2h}\frac{k_2^2+\kappa_{2,N}^2}{k_2^2-\kappa_{2,N}^2}\left(\frac{C_{2,N}}{U_{2,N}}-1\right)\exp\{-i\kappa_{2,N}(x-x_0)\}\,. \tag{98}$$

§ 5. Ratio of energy flux of transmitted or reflected Love waves to that of incident Love waves

We could obtain the transmitted and reflected waves for small $(k_2\delta)$. These waves are

summarized as follows:

(a) Case I.

Incident waves;

$$\left.\begin{aligned} v_{0,1} &= A\cos\tilde{\beta}_{2,N}H\cdot\exp\{-\tilde{\beta}_{1,N}z\}\cos[\omega t+\kappa_{1,N}(x-x_0)], \quad z\geqq 0,\\ v_{0,2} &= A\cos\tilde{\beta}_{2,N}(z+H)\cdot\cos[\omega t+\kappa_{1,N}(x-x_0)], \quad 0\geqq z\geqq -H, \end{aligned}\right\} \; x>0. \tag{99a}$$

Transmitted waves;

$$\left.\begin{aligned} v_{t,1} &= A\cos\hat{\beta}_{2,N}h\cdot\exp\{-\hat{\beta}_{2,N}z\}\cos[\omega t-\kappa_{2,N}x-\kappa_{1,N}x_0], \quad z\geqq 0,\\ v_{t,2} &= A\cos\hat{\beta}_{2,N}(z+h)\cdot\cos[\omega t+\kappa_{2,N}x-\kappa_{1,N}x_0], \quad 0\geqq z\geqq -h, \end{aligned}\right\} \; x<0. \tag{99b}$$

Reflected waves;

$$\left.\begin{aligned} v_{r,1} &= A\sum_{m=1}^{\infty}a_m\cos\tilde{\beta}_{2,m}H\cdot\exp\{-\tilde{\beta}_{1,m}z\}\cos[\omega t-\kappa_{1,m}x-\kappa_{1,N}x_0], \quad z\geqq 0,\\ v_{r,2} &= A\sum_{m=1}^{\infty}a_m\cos\tilde{\beta}_{2,m}(z+H)\cdot\cos[\omega t-\kappa_{1,m}x-\kappa_{1,N}x_0], \quad 0\geqq z\geqq -H, \end{aligned}\right\} \; x>0, \tag{99c}$$

$$a_m=\frac{\kappa_{1,m}\delta}{\tilde{\beta}_{2,N}\tilde{\beta}_{2,m}H}\,\frac{k_2^2+\kappa_{1,N}\kappa_{1,m}}{\kappa_{1,N}+\kappa_{1,m}}\left(\frac{C_{1,m}}{U_{1,m}}-1\right)\frac{\sin\tilde{\beta}_{2,N}\delta}{\sin\tilde{\beta}_{2,m}\delta}. \tag{100}$$

(b) Case II.

Incident waves;

$$\left.\begin{aligned} v_{0,1} &= A'\cos\hat{\beta}_{2,N}h\cdot\exp\{-\hat{\beta}_{1,N}z\}\cos[\omega t-\kappa_{2,N}(x+x_0)], \quad z\geqq 0,\\ v_{0,2} &= A'\cos\hat{\beta}_{2,N}(z+h)\cdot\cos[\omega t-\kappa_{2,N}(x+x_0)], \quad 0\geqq z\geqq -h, \end{aligned}\right\} \; x<0. \tag{101a}$$

Transmitted waves;

$$\left.\begin{aligned} v_{t,1} &= A'\cos\tilde{\beta}_{2,N}H\cdot\exp\{-\tilde{\beta}_{1,N}z\}\cos[\omega t-\kappa_{1,N}x-\kappa_{2,N}x_0], \quad z\geqq 0,\\ v_{t,2} &= A'\cos\tilde{\beta}_{2,N}(z+H)\cdot\cos[\omega t-\kappa_{1,N}x-\kappa_{2,N}x_0], \quad 0\geqq z\geqq -H, \end{aligned}\right\} \; x>0. \tag{101b}$$

Reflected waves;

$$\left.\begin{aligned} v_{r,1} &= -A'\sum_{m=1}^{\infty}a_m'\cos\hat{\beta}_{2,m}h\cdot\exp\{-\hat{\beta}_{1,m}z\}\cos[\omega t+\kappa_{2,m}x-\kappa_{2,N}x_0], \quad z\geqq 0,\\ v_{r,2} &= -A'\sum_{m=1}^{\infty}a_m'\cos\hat{\beta}_{2,m}(z+h)\cdot\cos[\omega t+\kappa_{2,m}x-\kappa_{2,N}x_0], \quad 0\geqq z\geqq -h, \end{aligned}\right\} \; x<0, \tag{101c}$$

$$a_m'=\frac{\kappa_{2,m}\delta}{\hat{\beta}_{2,m}^2h}\,\frac{k_2^2+\kappa_{2,N}\kappa_{2,m}}{\kappa_{2,N}+\kappa_{2,m}}\left(\frac{C_{2,m}}{U_{2,m}}-1\right). \tag{102}$$

Since waves in cases I and II are of the same form as seen from the above equations, we will proceed as follows only for waves in case I.

The rate of energy, which passes the plane perpendicular to x-axis, per unit time and per unit area, is given by

$$F=\mp\mu\frac{\partial v}{\partial x}\frac{\partial v}{\partial t}, \tag{103}$$

$-$ being taken when waves are propagated to the direction of positive x and $+$ to the opposite direction. Hence, we obtain

$$\left.\begin{aligned} F_{0,1}&=\mu_1\omega A^2\kappa_{1,N}\cos^2\tilde{\beta}_{2,N}H\cdot\exp\{-2\tilde{\beta}_{1,N}z\}\sin^2[\omega t+\kappa_{1,N}(x-x_0)]\,, && z\geqq 0\,,\\ F_{0,2}&=\mu_2\omega A^2\kappa_{1,N}\cos^2\tilde{\beta}_{2,N}(z+H)\cdot\sin^2[\omega t+\kappa_{1,N}(x-x_0)]\,, && 0\geqq z\geqq -H\,,\end{aligned}\right\} x>0\,. \quad (104a)$$

$$\left.\begin{aligned} F_{t,1}&=\mu_1\omega A^2\kappa_{2,N}\cos^2\hat{\beta}_{2,N}h\cdot\exp\{-2\hat{\beta}_{1,N}z\}\sin^2[\omega t+\kappa_{2,N}x-\kappa_{1,N}x_0]\,, && z\geqq 0\,,\\ F_{t,2}&=\mu_2\omega A^2\kappa_{2,N}\cos^2\hat{\beta}_{2,N}(z+h)\cdot\sin^2[\omega t+\kappa_{2,N}x-\kappa_{1,N}x_0]\,, && 0\geqq z\geqq -h\,,\end{aligned}\right\} x<0\,. \quad (104b)$$

$$\left.\begin{aligned} F_{r,1}&=\mu_1\omega A^2\sum a_m{}^2\kappa_{1,m}\cos^2\tilde{\beta}_{2,m}H\cdot\exp\{-2\tilde{\beta}_{1,m}z\}\cdot\sin^2[\omega t-\kappa_{1,m}x-\kappa_{1,N}x_0]\,, && z\geqq 0\,,\\ F_{r,2}&=\mu_2\omega A^2\sum a_m{}^2\kappa_{1,m}\cos^2\tilde{\beta}_{2,m}(z+H)\cdot\sin^2[\omega t-\kappa_{1,m}x-\kappa_{1,N}x_0]\,, && 0\geqq z\geqq -H\,,\end{aligned}\right\} x>0\,. \quad (104c)$$

The energy flow for a certain period $T=2\pi/\omega$ is, from $\bar{F}=\int_0^T F\,dt$, found to be

$$\left.\begin{aligned} \bar{F}_{0,1}&=\pi\mu_1A^2\kappa_{1,N}\cos^2\tilde{\beta}_{2,N}H\cdot\exp\{-2\tilde{\beta}_{1,N}z\}\,,\\ \bar{F}_{0,2}&=\pi\mu_2A^2\kappa_{1,N}\cos^2\tilde{\beta}_{2,N}(z+H)\,,\end{aligned}\right\} x>0\,. \quad (105a)$$

$$\left.\begin{aligned} \bar{F}_{t,1}&=\pi\mu_1A^2\kappa_{2,N}\cos^2\hat{\beta}_{2,N}h\cdot\exp\{-2\hat{\beta}_{1,N}z\}\,,\\ \bar{F}_{t,2}&=\pi\mu_2A^2\kappa_{2,N}\cos^2\hat{\beta}_{2,N}(z+h)\,,\end{aligned}\right\} x<0\,. \quad (105b)$$

$$\left.\begin{aligned} \bar{F}_{r,1}&=\pi\mu_1A^2\sum a_m{}^2\kappa_{1,m}\cos^2\tilde{\beta}_{2,m}H\cdot\exp\{-2\tilde{\beta}_{1,m}z\}\,,\\ \bar{F}_{r,2}&=\pi\mu_2A^2\sum a_m{}^2\kappa_{1,m}\cos^2\tilde{\beta}_{2,m}(z+H)\,,\end{aligned}\right\} x>0\,. \quad (105c)$$

Thus, the total flux of energy across the vertical plane of unit breadth is

$$[\text{T.F.}]_{\text{inc.}}=\int_0^\infty\bar{F}_{0,1}\,dz+\int_{-H}^0\bar{F}_{0,2}\,dz=\frac{1}{2}\pi\mu_2A^2\frac{\kappa_{1,N}}{\tilde{\beta}_{2,N}}\frac{\tan\tilde{\beta}_{2,N}H}{\sec^2\tilde{\beta}_{2N}H}\left[1+\frac{\tilde{\beta}_{2,N}^{\,2}}{\tilde{\beta}_{1,N}^{\,2}}+\tilde{\beta}_{2,N}H\frac{\sec^2\tilde{\beta}_{2,N}H}{\tan\tilde{\beta}_{2,N}H}\right]$$

$$=\frac{1}{2}\pi\mu_2A^2\frac{\tilde{\beta}_{2,N}}{\kappa_{1,N}}\frac{\tilde{\beta}_{2,N}H}{\left(\dfrac{C_{1,N}}{U_{1,N}}-1\right)}\qquad\text{for incident Love waves,}\quad (106a)$$

$$[\text{T.F.}]_{\text{trans.}}=\frac{1}{2}\pi\mu_2A^2\frac{\hat{\beta}_{2,N}}{\kappa_{2,N}}\frac{\hat{\beta}_{2,N}h}{\left(\dfrac{C_{2,N}}{U_{2,N}}-1\right)}\qquad\text{for transmitted Love waves,}\quad (106b)$$

and

$$[\text{T.F.}]_{\text{refl.}}=\frac{1}{2}\pi\mu_2A^2\sum a_m{}^2\frac{\tilde{\beta}_{2,m}}{\kappa_{1,m}}\frac{\tilde{\beta}_{2,m}H}{\left(\dfrac{C_{1,m}}{U_{1,m}}-1\right)}\qquad\text{for reflected Love waves,}\quad (106c)$$

Hence,

$$\frac{[\text{T.F.}]_{\text{trans.}}}{[\text{T.F.}]_{\text{inc.}}}=\frac{\kappa_{1,N}}{\kappa_{2,N}}\frac{\hat{\beta}_{2,N}^{\,2}}{\tilde{\beta}_{2,N}^{\,2}}\frac{h}{H}\frac{\left(\dfrac{C_{1,N}}{U_{1,N}}-1\right)}{\left(\dfrac{C_{2,N}}{U_{2,N}}-1\right)}=\frac{h}{H}\frac{C_{1,N}}{C_{2,N}}\frac{\left(\dfrac{C_{2,N}^{\,2}}{V_2^{\,2}}-1\right)}{\left(\dfrac{C_{1\,N}^{\,2}}{V_2^{\,2}}-1\right)}\frac{\left(\dfrac{C_{1,N}}{U_{1,N}}-1\right)}{\left(\dfrac{C_{2,N}}{U_{2,N}}-1\right)}\,, \quad (107a)$$

and

$$\frac{[\text{T.F.}]_{\text{refl.}}}{[\text{T.F.}]_{\text{inc.}}}=\sum a_m{}^2\frac{\kappa_{1,N}}{\kappa_{1,m}}\frac{\tilde{\beta}_{2,m}^{\,2}}{\tilde{\beta}_{2,N}^{\,2}}\frac{\left(\dfrac{C_{1,N}}{U_{1,N}}-1\right)}{\left(\dfrac{C_{1,m}}{U_{1,m}}-1\right)}=\sum a_m{}^2\frac{C_{1,N}}{C_{1,m}}\frac{\left(\dfrac{C_{1,m}^{\,2}}{V_2^{\,2}}-1\right)}{\left(\dfrac{C_{1,N}^{\,2}}{V_2^{\,2}}-1\right)}\frac{\left(\dfrac{C_{1,N}}{U_{1,N}}-1\right)}{\left(\dfrac{C_{1,m}}{U_{1,m}}-1\right)}\,. \quad (107b)$$

When $m=N$, i.e., the mode of reflected Love wave is equal to that of incident wave, it is

easily found

$$\frac{[\text{T.F.}]_{\text{refl.}}}{[\text{T.F.}]_{\text{inc.}}}=a_N{}^2 . \tag{108}$$

§ 6. Numerical examples

Fig. 2 shows phase- and group-velocities of Love waves (1st mode) in the layered structure of $\mu_1/\mu_2=2$ and $V_1/V_2=4/3$, and $[\text{T.F.}]_{\text{inc.}}/\frac{1}{2}\pi\mu_2 A^2$ for k_2H is shown in Fig. 3. We must remember the assumption that $k_2\delta=\omega(H-h)/V_2$ is very small. If we take $\delta/H=\alpha$, then $k_2H=k_2\delta/\alpha$ and $k_2h=k_2H\cdot(h/H)$. Hence, when α is not small, we can discuss only the waves for very small k_2H. For an example, if $h/H=0.8$ or $\delta/H=0.2$ and $k_2\delta\leqslant 0.01$, only the waves in the range $k_2H\leqslant 0.05$ or $k_2h\leqslant 0.04$ can be discussed. The smaller the value of h/H, the smaller the range that we can discuss for. And for the small values of δ/H or for the small values of k_2H, the value of $[\text{T.F.}]_{\text{trans.}}/[\text{T.F.}]_{\text{inc.}}$ is, of course, nearly 1.

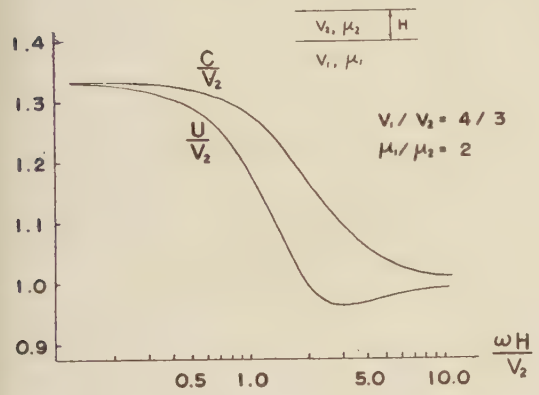

Fig. 2. Phase- and group-velocities of Love waves under considerations.

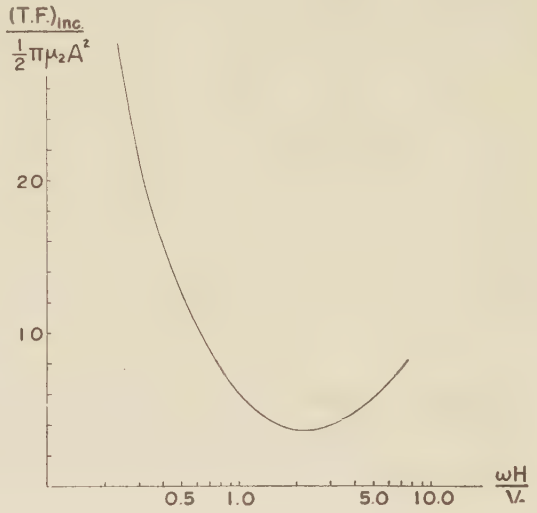

Fig. 3

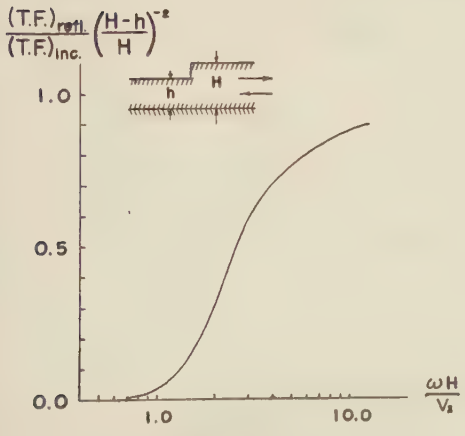

Fig. 4

Fig. 4 shows $\{[\text{T.F.}]_{\text{refl.}}/[\text{T.F.}]_{\text{inc.}}\}\times\{1-(h/H)\}^{-2}$ for the reflected Love waves of the first mode, i.e., $a_1{}^2\times\{1-(h/H)\}^{-2}$. From this figure, we can estimate $[\text{T.F.}]_{\text{trans.}}/[\text{T.F.}]_{\text{inc.}}$ to some extent.

§ 7. Conclusion

We studied the problem of propagation of Love waves in the layered media with a surface layer of variable thickness. It is difficult to see the exact behaviours of Love waves in such media, because we must solve an infinite set of simultaneous linear equations and calculate phase- and group-velocities of Love waves for infinite numbers of modes,

as stated at the beginning of § 4.

We derived approximate solutions for the case that the thickness difference of surface layer is small compared with the wave-length under consideration, leaving the solutions for larger thickness difference in the future.

If the incident Love wave is of the N-th mode, only the transmitted Love wave of the N-th mode predominates and the waves of other modes are small. But the amplitudes of reflected Love waves are of the order (thickness-difference/wave-length) for all modes.

The mean group-velocity U_m for the total epicentral distance Δ is, of course, given by

$$\Delta/U_m=\Delta_1/U_1+\Delta_2/U_2\,,$$

for longer periods, as illustrated in Fig. 5. The period for Airy phase, of course, differs from that for a uniformly layered structure.

The method used in this paper can be applied to solving the problem of propagation of Love waves in layered structures in which the boundary has a step form, as shown in Fig. 6, with some modifications.

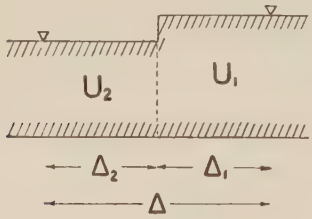

Fig. 5

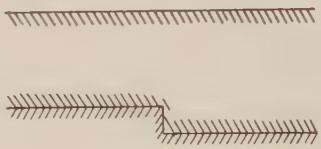
Fig. 6

§ 8. Acknowledgements

The author wishes to express his sincere thanks to Professor H. Honda for his guidance in this study.

APPENDIX. Decomposition of $\frac{\beta_2\delta}{\sinh\beta_2\delta}\frac{F_1(\zeta)}{F_2(\zeta)}=K_+(\zeta)K_-(\zeta)$ [cf. (30)]

According to the infinite product theorem (E. C. Titchmarsh (1939), p. 113), we can write

$$\frac{\sinh\beta_2\delta}{\beta_2\delta}=\prod_{n=1}^{\infty}\{p_n^2\delta_n^2+\zeta^2\delta_n^2\}=H(\zeta)\,, \tag{A1}$$

where

$$\left.\begin{aligned} &p_n\delta_n=(1-k_2^2\delta_n^2)^{1/2}=-i(k_2^2\delta_n^2-1)^{1/2},\\ &\delta_n=\delta/n\pi\,. \end{aligned}\right\} \tag{A2}$$

We decompose $H(\zeta)$ as follows;

$$H(\zeta)=H_+(\zeta)H_-(\zeta)\,,\qquad H_\pm(\zeta)=\prod_{n=1}^{\infty}\{p_n\delta_n\mp i\zeta\delta_n\}\exp\{\pm i\zeta\delta_n\mp\chi(\zeta)\}\,, \tag{A3}$$

taking $\chi(\zeta)$ as an arbitrary function. When ζ is very large,

$$H_+(\zeta)\sim\prod_{n=1}^{\infty}\{1-i\zeta\delta_n\}\exp\{i\zeta\delta_n-\chi(\zeta)\}=\frac{\exp\left\{iC\frac{\zeta\delta}{\pi}-\chi(\zeta)\right\}}{\Gamma\left(1-i\frac{\zeta\delta}{\pi}\right)}, \tag{A4}$$

where C is the Euler's constant and $\Gamma(z)$ the Gamma function. From Stirling's formula, we have

$$\Gamma\left(1-i\frac{\zeta\delta}{\pi}\right)\sim\sqrt{2\zeta\delta}\ \exp\left\{-\frac{\pi}{4}i+i\frac{\zeta\delta}{\pi}\left(1-\ln\frac{\zeta\delta}{\pi}\right)-\frac{\zeta\delta}{2}\right\}, \tag{A5}$$

hence,

$$H_+(\zeta)\sim\frac{1}{\sqrt{2\zeta\delta}}\exp\left\{\frac{\pi}{4}i\right\}\exp\left\{-i\frac{\zeta\delta}{\pi}\left(1-C-\ln\frac{\zeta\delta}{\pi}\right)+\frac{\zeta\delta}{2}-\chi(\zeta)\right\}. \tag{A6}$$

Thus, if we choose

$$\chi(\zeta)=-i\frac{\zeta\delta}{\pi}\left(1-C-\ln\frac{\zeta\delta}{\pi}\right)+\frac{\zeta\delta}{2}, \tag{A7}$$

then, $|H_+(\zeta)|\sim|\zeta|^{-1/2}$ as $|\zeta|\to\infty$. Since

$$H_-(\zeta)=H_+(-\zeta), \tag{A8}$$

$H_-(\zeta)$ has the same behaviour for $|\zeta|\to\infty$ as $H_+(\zeta)$.

If we write all zeros of $F_1(\zeta)$ and $F_2(\zeta)$, given by (29) and (18), as $\pm\kappa_{1,n}$ and $\pm\kappa_{2,n}$ $(n=1, 2, 3, \cdots)$, we can take

$$\frac{F_1(\zeta)}{F_2(\zeta)}=\prod_{n=1}^{\infty}\frac{(\zeta^2-\kappa_{1,n}{}^2)}{(\zeta^2-\kappa_{2,n}{}^2)}\frac{G_1(\zeta)}{G_2(\zeta)}, \tag{A9}$$

where

$$G_1(\zeta)=F_1(\zeta)/\prod_{n=1}^{\infty}(\zeta^2-\kappa_{1,n}{}^2),\qquad G_2(\zeta)=F_2(\zeta)/\prod_{n=1}^{\infty}(\zeta^2-\kappa_{2,n}{}^2), \tag{A10}$$

and both functions have no zero. Furthermore, we decompose $L(\zeta)=G_1(\zeta)/G_2(\zeta)$ as follows;

$$L(\zeta)=\frac{G_1(\zeta)}{G_2(\zeta)}=L_+(\zeta)L_-(\zeta), \tag{A11}$$

then, $L_+(\zeta)$ is given by the integral

$$\ln L_+(\zeta)=\frac{1}{2\pi i}\int_\Gamma\frac{\ln L(w)}{w-\zeta}dw, \tag{A12}$$

where we take the contour Γ as shown in Fig. A1, according to the definition of the upper sheet of the Riemann-plane ($\mathscr{R}\beta_1\geqslant 0, \mathscr{R}\beta_2\geqslant 0$). Hence,

$$\begin{aligned}\ln L_+(\zeta)&=\frac{1}{2\pi i}\int_\Gamma\frac{\ln F_1(w)}{w-\zeta}dw-\frac{1}{2\pi i}\int_\Gamma\frac{\ln F_2(w)}{w-\zeta}dw\\&=\frac{1}{\pi}\int_0^{\infty}\frac{\phi_1-\phi_2}{u-i\zeta}du-\frac{1}{\pi}\int_0^{k_1}\frac{\psi_1-\phi_2}{u+\zeta}du,\end{aligned} \tag{A13}$$

where

$$\tan\phi_1=\frac{\gamma\sqrt{u^2+k_1{}^2}\cos\sqrt{u^2+k_2{}^2}H}{\sqrt{u^2+k_2{}^2}\sin\sqrt{u^2+k_2{}^2}H},\qquad \tan\psi_1=\frac{\gamma\sqrt{k^2{}_1-u^2}\cos\sqrt{k_2{}^2-u^2}H}{\sqrt{k_2{}^2-u^2}\sin\sqrt{k_2{}^2-u^2}H} \tag{A14}$$

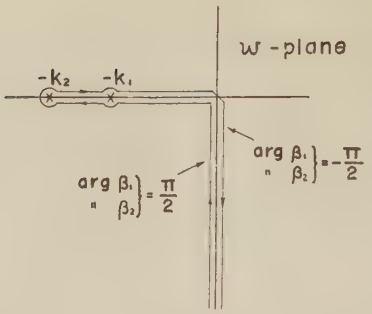

Fig. A 1

and ϕ_2, ψ_2 are given by the equations similar to (A14), taking h in place of H. And we have

$$L_-(\zeta)=L_+(-\zeta)\,. \tag{A15}$$

From (A1) and (A9), if we write

$$\frac{\beta_2\delta}{\sinh\beta_2\delta}\frac{F_1(\zeta)}{F_2(\zeta)}=K_+(\zeta)K_-(\zeta)=\frac{L_+(\zeta)L_-(\zeta)}{H_+(\zeta)H_-(\zeta)}\prod_{n=1}^{\infty}\frac{(\zeta^2-\kappa_{1,n}{}^2)}{(\zeta^2-\kappa_{2,n}{}^2)}\,, \tag{A16}$$

we can finally obtain

$$K_+(\zeta)=K_-(-\zeta)=\frac{L_+(\zeta)}{H_+(\zeta)}\prod_{n=1}^{\infty}\frac{(\zeta+\kappa_{1,n})}{(\zeta+\kappa_{2,n})}\,, \tag{A17}$$

and $|K_+(\zeta)|$, $|K_-(\zeta)|\sim|\zeta|^{1/2}$ as $|\zeta|\to\infty$.

References

Titchmarsh, E. C.:
1939 Theory of Functions, 2nd Ed., Oxford University Press.

Jones, D. S.:
1952 A Simplifying Technique in the Solution of a Class of Diffraction Problems, Quart. Journ. Math., (2)**3**, pp. 189–196.

Press, F.:
1957 A Seismic Model Study of the Phase Velocity Method of Exploration, Geophysics, **22**, pp. 275–285.

Takagi, A.:
1959 Seismic Model Study, Read at the Meeting of the Seismological Society of Japan on Oct. 30.

DISASTER PREVENTION RESEARCH INSTITUTE
KYOTO UNIVERSITY
BULLETINS

Bulletin No. 47 August, 1961

Observational Study on Microseisms (Part 2)

By

Kennosuke OKANO

Abuyama Seismological Observatory, Faculty of Science, Kyoto University
(Communicated by Prof. K. Sassa)

Observational Study on Microseisms (Part 2)

By

Kennosuke Okano

Abuyama Seismological Observatory, Faculty of Science, Kyoto University
(Communicated by Prof. K. Sassa)

1. Introduction

In the previous paper (Okano 1961) it was shown that microseismic waves are generated by the swells propagated from a disturbance source to the coasts near an observation point. Especially their arrival directions deduced from the orbital motions of ground which were recorded by the vector seismographs, made this inference reserve the writer's entire confidence. The further investigation was made by carrying out the observations at the Aso and the Yura stations. The former station is located at the nearly central part of Kyushu where is surrounded by seas on all sides, and the latter is located at the coast of Wakayama Pref. in the southward direction at the distance of about 100 km from the Abuyama Seismological Observatory. Both stations appear suitable to investigate furthermore the precise location of generation of microseisms. The frequency of arrival directions of microseismic waves obtained at the Aso station is very partially distributed and these partially distributed directions seem to be closely associated with the slope of continental shelves. The frequency distributions obtained at the Abuyama and the Yura stations also support this close relationship. Furthermore the writer intended to investigate whether microseismic waves are generated at the regions close by coast lines or at some distance from coasts. The amplitude of waves coming from different directions supplied some information regarding that problem. But the sufficient elucidation of this subject must be expected by further investigations.

When the typhoon no. 14 in 1960 passed through on the south ocean off Japan, there were appreciable differences of the periods among the microseismic waves coming from different directions. This result is explainable, if the periods of swells increase with an increase of distance of propagation.

2. Arrival directions of microseismic waves at Kyushu

With the same method used at the Abuyama Seismological Observatory, the arrival directions of microseismic waves were deduced by observing the orbital motions of ground at Kyushu. The station where the observation was carried out is the Aso Volcanological Laboratory, located nearly in the central part of Kyushu. The instruments used are the vector seismographs adjusted to the following constants ; $T_1=4.0$ sec., $T_2=6.0$ sec., h_1, h_2 = near critical and $V_{max.}$ = about 2800. Some of the orbital motions recorded are shown in Fig. 1. It is found that they are appreciably

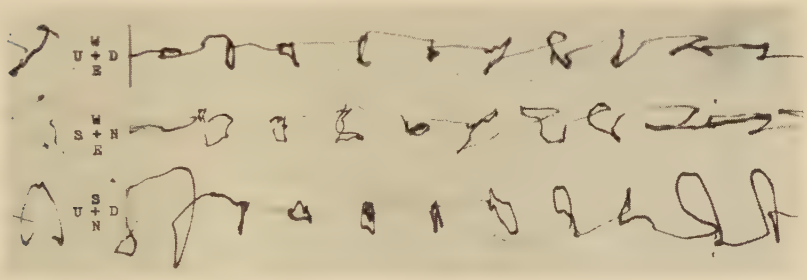

(1)

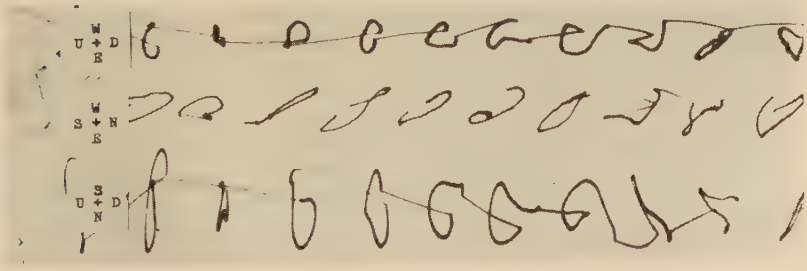

(2)

Fig. 1 Seismograms recorded at Aso station.

disturbed and complicated in comparison with those recorded at the Abuyama station, because of superposing by various types of volcanic microtremors (Sassa 1935). Notwithstanding the fact the waves of typical Rayleigh type, disregarding the slight deformation, are found so frequently that the frequency distribution of arrival directions can be obtained without difficulty. Fig. 2 shows the three distributions obtained from the microseismic

storms generated by the typhoon no. 6, no. 8 and no. 18 in 1960, and Fig. 3 shows the respective weather charts at the times when those distributions were obtained. When those distributions were obtained, the typhoons regarded as the disturbance sources were on the south-westerly ocean far off Kyushu. Most of the arrival directions do not point toward the centers of the typhoons, though there are a few pointed toward the south-westerly coast where considerable parts of swells arised in the typhoon areas are supposed to be sent, judging from the location of the typhoons. A great part of the frequencies is concentrated in the south-easterly direction (the Hyuga Sea), and a small part of them indi-

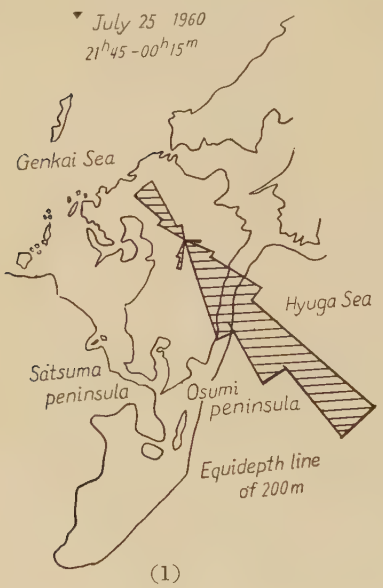

(1)

(2)

(3)

Fig. 2 Frequency distributions of arrival directions of microseismic waves observed at Aso station.

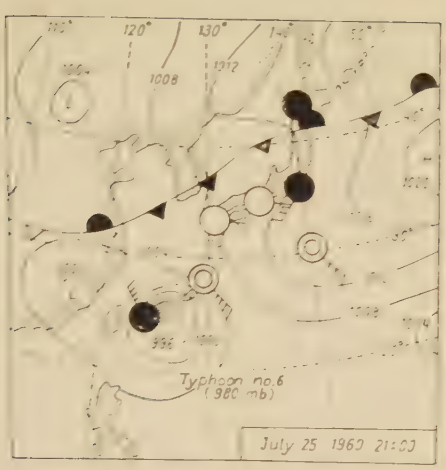

(1)

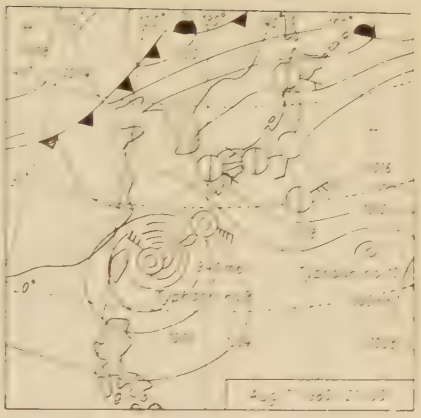

(2)

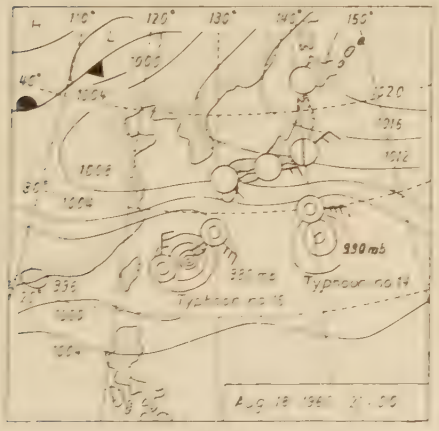

(3)

Fig. 3 Weather charts at the respective times when Fig. 2 was obtained.

cates the north-westerly direction (the Genkai Sea), though the microseismic storm on July 25 in 1960 when the cold front passed over the Genkai Sea distributes considerable frequencies in that direction. And a little rests of the frequencies are distributed only in the direction of the Satsuma Peninsula. Previously the writer deduced from the arrival directions of microseismic waves at the Abuyama station that there are some districts where microseismic waves are frequently generated and some other districts not frequently. These observations at Kyushu supported more firmly this inference. Vertical components, as shown in Fig. 1, are small in amplitude as compared with horizontal, whereas the seismographs at the Abuyama station recorded the microseismic waves with similar amplitudes in two components. This may be due to the property of the ground on which the Aso station is founded.

3. Arrival directions of microseismic waves at the Wakayama Pref.

To obtain further information on the generating district of microseismic waves, the arrival directions were observed at the Yura observing station of the Wakayama Pref. by the vector seismographs used for the same purpose at the Abuyama station.

When the seasonal wind stirred up the Japan Sea on Dec. 6 in 1960, the observation was carried out for about five hours. The seismographs recorded frequently the orbits of the considerably typical Rayleigh motion, having the amplitudes in vertical component similar to those in horizontal, as recorded at the Abuyama station. An example of those orbital motions is shown in Fig. 4. Fig. 5 shows the frequency distribution

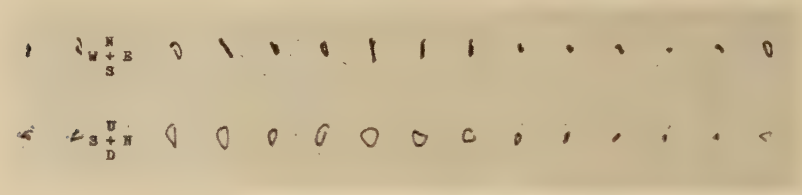

Fig. 4 Seismogram recorded at Yura station.

of arrival directions read from those orbits. Notwithstanding that the Yura station is far more distant from the coast of the Japan Sea than that of the Pacific, almost all arrival directions point toward the Japan Sea. And the pattern of the distribution is very similar to that of the Abuyama station, that is, the microseismic waves do not come from the easterly and westerly directions in which there are no coasts of the Japan Sea close to the station. The direction indicating the maximum frequency does not coincide with the northward direction in which the station is nearest to the

Fig. 5 Frequency distribution of arrival directions of microseismic waves observed at Yura station.

Japan Sea, but deviates somewhat westwards. We may recognize the difference of about 10 degrees between the deviation of arrival directions at the Abuyama station and that at the Yura station. The existence of the difference appears to support the writer's opinion on the origin of microseisms.

4. The microseismic storm observed at the Abuyama station on Aug. 20 1960

The strong microseismic storm was raised when the typhoon no. 14 passed over the southerly ocean of Japan. The vector seismorgraphs recorded the orbital motions of ground in horizontal and only one vertical (UD-NS) planes, and simultaneously an ordinary seismograph with the same constants as the vector seismographs recorded the ground vibration in NS component. The arrival directions were read from the former and the wave period from the latter, because the vector seismographs are hard to give the wave period so exactly as read from an ordinary seismograph. And if we intend to select only the waves of the typical Rayleigh form, the orbital motions in the horizontal and only one vertical (UD-NS) planes may supply the sufficient information for the arrival direction. Of course, if the microseismic waves come from

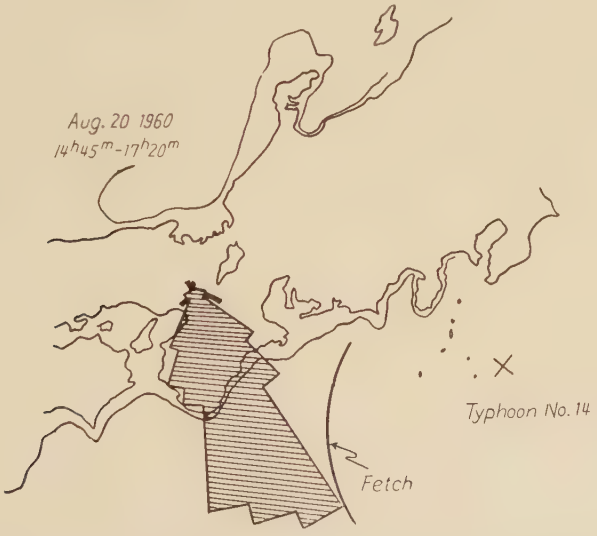

Fig. 6 Frequency distribution of arrival directions of microseismic waves observed at Abuyama station on Aug. 20 1960 and location of the typhoon.

the easterly or westerly direction, the orbits in another vertical (UD-EW) plane are necessary to detect such waves. But the writer could save the necessity of those orbits, because he did scarcely find the east-westerly linear orbits with comparable amplitudes in the horizontal plane. The frequency distribution of arrival directions is shown in Fig. 6. The arrival directions do not point toward the center of the typhoon, and the direction of maximum frequency deviates considerably eastwards from the south, differing from that obtained previously. This may be ascribed to that the typhoons were westwards from the Kii Peninsula in the previous case and eastwards in this case and hence the swells propagated from the respective typhoon areas were interruped by the Peninsula.

5. Consideration on the district where microseismic waves are generated

The frequency distribution of arrival directions of microseismic wave having the typical Rayleigh motions is shown in Fig. 7, including the new data obtained by the observation at the Abuyama station. Examining these distributions obtained at the Abuyama, the Aso and the Yura stations, it comes into notice that the microseismic waves originate definitely in the particularly limited regions while the center of typhoon moves. The writer recognized that the frequency of generation is closely connected with the slope of the continental shelf. The equidepth lines of 200 meters drawn in those figures suggest that fact, and it is indicated furthermore clearly by Fig. 8. In this case the frequency of generation is supposed to be also associated with an angle of the arrival direction formed with the continental margin, besides a slope of the continental shelf, because the origin of

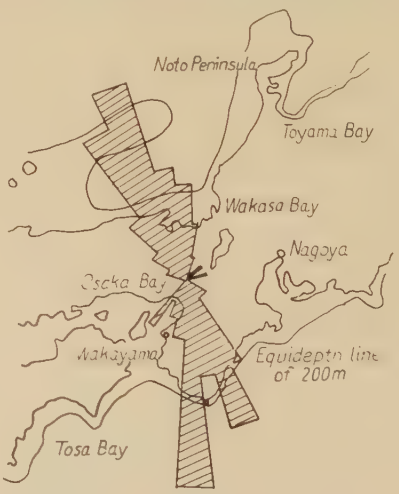

Fig. 7 Frequency distribution of arrival directions of only microseismic waves having the typical Rayleigh form. (at Abuyama station)

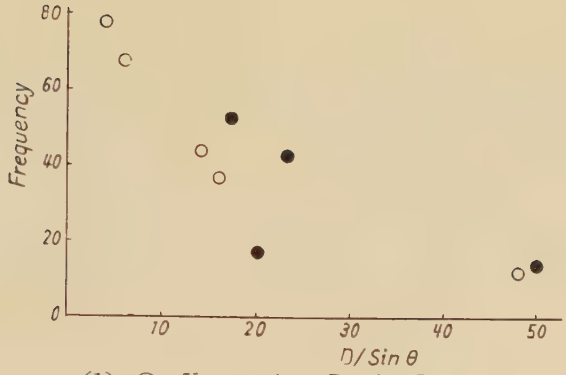

(1) ○– Yura station, ●– Aso Laboratory

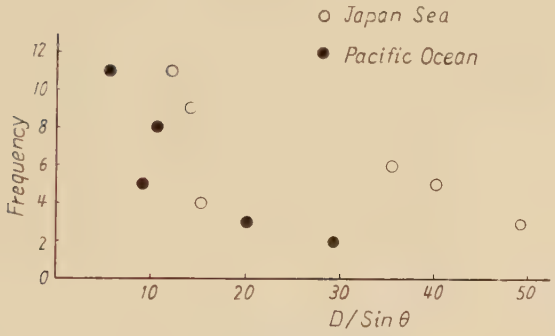

(2) Abuyama Observatory

Fig. 8 Relationship between the frequency of microseismic waves and the ratio of D to Sin θ.
D : Distance from coasts to continental margins
θ : Angle of arrival directions formed with continental margins

microseisms is taken as the line source which is parallel with the continental margin. Therefore $D/\sin\theta$ was adopted as the abscissa, in which D is the distance from the coast to the continenental margin and θ is the above mentioned angle. It may be readily understood from the above mentioned inference that there are minimum frequencies in the southerly direction in their distributions at the Aso station and also in the direction of the Wakayama district and the Noto Peninsula in the distributions at the Abuyama station.

Let us consider why we observe frequently the microseismic waves coming from the regions possessing the continental shelves of steep slope. As the wave length of sea waves is comparable to the depth of the

continental shelf, the wave energy is dissipated as a result of friction by the oscillating motion of waves at the sea bottom, and in consequence the wave height reduces as the waves propagate shoreward. Accordingly as a decrease of the slope of shelf, the sea waves reduce in height in the vicinity of the coast, because of dissipating of the energy due to an increase of the distance of propagation, and then it results in the reduction of amplitudes of microseismic waves. The arrival direction may be thus not frequently observed by us in the direction of the gently sloping continental

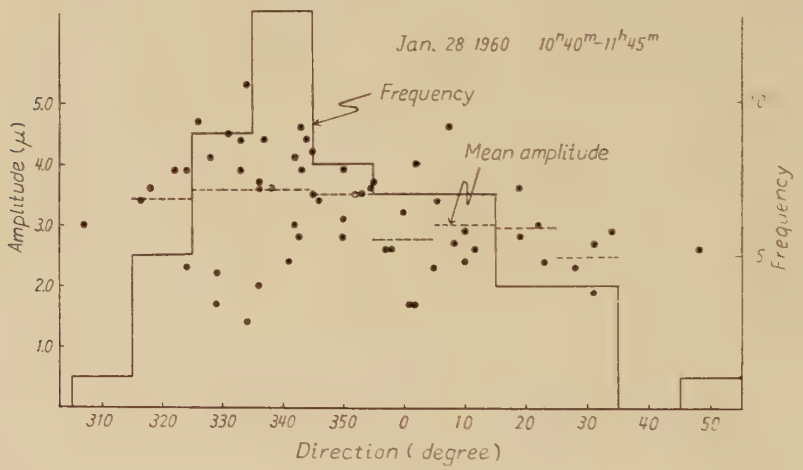

(1)

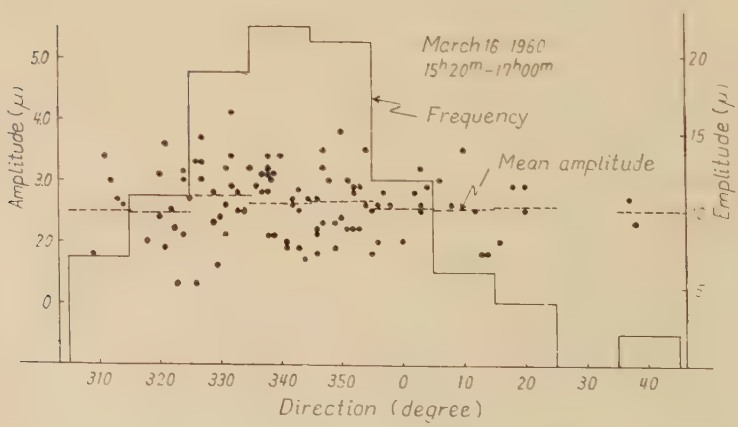

(2)

Fig. 9 The amplitude of microseismic waves versus the arrival direction.

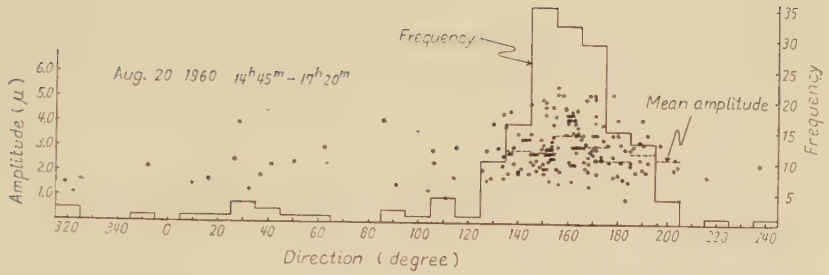

Fig. 10 The amplitude of microseismic waves versus the arrival direction.

shelf. If it is so, the amplitude of microseismic waves should be in proportion to the frequency of arrival directions. The relation between the amplitude and the arrival direction is shown in Fig. 9 for the microseismic waves coming from the Japan Sea and in Fig. 10 for those coming from the Pacific. The broken lines in those figures indicate the mean amplitudes. We may observe the upper limiting points plotted to be somewhat proportional to the frequency, but the fluctuation of the amplitude fad into insignificance in comparison with that of the frequency, especially for the mean amplitude. The writer could not thus recognize the close connection between the amplitude of microseismic waves and their frequency of generation. From this fact it is hardly likely that microseismic waves with the energy enough to be propagated to the Abuyama station may be generated at the regions close to the coastlines. The writer does not readily accept the consideration that the microseismic waves should be generated by the standing sea waves due to the interference of incident and reflected waves produced by a steep coast, because he wonders if the standing sea waves can so strongly generate elastic waves in the crust that the ground displacement is able to attain to a few microns after propagating the path of more than 100 km.

According to the experimental study of Cooper and Longuet-Higgins (1951), the first order pressure variations by progressive water waves give considerable energy in the bed of tank, if the water depth is small as compared with half the wave-length. Therefore, the progressive sea waves must more strongly generate microseismic waves than the standing sea waves in sea beds close to coastlines, because the progressive waves, in

general, give more energy in phase in sea beds than the standing sea waves.

The writer prefers the district at a distance from the coast, that is, rather near the continental margin, to the district close to the coastline as the origin of generation of microseisms.

In conclusion steeper inclination of the sea bed must be accompanied by the condition to generate more frequently micorseismic waves, and at present we can but guess that the standing sea waves are frequently produced under such a condition.

6. Investigation of the wave period of microseisms coming from different arrival directions

It is interesting and very significant to the investigation of microseisms to observe whether the microseismic waves with different periods come from different arrival directions. The observation to this purpose was carried out at the Abuyama station for the microseismic waves coming from the Japan Sea and the Pacific.

When the progression of microseismic waves was previously investigated (Okano 1960), the ordinary seismograms in NS component were obtained together with the vector seismograms. Therefore the wave period could

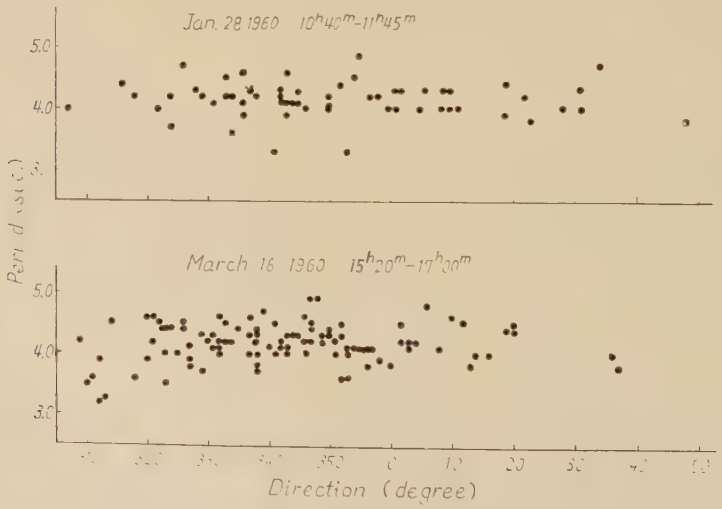

Fig. 11 Relation of the period to the arrival direction of microseismic waves caused by seasonal winds in winter season.

be exactly read from the former and the arrival direction from the latter, and those relations are illustrated in Fig. 11. Although the period are considerably scattered centering around about 4.2 sec., on the whole there is little if any difference among those of waves coming from different directions. The writer supposed that those facts can be interpreted as follows. Since the seasonal wind stires widely up the Japan Sea in winter season, the disturbance source also covers a wide range of the Sea, and hence it is not so distant from the continental margin where the writer considers to be the origin of generation. Accordingly the wave period of microseisms is not so large because of the short distance of propagation of sea waves and it is not so different among the waves generated at the different districts.

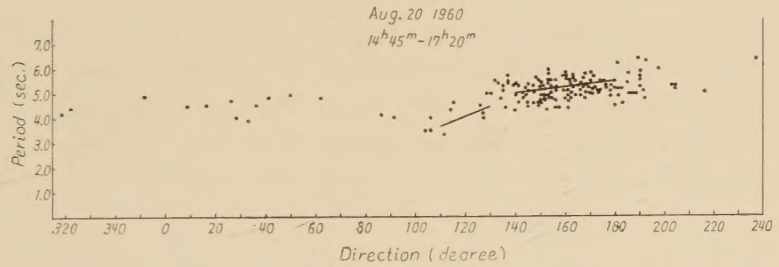

Fig. 12 Relation of the period to the arrival direction of microseismic waves caused by typhoon No. 14.

Fig. 12 shows the relation of the period to the arrival direction of microseismic waves when the typhoon no. 14 was situated as shown in Fig. 6. The difference of the periods among arrival directions is considerably noticed, excepting the waves propagated from the Japan Sea. Then we assume that the swells leave the end of the fetch shown in Fig. 6, propagate on the open sea and generate the microseismic waves in the vicinity of the continental margin. According to Sverdrup and Munk (1947), the relation of the wave period of swells at the end of the decay distance to that at the end of the fetch was indicated as follows.

$$\frac{T_D}{T_F}=\sqrt{1+16\pi^2\,\mathrm{Ar}\,\left(\frac{D}{gT_F^2}\right)}$$

$$A\ :\ 2\gamma^2\rho'/\rho=6.35\times10^{-5}$$

γ^2 : Resistance coefficient applicable to wind (2.6×10^{-3} for wind velocities 5m/sec)

ρ' : Density of air (1.25×10^{-3} g/cm^3)

ρ : Density of water (1.025 g/cm^3)

r : Coefficient of energy partition (0.580)

D : Distance of decay

Based on the probable assumption that T_F is 6.0 sec., T_D was calculated for each arrival direction, and the relation are indicated by the solid lines in Fig. 12. In this case the writer applied the Longuet-Higgins's theory to the relation between the period of microseismic waves and that of swells, according to which the former is half of the latter. Comparatively good coincidence is recognized between the observation and the calculation. This is one of the evidences to show that the microseismic waves should be generated in the neighbourhood of the continental margin by the swells propagated from the disturbance source. The waves of the short period coming from the direction of 100–110 degrees may be the 3-second microseisms which are very frequently observed at Nagoya. (National Comittee for I.G.Y. 1959 and 1960).

7. Summary

1. The inference that microseismic waves are generated not in the neighbourhood of a low pressure center but at the regions near coasts, became quite obvious from the observations at the Aso and the Yura stations.

2. The microseismic waves are more frequently generated at the district where the continental margin is more shoreward, namely, the slope of the continental shelf is steeper.

3. The writer could not see the appreciable differences in mean amplitude among the waves coming from different directions. This fact suggests that microseismic waves should be generated at the districts not close to coastlines but rather near continental margins, because the swells are supposed to be alike in height everywhere in the vicinity of continental margins.

4. The microseismic waves coming from different arrival directions are alike in mean period when the waves are generated by the seasonal

wind in winter season. When the microseismic waves are generated by the typhoon, we may observe longer periods for the waves propagated from the district having longer distance of propagation of swells.

8. Acknowledgment

Much of this work was suggested by Professor Kenzo Sassa of Kyoto University, to whom the writer owes thanks for his interest and encouragement. The writer wishes to express his thanks to Professor Haruo Miki of Kyoto University for his encouragement. The writer is greatly indebted to Mr. Kosuke Kamo of the Volcanological Laboratory of Kyoto University for the observation at the Aso station.

References

1) Cooper, R. I. B. and M. S. Longuet-Higgins : An experimental study of the pressure variations in standing water waves, Proc. Roy. Soc. A, 206 (1951), 424–435.
2) National Comittee for I. G. Y. : Report of microseismic and sea wave observations in Japan during I. G. Y., 1957–1958. No. 1 (1959) and No. 2 (1960).
3) Okano, K. : Observational study on microseisms (Part 1), Disaster Prevention Res. Inst. Kyoto Univ. Bull., No. 44, 1–22 (1961).
4) Sassa, K. : Volcanic micro-tremors and eruption-earthquakes (Part 1 and 2), Mem. Coll. Sci., Kyoto Univ., A, 18 (1935) and 19 (1936).
5) Sverdrup, H. U. and W. H. Munk : Wind, sea and swell : theory of relations for forecasting, Publ. Hydrog. Office, Wash., No. 601 (1947).